Dimensional stability of biaxially drawn PET: effects of processing and material composition

DIMENSIONAL STABILITY OF BIAXIALLY DRAWN PET: EFFECTS OF PROCESSING AND MATERIAL COMPOSITION

by

ZAKIA FEKKAI

A Doctoral Thesis submitted in partial fulfilment
of the requirements for the award of the
Degree of Doctor of Philosophy
of
Loughborough University of Technology

1991

Supervisor: Dr L Mascia

Institute of Polymer Technology and
Materials Engineering

Dedicated to my loved ones:
my family and my husband Nazir

* * * * *

ACKNOWLEDGEMENTS

I would like to express my sincere gratitude to Dr L Mascia for the opportunity to undertake this project. His enthusiasm, knowledge and tireless effort was a continual inspiration. Also for the advice that arose from our numerous discussions, which was invaluable.

The completion of this programme was greatly aided by Messrs P Ramsey and R Owens who were always available to steer me in the right direction with all technical problems. I would like to thank Mr F Miller for his time, knowledge and friendship, and Mr F Page for his help on the SEM work.

I would like to thank all my friends for their moral support and the useful discussions we had.

A special thank you to Janet Smith for typing this thesis.

Finally I would like to thank the directors of Enichem Fibres SpA for the financial support without which this project would not have been possible.

ABSTRACT

Biaxial orientation of PET for the production of high strength films for demanding applications, such as slot liners for electrical motors and sound and audio visual tapes, is a well established process. More recently biaxial orientation of PET has been utilised for the production of carbonated beverages, bottles and cans for processed food packaging to achieve high strength and impact resistance. These containers, however, are not suitable for hot filling and high temperature sterilisation purposes owing to the lack of dimensional stability.

Heat setting operations, which are well proven methods for fibres and films, have also been proposed for bottles, but this operation requires complex and expensive machinery to prevent distortion of the containers and to achieve the desired degree of control on dimensions. Furthermore thermally induced crystallisation in heat setting operations in areas where the amount of orientation is very small, such as the neck regions of the bottle, causes severe embrittlement and the development of opacity.

This study was initiated, therefore, with the aim of establishing the factors that affect the shrinkage of PET bottles when exposed to high temperatures (particularly in the range 85-100^{o}C) and to examine the means by which the problem can be alleviated. Two approaches have been used: model stretching experiments and evaluation of compatible blends. Uniaxial and biaxial stretching experiments were carried out on PET sheets and samples were examined primarily by thermal analysis, density measurements, shrinkage tests and microscopy.

The results have shown that the lowest shrinkage is obtained with samples exhibiting a very low amount of residual crystallisability after drawing, which is generally achieved at high draw temperatures. Moreover it was discovered that biaxial stretching with additional in plane distortions is very effective in decreasing the amount of shrinkage taking place at high temperatures owing to the greater level of crystallinity developed in the stretching operation.

Blending PET with compatible high Tg amorphous polymers, such as polycarbonate (PC) and polyarylate (PA) was not found to be an effective method to improve dimensional stability. Increasing the Tg of the polymer mixture with amorphous polymers has, in fact, the opposite effect, owing to the lower level of crystallinity developed during stretching. Mixing PET with the crystalline polymer, polymetaxylene adipamide, which is incompatible but produces transparent blends, on the other hand, reduces the level of shrinkage considerably, particularly when the level of polymetaxylene adipamide approaches 30%. This has been attributed to a nucleation effect which increases the level of crystallinity during stretching.

TABLE OF CONTENTS

CHAPTER 1
INTRODUCTION

1.1 HISTORICAL DEVELOPMENT OF PET ORIENTED PRODUCTS

Polyethylene terephthalate (PET) is a well known commercial polymer used for fibres, films and recently for food and beverage containers.

The discovery of polyethylene terephthalate as a fibre forming polymer was made in England in 1941 by Whinfield and Dickson, of the Calico Printers Association Ltd. It was recognised at an early stage to be a material of unusual interest, and developmental investigations on the polymer and its fibres were undertaken first by British Government research laboratories and later by Imperial Chemical Industries. In the early 1950s polyethylene terephthalate first appeared in commercial quantities under the trademarks Terylene in the United Kingdom and Dacron in the United States.

The technology of polyester fibre production is well documented [1,2]. Through a number of variations in the melt spinning, drawing, and setting procedures, numerous types of yarn are produced, which find use in many industrial applications (e.g. conveyor belting, filter fabrics, laundry bags, webbing, tyre cords, sewing threads, ropes etc) and particularly in blends with cotton, wool, linen, or rayon as lightweight permanently pleatable fabrics [3].

Concurrently with its role as a fibrous material, polyethylene terephthalate has come into use as a source of high-strength biaxially

drawn films (e.g. Melinex in the United Kingdom, Mylar in the United States) which are noted for their high transparency, strength and dimensional stability. These are used extensively for electrical insulation, as bases for magnetic recording tapes and typewriter ribbons, in decorative laminates and panelling and as a vacuum-formable coating and packaging material.

In 1977, its use was extended to beverage bottles because of several characteristics such as the ease of producing orientation, mechanical strength, low permeability to CO_2, transparency, non-toxic nature and devoid of any effect on flavour [4]. The manufacturing procedure mostly used to produce impact-resistance bottles from polyethylene terephthalate is the stretch-blow moulding process, by which rotationally symmetric containers with narrow as well as wide necks are produced. This process is widely used because of its many advantages [5-8]. It gives products of considerably better mechanical and optical properties, and improved barrier properties against permeation by gases and water vapour [9].

The stretch blow moulding technique is a two stage process. In the first stage, the polymer is injection moulded into preforms. These preforms are rapidly quenched in mould cavities at a temperature of $5^{o}C$ to $10^{o}C$ to obtain a transparent product. In the second stage these preforms are reheated and conditioned at an orientation temperature between the Tg and the melting point, and are then transferred to a stretch blow moulding machine, where a rod is inserted into the preform to stretch and orient it axially and to position it centrally in the mould. High pressure air is then

injected in two steps to expand the preform against the walls of the mould, thereby providing orientation in the hoop direction.

Degradation during polymerisation and processing causes the formation of small amounts of acetaldehyde. Copolymers are used to minimise this drawback, while a newer process called compress-orient blow moulding is also claimed to reduce acetaldehyde content [10]. The polymer is injected into the mould at low temperature and pressure. A core is inserted to compress the polymer, causing it to flow and to fill the cavity. These mild moulding conditions reduce the acetaldehyde content by 50% because of less thermal degradation of PET. The acetaldehyde content in the final bottle is an important factor to consider as it must be kept below 6 ppm. Above this level the acetaldehyde imparts a fruity flavour to the contents of the bottle and is not toxicologically safe. Polymers with minimum acetaldehyde content can be prepared by conducting the final stages of the polymerisation in the solid state, thereby minimising thermal degradation and purging the acetaldehyde residues and other volatiles from the polymer.

1.2 BLENDS BASED ON PET

In recent years, PET blends have been a subject of great interest in both industrial and University research laboratories. The advantages of blending two polymers and the associated properties have been summarised in a series of recent reviews [11-12].

Polymer blends can be characterised by their phase behaviour as being either miscible or immiscible. Immiscible blends show multiple amorphous phases. Each phase of a completely immiscible blend contains an essentially pure blend component whereas the phases of partially immiscible blends will contain some of each material in the blend. Finally, blends can also be found which are completely miscible and have only one amorphous phase [13].

One of the most important properties of polymer blends is their mechanical behaviour. A compatible polymer blend exhibits mechanical properties that are intermediate between those of the two components [14]. In crystallisable polymer blends the mechanical behaviour is affected by the properties of individual constituents, mode of dispersion, degree of crystallinity, morphology and compatibility in the amorphous state [15-16]. It is very rare to achieve compatibility in the crystalline phase.

In general the mechanical, thermal, rheological and other properties of a polymer blend depends strongly on its state of miscibility. Conceptually, this state is determined by the thermodynamics of the interactions between the blend components which depend on their chemical structures and stereo configurations.

Polyarylate (PA) and polycarbonate (PC) have a relatively high glass transition temperature and are amorphous, while polyethylene terephthalate (PET) has a semi-crystalline structure. All three polymers have the ester groups in common, which may result in interaction between the similar chemical moieties. In recent studies

it has been reported that PET is miscible with PC for a wide composition range [13-17,18-19] where the physical blends of PET and PA are phase separated in their amorphous state involving a pure PET phase and a mixed phase rich in PA.

However the ester exchange reactions can convert the immiscible blends of PET to single-phase materials [20], for example blends of PET and PA which are initially immiscible, become single-phase mixtures during melt processing, as determined by optical transparency and a single Tg [21]. Similarly, immiscible mixtures of PET or PA with phenoxy are converted to single-phase systems through ester exchange, these systems, however, rapidly crosslink via the hydroxyl functionality of the phenoxy at processing temperatures.

1.3 MEASUREMENT OF ORIENTATION

1.3.1 Optical Anisotropy and Birefringence

The measurement of optical anisotropy is one of the simplest and most used methods for studying orientation in polymers. It is based on the principle that a given material has associated with it unique optical properties that are determined by its polarisability [22]. Since polarisability is related to the refractive index by the Lorenz-Lorenz equation:

$$\frac{n^2 - 1}{n^2 + 1} = \frac{4}{3}\pi P \qquad (1)$$

where P is defined as αN, N being the number of molecules per unit volume and α is the polarisability of the molecular unit having the dimensions of volume. Orientation can, therefore, be assessed by directly measuring two principal refractive indices, $n_{||}$ and $n_{\perp}$, and calculating the difference [23]:

$$D_n = n_{||} - n_{\perp} \qquad (2)$$

For the case of fibres, D_n is the birefringence, $n_{||}$ being the refractive index along the fibre axis, and $n_{\perp}$ the refractive index perpendicular to the fibre axis as viewed through a cross-polarised light.

This method requires the use of an immersion fluid [23] that matches the refractive index of the fibre. As the matching fluids for highly oriented synthetic fibres are often toxic, other methods are normally used, such as the compensator and spectrophotometric methods.

The basic principle of the spectrophotometric method [24,25] is to measure the distribution of intensity as a function of the wavelength with a spectrophotometer and to compute the optical retardation of the stretched sample. The experimental arrangement for this method is that the monochromatic light transmitted from the analyser is measured by a detector and compared with a reference beam; the difference is recorded on a chart. The birefringence is given by $D_n = m \lambda m/h$, where m is the peak number, λm is the peak wavelength and h is the sample thickness.

The comparator technique basically involves [22] a known retardation to nullify or compensate the retardation induced by the sample. This amounts to placing a birefringent (anisotropic) material into the light path, e.g. a wedge or plate of quartz or calcite, which can be rotated precisely by tilting it about an axis parallel to the plane of the plate

$$D_n = R/t$$

where D_n is the birefringence

t = thickness and R is the retardation.

1.3.2 Wide Angle X-Ray Diffraction

Wide angle X-ray diffraction is another technique which has been of vital importance in the understanding of oriented polymers. When a crystalline polymer is oriented, the random circular diffraction pattern transforms into a collection of defined arcs that are correlated with a particular (hKl) plane that can be identified, based on the crystal structure and Bragg relationship [22]. It follows that the magnitude of the azimuthal spread (X/2) of these reflections is indicative of the degree of orientation. The breadth, K, of the reflection is related to crystal size and imperfection [26]. Also, the location of the reflection with respect to the sample axes indicates the orientation of the crystallographic planes. In general, the distribution of orientation is determined for a single (hKl) plane, usually a (h00), (0K0) or (00l) plane, if sufficient diffraction exists. The data are then presented either in a pole figure or may be used to determine the Herman's orientation function defined as:

$$f_{hKl,i} = \frac{3\cos^2\phi\, hKl,i - 1}{2}$$

where $\cos^2 \phi_{hKl,i}$ is the average angle that the normal to the set of (hKl) planes makes with some specified ith axis, usually the principal deformation direction of the sample [22].

The Herman's orientation factor has been generalised by White and Spriuell who found that it is more useful to represent orientation in terms of planar or biaxial orientation factors:

$$f^{B}_{c1} = 2\cos^2\phi_{c1} + \cos^2\phi C_{c2} - 1$$

$$f^{B}_{c2} = 2\cos^2\phi_{c2} + \cos^2\phi C_{c1} - 1$$

defined in terms of angle ϕ_{c1} and ϕ_{c2} between the polymer crystal axis **c**, and machine, 1, and transverse, 2, direction. The direction 3 is taken normal to the surface of a film sheet or bottle [27]. For uniaxial orientation in the machine direction, f^{B}_{c1} is unity and f^{B}_{c2} is zero. For uniaxial orientation in the transverse direction, f^{B}_{c1} is zero and F^{B}_{c2} is unity. For balanced biaxial orientation f^{B}_{c1} and f^{B}_{c2} are equal to 1/2.

1.3.3 Small Angle X-ray Scattering

Small angle X-ray scattering (SAXS) is often used as a complementary method to wide angle X-ray diffraction to define the structure and morphology of oriented crystalline polymers [22]. It is one of the techniques used to study superstructural development in multiaxially stretched products [28]. It is found [22], however, that there is an inverse relationship between scattering angle θ and the ratio of the

size of the scattering structure to the wavelength of radiation which is used. Consequently, the technique of small-angle X-ray scattering is used for studies of structures of size 100-10000 Å with X-rays of wavelength of ∿1Å. The equation for scattering can be expressed in terms of a reduced variable of the form

$$U^* = C^* (a/\lambda) \sin (\theta/2)$$

where a is some dimensional parameter of the scattering structure. C* is a constant characteristic of the experiment, being close to one. Measurements are usually in the range of convenient observation when U* is of the order of unity.

1.4 AIMS OF THE INVESTIGATION

Polyethylene terephthalate (PET) is widely used for the production of biaxially stretched films in view of its high melting point, making these particularly suitable for high temperature applications and convenience food packaging. In such cases the required dimension stability at high temperatures is achieved by heat setting operations which allow a small amount of relaxation while increasing the level of crystallinity in the film. The aim of this study is to provide a method that makes it possible to enhance the dimension stability of biaxially stretched PET products without the expedient of heat setting operations, making it particularly useful for the production of bottles and containers destined for hot-filling and high temperature sterilisation of beverages and processed food. The overall objectives of the study are to explore the possibility of achieving high temperature dimension stability by:

i) The processing route using model stretching experiments. The factors that affect the dimensional stability of PET bottles are studied by simulating the expansion process with uniaxial and biaxial stretching experiments from which we would deduce the conditions leading to zero shrinkage.

ii) The materials route using blends that produce transparent products. This objective seeks to decrease shrinkage by blending PET with compatible high Tg amorphous polymers (polycarbonate-polyarylate) and a semi-crystalline polyamide (polymetaxylene adipamide), which has received FDA approval for such products in mixtures with PET.

CHAPTER 2
LITERATURE REVIEW

2.1 CRYSTALLISATION STUDIES ON POLY(ETHYLENE TEREPHTHALATE)

2.1.1 The Amorphous and Crystalline States

Crystallisation is a two stage process consisting of nucleation and growth. In a quiescent state, once nuclei are formed, they develop into crystals by chain folding, resulting in lamellar crystals, which tend to organise themselves into larger entities called spherulites. It is found experimentally [29] that under isothermal conditions the radius of a spherulite increases linearly with time until different spherulites begin to impinge on each other.

The crystallisable nature of PET is well known [30]. By rapid quenching from the melt it is possible to obtain a completely amorphous polymer. If, on the other hand, it is allowed to cool slowly it crystallises to a degree of crystallisation that depends on the cooling rate. Hence the morphology and percentage of crystallinity are controlled by the processing conditions.

2.1.2 Isothermal Crystallisation

The structural changes accompanying the crystallisation process of PET have often been investigated using differential scanning calorimetry (DSC) and it has been found that when PET is crystallised under different conditions, frequently it exhibits two endothermic fusion peaks [31-32]. The main peak, peak I, is constant, while the second peak, peak II, is only observed after heat treatments at temperatures

below the main melting peak. Initially peak II is small but, with increasing crystallisation temperature or crystallisation time, it increases in size and moves to higher temperature and merges with peak I, which gradually decreases in size and eventually disappears completely. At present there are conflicting views about the origin of these peaks. Bell and Murayama [33] have proposed that peak I is associated with chain folded crystals and peak II with crystals containing partially extended chains. Roberts [34], on the other hand, has interpreted peak I as being due to bundle-like crystals and peak II to chain folded crystals. Both authors tacitly assumed that no structural changes took place in temperature scans in a DSC apparatus. On this basis, the melting peaks were assumed to be directly related to the structure of the material at room temperature prior to the scan. These assumptions were proved later to be incorrect by various authors [34-35]. Zachmann and Stuart [36] found, in particular, that only imperfect crystallites were formed at low crystallisation temperature. By subsequent heating to higher temperatures, the perfection of the crystallites increased, often within very short times, leading to the conclusion that the low temperature peak was due to partial melting and recrystallisation.

Hughes and Sheldon [37] carried out a DTA study on amorphous PET and found that the apparent area under the melting peak was significantly larger than the apparent area under the exothermic crystallisation peak. They suggested that the crystallisation peak was followed by a continuous crystallisation process which was not detectable in the thermogram baseline.

Bair [38] et al have shown conclusively that multiple melting peaks observed in DSC thermograms of polyethylene single crystals are the result of annealing during scanning.

Finally Holdsworth and Turner-Jones [30] concluded that when amorphous PET is heated in a scanning calorimeter, there is a crystallisation process which converts the material into an assembly of imperfect crystallites. This is revealed by a large exothermic peak. The peak width suggests that crystallites with differing degrees of perfection are formed. Also in the intermediate temperature range there is a continual increase in crystallinity. This is due primarily to an increase in the average perfection of the crystallites by a continuous melting and recrystallisation process, producing a gradual increase in crystallinity which takes place over a wide temperature range and making it undetectable in the DSC baseline.

When the temperature is sufficiently high, the crystallites that are melting can no longer recrystallise and, therefore, give rise to a broad endothermic melting peak.

According to Roberts [32] crystallisation of PET occurs most rapidly in the temperature range 140-220^{o}C with 50 per cent of the resulting crystallinity developing in less than 30 seconds. The overall degree of crystallinity achieved [39], however, depends on the annealing temperature and to attain the highest degree of crystallinity the polymer has to be annealed at temperatures approaching the melting point.

The DSC analysis revealed that when PET is subject to heat treatments above its glass transition temperature and below its melting point (Tm) morphological changes occur which can be detected as an additional fusion endotherm appearing at a temperature (T'm) up to 40°C higher than the annealing temperature. The heat of fusion ($\Delta H_f'$) and melting temperature peak of this additional endotherm increases with treatment time at a particular temperature and with annealing temperature for a fixed treatment time.

The morphological changes occurring when partially crystalline poly(ethylene terephthalate) is annealed have been studied by various authors [40,41]. Petermann and Rieck [41] showed that annealing below 150°C leads to an increase in crystallite size and degree of crystallinity, but a micellar structure is always observed. When annealing is carried out above 180°C, on the other hand, the amorphous regions between the side faces of the micellar blocks begin to crystallise and large crystalline aggregates are formed without losing their micellar characteristics. On the other hand Klement and Geill [42] reported that thermal crystallisation of both uniaxially and biaxially drawn PET occurs with the formation of coarse 200-500 Å nodular aggregates which, in turn, may consist of the 75-100 nodules, detectable by electron microscopy. At annealing temperatures above 180°C, lamellar fibrils are formed which are arranged perpendicular to the draw direction in uniaxially drawn samples and at random in biaxially drawn samples. The lamellar fibrils orientation in uniaxially drawn PET is not unique and has been observed for many polymers crystallised after being subjected to large uniaxial strains [43].

2.1.3 Stress-Induced Crystallisation

Stress-induced crystallisation, also called strain-induced crystallisation, differs from isothermal crystallisation by its origin, kinetics and morphology.

Several studies have been made on induced crystallisation during stretching of amorphous PET [43,44,45,40]. They all show that, compared with isothermal crystallisation, the origin of the induced crystallisation is related to an entropic effect due to the orientation of the polymer chains. Bourvellec, Monnerie and Jarry [36] reported that the initial orientation of the material and the ambient temperature are the two parameters which control the kinetics of strain-induced crystallisation, which is always much faster than for the case of isothermal crystallisation of undrawn samples. For example, at 120^{o}C the half-time of the isothermal crystallisation of PET is a few minutes, but it becomes less than 0.01s in a strain-induced crystallisation process at the same temperature [36].

According to Bragato and Gianatti [46], as the initial level of orientation increases, the mechanism of crystallisation changes from a three dimensional growth, to a two dimensional one, and finally to a one dimensional rod like growth at high levels of orientation.

The crystalline textures obtained by induced crystallisation have a common feature, i.e. the crystallites are oriented contrary to the crystallites obtained by isothermal crystallisation of isotropic samples which are arranged into three dimensional spherulites.

De Vries et al [43] found that stress-induced crystallisation strongly depends on the stretching temperature as well as on the extensional strain rate. The most appropriate temperature range for stress-induced crystallisation to occur was found to be just above the glass-transition region. Also the rate of deformation has to be much larger than the reciprocal of the characteristic relaxation time of the polymer network in order to avoid disorientation during stretching, and the polymer has to be subsequently cooled to temperatures below Tg.

Previous studies [47,48] have shown that PET films do not change appreciably in crystallinity until they have been stretched to, at least, 150 per cent.

For PET bottles processed by the stretched blow moulding process Spruiell [49] reported that relatively high bulk crystallinities are produced, primarily due to stress-induced crystallisation resulting from the highest stretch ratio and strain rates experienced in this process.

The effects of chain branching on stress-induced crystallisation phenomena have been studied and reported by a few authors [50,51]. Hennessey and Spatorico [51] reported that the extent of crystallisation induced by stretching remains about the same, or perhaps decreases slightly, as the amount of branching increases in PET. The amount of crystallinity increases somewhat as the stretching temperature is increased for strains greater than >200%. The development of crystallinity as samples are drawn to various extents

does not appear to be strongly dependent on strain rate, at least in the range of 54-267%.

Yeh and Geil [52,53] pointed out that a glassy PET material is composed of a "ball-like" structure in which molecules are in paracrystalline order, and that strain-induced crystallisation is caused by rotation and alignment of molecular chains resulting in an increased perfection of the internal order of the paracrystalline "ball-like" structure.

2.1.4 Measurements of Crystallinity

The measured crystallinity in oriented PET depends on the method adopted and there is considerable confusion as to the type of structures present [54]. Prevorsek et al [55,56], from wide-angle X-ray diffraction (WAXD), revealed the presence of both crystalline, amorphous and an intermediate mesomorphic structures. The proportions of the mesomorphic phase were determined from the intensities of the diffraction peaks from the (110), (010) and (100) planes.

Others have put forward the concept of an oriented amorphous phase and random unoriented amorphous phase [57,58]. Each of these phases is an idealised model and there will be regions of intermediate structure. Each experimental technique, however, makes a separate assessment of the relative abundance of the three phases, and gives a different measure of the degree of crystallinity present in the sample.

Differential scanning calorimetry (DSC) has been used [59,60] widely to assess the percentage crystallinity assuming ΔH_m^o = 32.5 cal/g for

a 100 percent crystalline sample [61]. When a cold crystallisation exotherm is found during the heating scan, the value of the associated heat of crystallisation, ΔH_c, is subtracted from that for the heat of fusion ΔH_m, in order to calculate the crystalline weight fraction.

Sun and Magill [62] reported that shrinkage, crystallisation and melting can occur together during heating so that the crystallinity estimated by DSC for oriented materials has to be corrected by other independent measurement techniques, such as density measurements. For this reason, density (d) is also widely used a a measure of the degree of crystallinity (X) [40,63,64], determined by the relation

$$X = \frac{d - d_a}{d_c - d_a}$$

where the density of samples with 100% crystallinity, d_c, is taken to be equal to 1.457 g/cm^3 and the density for a 100% amorphous sample is taken as d_a = 1.335 g/cm^3 [65].

It is well known [66], however, that crystallinity can be overestimated when it is calculated from the density measured on oriented samples, owing to the increase in density of the amorphous phase as a result of the orientation of the molecular chains. Ward [67] showed that up to a level of amorphous orientation corresponding to an orientation factor of 0.3, the density of the amorphous phase of PET does not exceed 1.340, i.e. a variation of less than 0.3%, and can be neglected for the determination of crystallinity.

2.2 ORIENTATION AND SHRINKAGE

2.2.1 The Phenomena Related to the Amorphous and Crystalline Regions

Orientation in films and sheets can be produced in different ways, most frequently by drawing and stretching [22]. In all cases orientation is obtained by applying a large deformation in one or in two perpendicular directions at a suitable temperature. When the temperature is too low, e.g. when the polymer is in the glassy state, such deformations will generally lead to rupture and require excessively high stresses. At too high temperatures, i.e. in the viscous state, deformations can easily be applied but will not result in molecular orientations because of rapid molecular relaxation. Suitable conditions are those where the relaxation rate is exceeded by the rates of deformation and the sample is rapidly cooled. In such cases, rubber elastic deformations occur and are frozen in as molecular orientations [22]. For amorphous polymers this is the case in a temperature range between the glass-rubber transition point, Tg, and a somewhat higher value, depending on molecular weight. Crystalline polymers above the melting point, T_m, may have a temperature region in which a degree of permanent orientation can be produced, but this again depends on relaxation rate relative to drawing rate and cooling rate. In both these cases molecular weight and distribution are important parameters since the relaxation time of a polymer melt strongly increases with increasing chain length and widening of the distribution. If crystalline polymers are stretched below T_m the type of orientation will depend on the morphology of the polymer. Initially it was believed that oriented polymers consisted of a continuous amorphous phase surrounding dispersed crystalline regions, i.e. the so-called crystallites or fringed micelles [68] concept. During deformation the amorphous part would orient as an

amorphous polymer and the crystalline regions would rotate and orient in the direction of stretching. Since it is known that the crystalline domains in spherulites are continuous [69] and usually consist of folded molecules in lamellae, a different behaviour during stretching is assumed. At very low temperatures the crystalline lamellae are rigid and will, therefore, break up during drawing. Above a certain temperature slippage and twinning of the crystalline phase can occur and the molecules will orient themselves in the drawing direction through rotations of the lamellae and finally causing the unfolding of the molecules [70] to produce the so called chain extended crystals.

When oriented polymers are heated, they will try to regain their original high entropy, hence shrinkage will occur as soon as the molecules can move sufficiently to recoil to their original dimensions. For amorphous polymers this will be the case when the temperature exceeds the glass transition point, Tg. For crystalline polymers the behaviour is more complicated. At any temperature above the Tg of the amorphous phase, the oriented molecules in the amorphous regions will try to reach a higher entropy, but their coiling is hindered by the crystalline material. With increasing temperature the internal stresses in the amorphous regions are released and shrinkage occurs as a result. Most of the shrinkage is observed near the melting point, while above the melting point the orientation is lost completely. The theory of orientation discussed above is based primarily on deformation considerations and does not take into account the crystallisation phenomena occurring during the development of orientation, which is known as stress or strain-induced crystallisation. PET is known to exhibit such phenomena [71,72].

2.2.2 Molecular Orientation in Drawn Poly(ethylene Terephthalate)

The molecular orientation of poly(ethylene terephthalate) induced by stretching has been used for many years for manufacturing polyester fibres (uniaxial orientation) [73,74,75], films [76,77] and bottles [78,79] (biaxial orientation). The effect of draw ratio, temperature and strain rate on the orientation produced upon drawing amorphous PET have been well studied and widely reported [80,81,82]. Jabarin [83] showed that the molecular orientation in PET is a function of at least four independent but interrelated variables, namely amount of extension, molecular weight, temperature of orientation and stretch rate. He found that the birefringence between the plane and thickness direction of the samples stretched biaxially to equal draw ratio in both directions, increased with increasing amount of extension. For unequal biaxial extension, the greatest birefringence value occurs in the direction of the greatest extension. He studied the effect of temperature, molecular weight, extension ratio and stretch rate, on the amount of orientation by measuring the birefringence and found that the birefringence decreases with increasing drawing temperature, suggesting a decrease in molecular orientation. In the case of the high molecular weight samples (I_v = 0.7-0.8), the decrease in birefringence with temperature is gradual for drawing temperatures up to 90°C, but it is very steep when stretching is performed above 90°C. In general, the higher the molecular weight the higher the stretching temperature which can be used to achieve high levels of birefringence.

The effect of strain rate on birefringence was very significant at the higher end of the drawing temperature range (i.e. above 120°C).

Nicolas et al [84] studied the effects of orientation on the melting of poly(ethylene terephthalate) and reported that during drawing, PET

crystallises and that both the glass transition and crystallisation exotherm no longer appear in the thermogram. Furthermore, DSC measurements of the melting endotherm showed that orientation progressively increases the temperature for the onset of the melting process. The heat of fusion, on the other hand, was found to be comparatively insensitive to draw ratio, while the relative height of the melting endotherm increased to some extent with draw ratio and, therefore, could be used as an indirect measure of orientation. Samples with draw ratios greater than 3.5, which are difficult to distinguish by wide-angle X-ray diffraction measurements, can be distinguished, therefore from measurements of the height of the melting peak. Although extensive work has been reported to explain the mechanism of molecular orientation and the structure of oriented PET drawn above the glass-transition temperature [71,85,86,87] relatively little work has been done on oriented PET drawn below its glass transition temperature [88,89].

It has been shown [90] that during cold drawing (orientation below Tg) of pure polyethylene terephthalate at a temperature less than 70^{o}C and with a draw ratio = 5:1, silvery striations were frequently obtained perpendicular to the direction of draw. This observation was explained by the formation of microvoids.

In the wide angle X-ray diffraction pattern of drawn PET [91], reflections are often displaced, some up and some down, from normal layer line positions, this shows not only that the molecular chain axes of crystals are tilted with respect to the draw axis, but also that they are all tilted by about the same amount and in the same direction with respect to the unit cell. Thus, some definite crystallographic axis, which deviates slightly from the crystalline

c-axis, is parallel to the draw axis. This type of orientation is known as the tilted orientation, and was first studied in PET by Dunbeny, Bunn and Brown [91]. They reported that crystals in PET fibres, drawn at 75°C and annealed at 210°C are tilted by about 5° in such a precisely defined direction that the crystallographic (230) plane remains vertical while the inclination of the (001) plane to the draw axis increases.

Bonnant [92] explained that the tilt of PET crystals results from an inclined layer structure with the molecular axis having opposite tilts in the alternating crystalline and amorphous layers. He indicated that the above mentioned (230) orientation is realised when the surface of the crystalline layer coincides with a crystallographic plane such as (112) or (111).

There have been various studies on SAXS of uniaxially and biaxially stretched PET films [93,94]. Two structural models have been proposed to represent the superstructure of uniaxially oriented PET. A model by Statton and Goddard [93] which consists of parallel platelets stacked one upon another and within each platelet individual crystallites are arranged in a chessboard array in an amorphous matrix. The second model by Fischer and Fakirov [95] suggests that crystallites are made up of molecules staggered along (100) crystallographic planes. These models were used to explain two-point and four-point SAXD patterns obtained from oriented PET films and fibres. These two- or four-point [93,96,97] patterns are observed depending on the deformation levels, annealing conditions, and relative orientation of incident X-ray beam with respect to major axes of the oriented samples.

2.2.3 Thermal Shrinkage of Oriented PET

The dimensional stability of oriented polymers is an important feature in their application. During drawing chain orientation occurs and, depending on drawing conditions, such orientation may be frozen in, resulting in a thermodynamically unfavourable state for the amorphous chains [98]. If the polymer is subsequently heated above the glass transition temperature, Tg, the frozen-in orientation can be relaxed and the polymer will shrink to a more favourable random conformation. If external constraints are imposed on the sample to prevent shrinkage, a force will develop [99]. Parameters such as time, temperature, draw ratio, degree of orientation and crystallinity are important factors affecting shrinkage.

There have been many investigations on thermal shrinkage and heat setting of oriented PET [100-101]. In addition to molecular disorientation, crystallisation may also occur during shrinkage. The mechanism of contraction is not well established and controversies exist. For example, Statton et al [102] have proposed that crystallisation by chain folding is a major mechanism during shrinkage. Subsequently, however, it has been suggested that the basic mechanism for dimensional changes involves relaxation of orientation in the amorphous phase [103,104,105]. Infra-red spectroscopy has shown that chain folding occurs only during the actual crystallisation process, which may or may not be associated with change in length. However, as noted by Wilson [104], this does not imply that during shrinkage no crystallisation occurs before the completion of the disorientation of the amorphous phase. Heffelfinger [106] has shown that the crystalline trans content does not change during shrinkage at 100^{o}C for a short period of time. In contrast, the amorphous trans content markedly decreases. Consequently, the mechanical and other physical properties are significantly changed.

Several researchers [107-109] investigated the thermal shrinkage of drawn PET using the statistical theory of rubber elasticity. The most complete study was done by Pinnock and Mexhard [108]. They found that the optical and mechanical properties of amorphous PET filaments were similar to those of rubber, but their work was performed on samples which had a maximum effective draw ratio of 2:1. Above this value, strain-induced crystallisation occurred.

Recent studies by Samuels [110] and by Wilson [111] have shown that semi-crystalline PET fibres can be treated as a two-phase system, and that macroscopic shrinkage in PET fibres results from a disorientation of the oriented amorphous regions. The shrinkage arising from the recrystallisation by chain folding near the melting point of the polymer was also significant [112]. Sun and Magill [113], on the other hand, reported that shrinkage in oriented systems (crystalline or amorphous) is exothermic and it is responsible for multiple melting peaks observed in DSC measurements. In highly-oriented crystalline polymers, shrinkage occurs simultaneously with melting. For systems with low to moderate draw ratio, shrinkage often occurs between Tg and Tm, while oriented amorphous samples show shrinkage at or above Tg.

2.4.2 Polyethylene Terephthalate/Polycarbonate Blends

Blending of poly(ethylene terephthalate) (PET) and bisphenol-A polycarbonate (PC) has been studied extensively in recent years [17,114,115,116]. Nassar et al [17] and Murff et al [114] have studied PET/PC blends prepared by melt mixing, using thermal analysis and mechanical testing. Huang and Wang [115] and Harraham et al [116] have also studied PET/PC blends by thermal analysis. Thermal analysis of polymer blends has shown that a miscible polymer blend will exhibit a single glass transition temperature (Tg) between the Tgs of the pure

component [117,118] while for partially miscible systems the two Tgs approach each other, but do not become identical [119-121].

Nassar et al [17] reported that blends of PC and PET that contain more than 70% PET by weight form a single amorphous phase, whereas at lower PET levels two amorphous phases exist. From dynamic mechanical tests and thermal analysis they concluded that, for PET-rich compositions, PC and PET are completely miscible in the amorphous phase and show a single Tg, whose location depends on the blend composition, whereas, for PC-rich blends, two separate amorphous phases are observed. They examined the crystallisation and melting behaviour of PET/PC blends and found that T_c (crystallisation temperature) initially increases as PC is added to PET, which is what is expected for kinetic reasons if the PC were miscible with the PET. However, the peak crystallisation temperature, T_c, reaches a maximum at about 70% PET and then decreases as more PC is added (but presumably will never go below the T_c value for pure PET). This is another indication of the presence of two phases where the two phases are observed. Interestingly, this maximum occurs in the same composition region. Based on these observations they concluded that the presence of PC greatly alters the crystallisation behaviour of the PET but does not completely prevent its development. On the other hand they showed that T_m (melting temperature) decreases from the value observed for pure PET as PC is added up to about 80% PET, after which it remains constant. This decrease is of the order of 5-8^{o}C [122], which is much lower than is expected from crystal direction effects alone and is more consistent with the interpretation that a small degree of interchange reactions has occurred producing random copolymer species. Murff et al [123] reported that the mechanical properties of PET/PC do not show any significant negative departures from additivity, which is typical of many phase separated blends (i.e. exhibiting partial compatibility).

R. Legras et al [124] have studied the nucleation of PET/PC by the use of alkali metal salts of organic acids and found that PET and PC undergo chain scission by reacting with the alkali metal salts, forming polymeric species with ionic end groups. This chemical attack has been confirmed by infra-red spectroscopy and it has been shown in particular that the PET ionic chain ends are aggregated in the molten polymer. It is believed that these aggregated ionic chain ends form the true nucleating species of the crystallisation of PET. For the case of the PC salt system, the chemical attack of the carbonate linkage is complicated by other reactions, leading to crosslinking and loss of crystallisability of the polymer.

2.4.3 Poly(ethylene terephthalate)/Polyarylate Blends

Polyarylates based on bisphenol-A and a mixture of terephthalic and isophthalic acid have become an important class of polymeric materials for over two decades [125,126], in view of the attractive combination of properties, such as high heat distortion temperature (185^{o}C) (resulting from the high Tg, i.e. 187^{o}C), high toughness and retention of mechanical property after long term ultra-violet (UV) exposure [127,128,129]. The random distribution of terephthalate and isophthalate units make this polymer completely amorphous. Blends of polyarylates with other polymers have been mentioned in various patents and several references in the literature. Polyarylates based on bisphenol-A and tere-isophthalate units were noted to be miscible with bisphenol A polycarbonate by Mondragon et al [130]. Also binary blends of poly(ethylene terephthalate) and polyarylate have been claimed in several patents [131-133], while other data in the literature suggest the possibility of miscible behaviour [134,135].

Kimura, Salee and Porter [134] reported that physical blends of poly(ethylene terephthalate) (PET) and polyarylate (PA) show two amorphous phases; an essentially pure PET phase and a mixed phase rich in PA. From DSC measurements the above authors showed that the % crystallinity in the blend, normalised by its weight fraction, is found to go to a maximum at about 25% PA content. Wide angle X-ray diffraction measurements suggest that the sizes of PET crystals decrease systematically with increased PA content. Therefore, the number of PET crystallites would also be the largest near 25% PA. Transesterified blends of PET and PA, however, are non-crystallisable and exhibit a single Tg between the values of the two constituent polyesters and little lower than the linear interpolated value.

On the other hand, Equizabel, Ugar, Cortazar and Irwin [135] reported that blends of polyarylates/PET subjected to first DSC scan between 320°K and 570°K showed only one melting peak corresponding to PET fusion, at a temperature of 530°K, independently of the blend composition. In a second scan under identical conditions,i.e. up to 570°K, they observed that all the mixtures except 80:20 and 90:10 PA/PET exhibited a glass transition identical to that of the pure PET polymer. This glass transition indicated that the amorphous blend is composed of two well distinct phases. They also found that all the blends, again except those of 80/20 and 90/10 compositions, showed a PET crystallisation peak in the second scan. The peak temperature was practically independent of the composition at low polyarylate content but it increased when the amount of PA was higher than 40%. In the PET-rich composition a melting peak in the second scan was observed at a temperature slightly lower than that encountered in the pure PET (530°K).

Robenson [21] concluded, however, that polyarylate/PET blends undergo phase separation before ester exchange reactions but will exhibit a single phase after ester exchange reaction. The addition of polyarylate to PET leads to a decrease in crystallisation rate for PET which is greater for miscible blends than for phase-separated blends. An increase in the Tg of PET (as a result of the dilution by polyarylate chains), and covalent bond formation (due to ester-exchange between the constituents) are all contributory factors leading to decreased crystallisation rates, as has been widely documented in the literature on miscible polymer blends [136,137].

2.4.4 Phenoxy Blends

J. Mondragon et al [138] have studied the properties of melt-mixed blends of polycarbonate with phenoxy, before and after interchange reactions by controlling the processing time. From dynamic mechanical tests, they confirmed that both physical blends and reacted blends are not completely miscible at all compositions. A displacement in Tg values, however, was more clearly discernible in the case of reacted mixtures. For phenoxy-rich compositions, a single phase occurs. The exchange reactions resulted in a mechanical behaviour that showed both a higher modulus and a greater tensile strength for the reacted blends.

With studies on polyarylate/phenoxy blends, on the other hand, Robeson [21] demonstrated the potential for polymeric transesterifications even with phase separated systems and that the uncrosslinked, phase separated blends of phenoxy and polyarylate are eventually transformed into a single phase crosslinked blend at high temperatures. Similar results were reported by Equizabal et al [135] for solution cast films of phenoxy and polyarylate. Similar crosslinking reactions have been noted for poly(ethylene terephthalate) and phenoxy [138].

Cheung, Golovoy, Carter and Van Oene [139] showed that when semi-crystalline polyesters are used as one of the ingredients of a blend, the ester-interchanged products may not crystallise. They concluded that the addition of an organophosphite to a PET/PA/PC ternary blend effectively retards ester-exchange reaction when the extrusion temperature is up to 280°C. (The criterion used for stability was the retention of crystallinity of the polyethylene terephthalate phase).

Above 280°C and up to 300°C, the addition of both organophosphite and carbodimide produces a system which is stable with regard to the melting point and the heat of fusion of PET. Incorporation of a hindered phenol as a third stabiliser allows an extrusion temperature of 325°C.

CHAPTER 3
MATERIALS AND EQUIPMENT

The purpose of this section is to describe the raw materials and equipment used in this investigation.

3.1 MATERIALS

To study the factors affecting the shrinkage of PET bottles when exposed to high temperatures two aspects were studied:

a) stretching behaviour by model experiments, and

b) evaluation of compatible blends.

For the stretching experiments, nucleated and non-nucleated PET sheets, supplied by Enichem, were used. These sheets were made in the company using a chilled-rolls extrusion line. The data supplied with the sheets are shown in Table 3.1.

TABLE 3.1: SHEETS SPECIFICATION

Materials	I.V.	Tg (°C)	Tc (°C)	Tm (°C)	Nucleating Agent
Non-nucleated PET sheets	0.74	75	145.34	251.92	None
Nucleated PET sheets (1)	0.8	75	130.85	250.92	Na Montanate (0.5%)
Nucleated PET sheets (2)	0.8	75	137.38	252.18	Ca-Montanate (0.5%)

I.V. = Intrinsic viscosity
Tg = Glass transition temperature
Tc = Cold crystallisation temperature
Tm = Melting temperature

The first logical choice of blends was the use of compatible polymers exhibiting a higher Tg than the base PET polymer. Therefore, blends with high Tg amorphous polymers were investigated first. The amount of residual crystallinity in the polymer after moulding and after drawing was considered to be the predominant factor underlying high temperature shrinkage. In a second stage the use of nucleating agent and stabilisers as well as blends with semi-crystalline polymers were investigated.

For the preparation of the different blends, the materials used and their characteristics are given in Table 3.2.

TABLE 3.2: MATERIALS SPECIFICATION

Materials	Grade	Company	Tg (^{o}C)	Tm (^{o}C)
Poly(ethylene terephthalate) PET	Bottle	Enichem	75	251
Polycarbonate (PC)	Lexan 161	BASF	145	-
Polyarylate (Par)	Ardel 100	Amoco	185	-
Phenoxy (PH)	PKHH	Union Carbide	85	-
Polyamide-MXD6 (N-MX)	Nyref	Unitika	80	245
Sodium benzoate (NaB)	-	Aldrich	-	>300
Irganox 1010 (Irg)	B561	Ciba Geigy	-	185

a) Poly(ethyleneterephthalate) (PET):

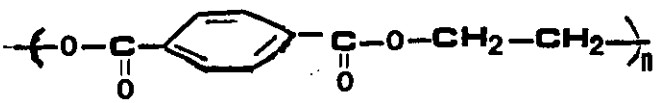

b) Polycarbonate: bis-phenol A polycarbonate

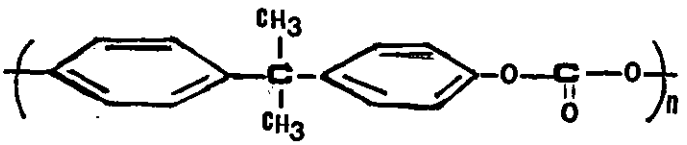

c) Phenoxy: polyhydroxy ether of bisphenol A

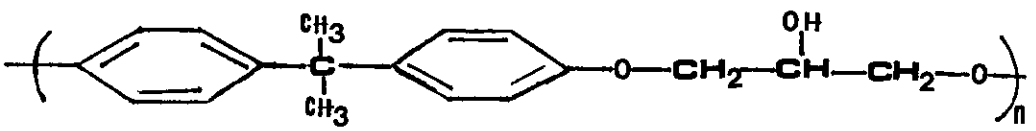

d) Polyarylate: aromatic polyester based on mixed terephthalic and isophthalic acid.

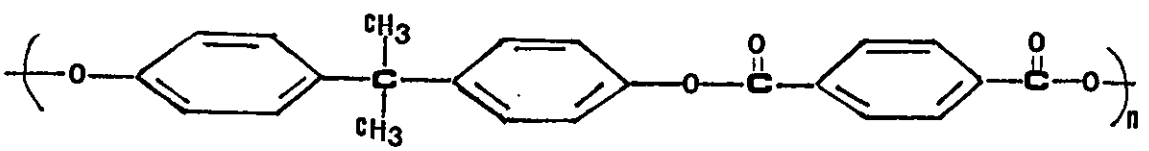

e) MXD6: crystalline polyamide resin, polymetaxylene adipamide:

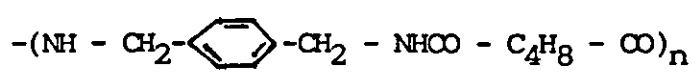

f) Irganox B561: stabiliser - mixture of Irgafox 168/Irganox 1010 - 4:1.

g) Irgafox 168: tris-(2,4-di-tert,butylphenyl)phosphite

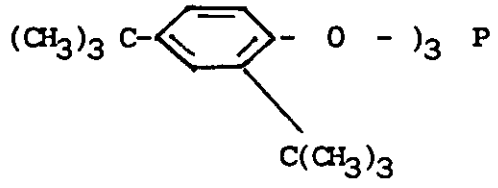

h) Irganox 1010: Pentaerythrityl-tetrakis[3-(3,5-di-ter-butyl-4-hydroxyphenyl)-propionate].

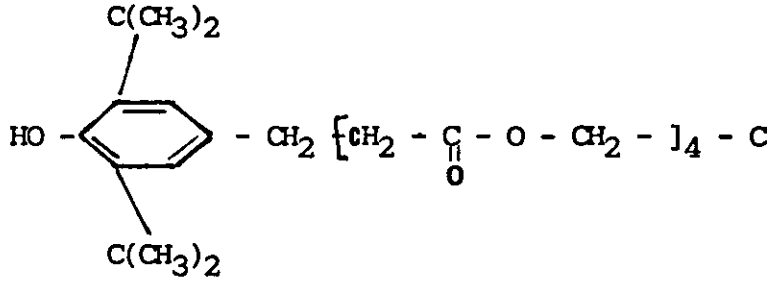

3.2 EQUIPMENT

a) Monoaxial Stretching Experiments

For monoaxial stretching experiments, the equipment used was a J.J. Lloyd Type T5002 tensile tester fitted with a thermostatically controlled conditioning chamber.

b) Biaxial Stretching Experiments

For biaxial stretching experiments the equipment used was an Instron tensile machine equipped with an Amstrad PC 1512DD computer and fitted with a thermostatically controlled conditioning chamber. A purpose built biaxial stretching jig was used, fitted with a device which

converted the vertical movement of the jaws into biaxial drawing of small sheet (see Figure 3.1).

c) **Blending and Specimen Preparation**

All the blends were prepared in a laboratory model twin screw compounding extruder APV (MP2000) equipped with a water bath, grinder and a dehumidifier.

The technical specification of the twin screw extruder is given in Table 3.3:

TABLE 3.3: TECHNICAL SPECIFICATIONS OF THE APV (MP2000)

Length: diameter ratio	15/1
Drive power, Kw	7.5
Maximum screw speed (rpm)	500
Barrel diameter (mm)	28
Number of temperature control zones	6
Mixing segments geometry	

All the mouldings were prepared on a Bipel 1301 injection moulding machine operated with a chiller to cool the mould to 5^{o}C.

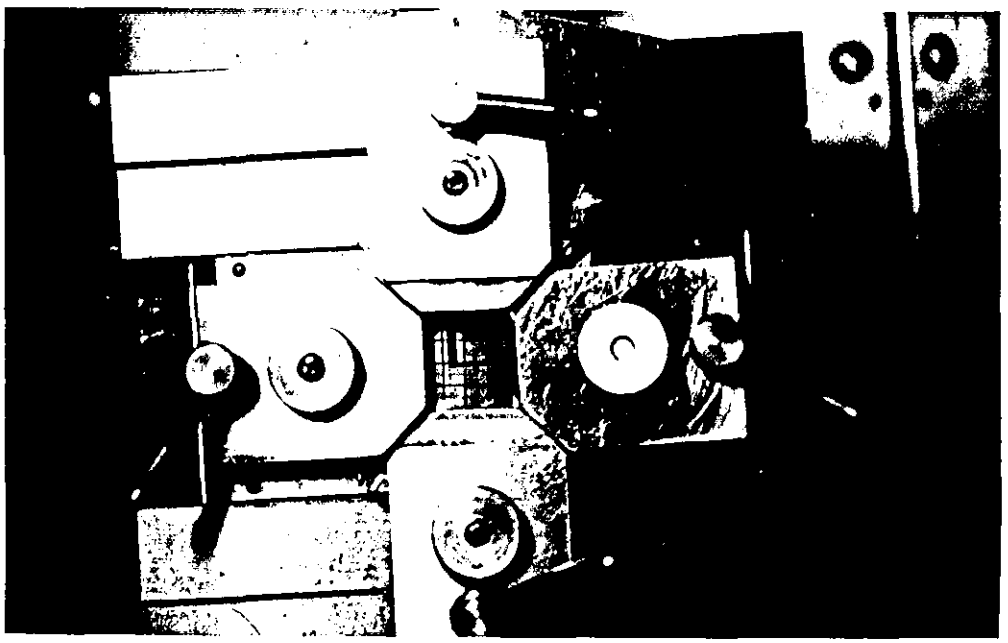

Before biaxially drawing

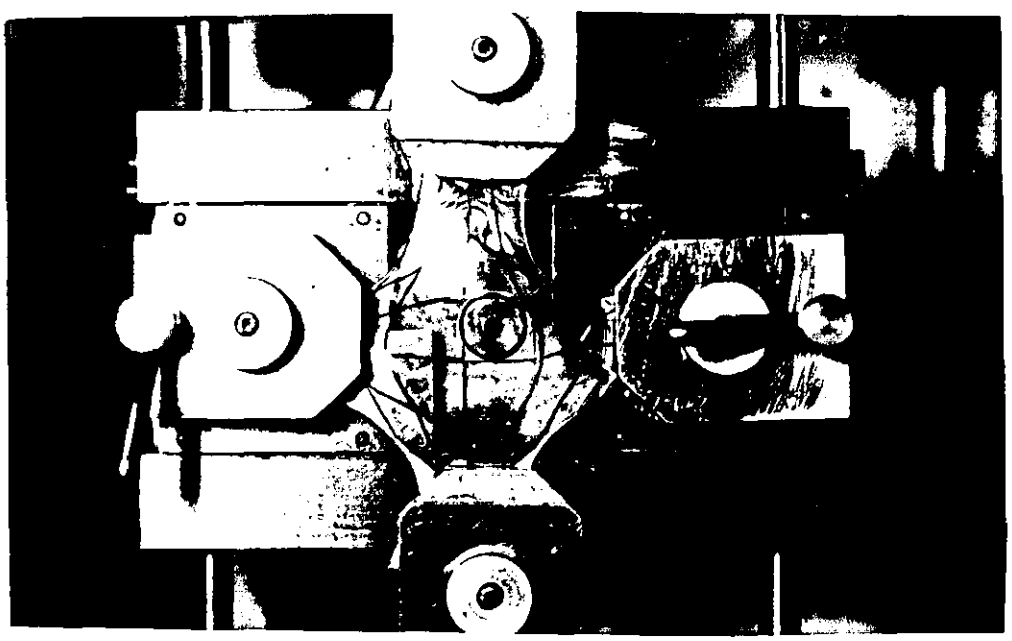

After biaxially drawing

FIGURE 3.1: BIAXIAL STRETCHING JIG

(a) Biaxial Drawing Without In-Plane Distortion

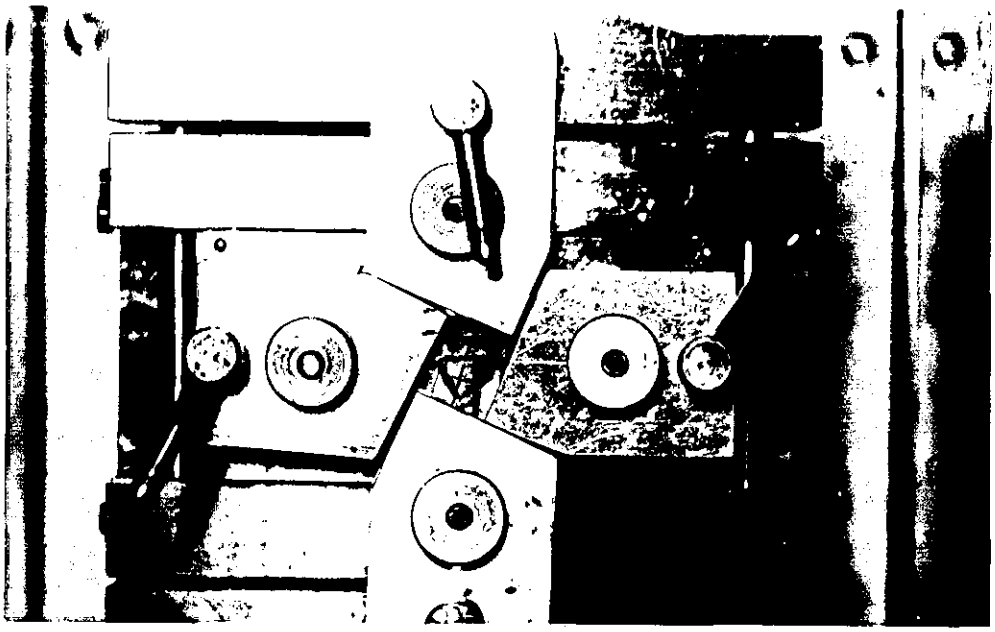

Before biaxially drawing

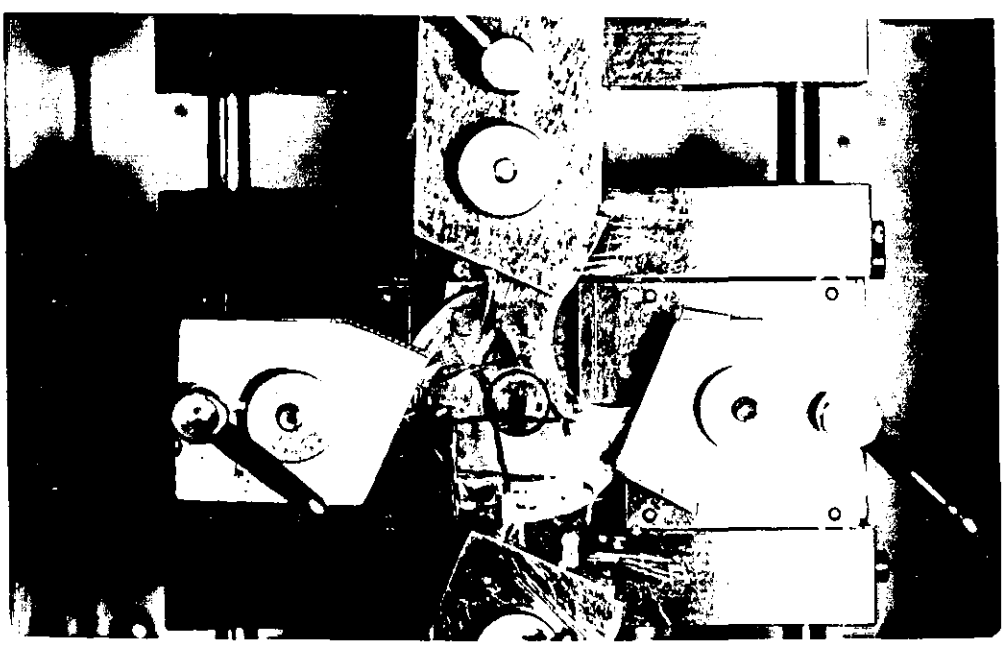

After biaxially drawing

(b) Biaxial Drawing with In-Plane Distortion

The equipment used for evaluation purposes were:

a) Differential scanning calorimeter (DSC):

A Du Pont Instruments Model 2000 was used. It consists of a constantan disc from which heat is transferred to the sample and reference position. The sample which may vary in weight from 0.1 mg to 25 mg is placed in small aluminium pan (with lid); a similar pan and lid is normally used as a control. The sample holders can be cooled or heated at various fixed rates (from 0.5°C/min to 50°C/min) in an atmosphere of nitrogen. In the course of an experiment even a slight change in heat content of the sample produces a high voltage output. This means that when some thermal transition takes place in the sample, the differential heat is monitored. This difference in heat flow per unit of time is recorded as a function of the temperature or time. Moreover this equipment is attached to a computer that calculates Tg values, T_c values, T_m values as well as the heat of crystallisation (ΔH_c) and/or heat of fusion (ΔH_f) of the sample.

b) Density column:

The density column used in this study was a Davenport apparatus, Serial No DMA 718M75. This equipment employs the density gradient column principle for determining densities, as described in many papers (40,63,64) and as specified in the standard method of BS 2782-508, BS 3715 and ASTM D.1550. The general arrangement is that six density gradient column tubes are contained in a thermostatically controlled water jacket, which is supported on

the base ledge of the apparatus cabinet. The column tubes themselves are not graduated and the positions of the marker floats and the specimens are read by means of a specially designed cathetometer mounted on the cabinet. The top of the cabinet is used to support the filling column and sweeping equipment.

c) Dynamic Mechanical Analyser (DMA)

The equipment used for DMA tests was a Du Pont Instruments, Model 2000. The sample is clamped between the ends of two parallel arms, which are mounted on low-force flexural pivots allowing reciprocating motions in the horizontal plane. The distance between the arms is adjustable by means of a precision mechanical slide to accommodate the sample length. An electromagnetic motor attached to one arm drives the arm/sample to a selected amplitude, normally 0.5 mm. As the arm/sample is displaced, the sample undergoes a flexural deformation.

A linear variable differential transformer (LVDT) mounted on the motorised arm, measures the sample's response (i.e. deflection and frequency) to the applied force, and provides a feedback control to the motor. The sample was positioned in a temperature-controlled chamber containing a radiant heater which provides convective heating of the sample.

d) Spectrophotometer:

A Beckman Acta MVII spectrophotometer was used to measure the birefringence of drawn samples. The experimental arrangement is shown schematically in Figure 3.2. [24].

A single sample is placed in a polarised light field in the sample chamber of the spectrophotometer. The monochromatic light transmitted from the analyser is measured by a detector and compared with a reference beam, and the difference is recorded on a chart. As the wavelength of the polarised incident light is changed, the intensity-wavelength chart permits calculation of birefringence.

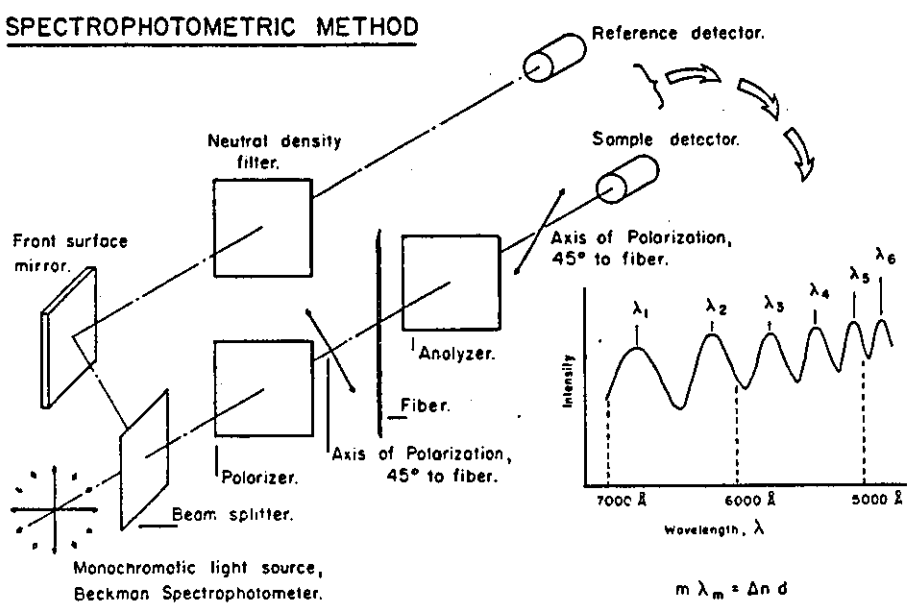

FIGURE 3.2: Experimental arrangement of a spectrophotometric method

CHAPTER 4
EXPERIMENTAL

The purpose of this section is to:

i) examine the draw ratio and shrinkage in various parts of the PET bottles which are produced by Inca International, so that these could be compared with those obtained from PET samples drawn on the laboratory jig.

ii) describe the experimental procedures used in this investigation.

4.1 EXAMINATION OF THE DRAW RATIOS AND SHRINKAGE OF PET BOTTLES PRODUCED BY INCA INTERNATIONAL (a subsidiary of Enichem)

10 mm square grids were drawn on the preform shown below (Figure 4.1) and then sent back to the company to be blown into bottles on the Inca production line (see Figure 4.1).

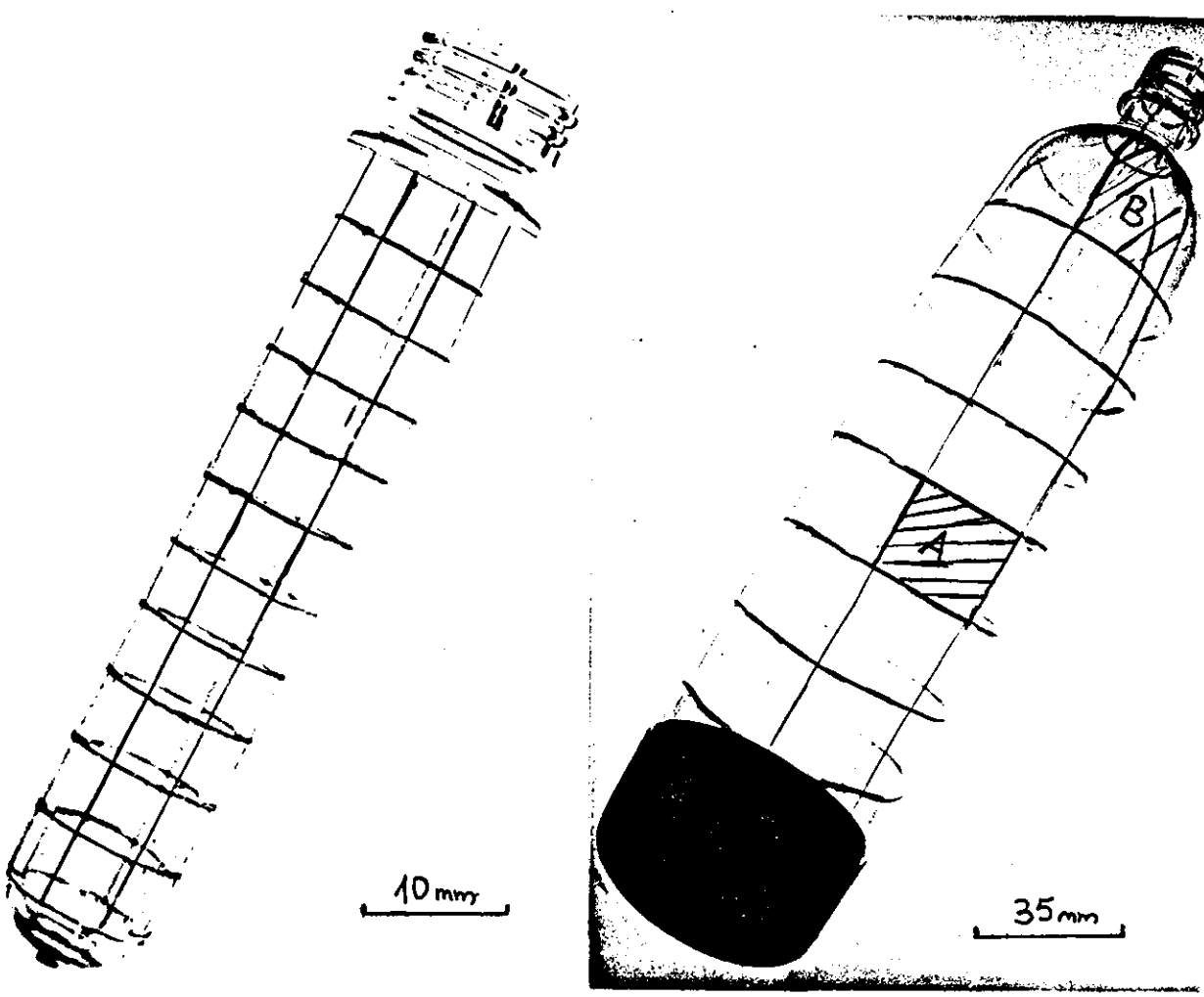

. The draw ratios in the longitudinal and hoop directions were calculated as follows:

$$\lambda_L = \frac{L_F}{L_i}$$

where λ_L = draw ratio in the longitudinal direction

L_F = final length

L_i = initial length

$$\lambda_h = \frac{W_F}{W_i}$$

where λ_h = draw ratio in the hoop direction

W_F = final width

W_i = initial width.

Shrinkage measurements in boiling water and in water at 85°C were also carried out on:

a) Non-annealed samples taken from the middle (Region A) and the top (Region B) of the bottles (see Figure 4.1).

b) Samples annealed at 100°C and 180°C for 30 secs (see later for details of annealing operation).

To complete the examination of the bottles, DSC measurements were carried out on samples taken from the preform, the top (region B) and the middle (region A) of the bottles. The glass transition

temperature (Tg), the cold crystallisation temperature (Tc), the heat of crystallisation (ΔHc), the melting temperature (Tm) and the heat of fusion (ΔHf) were measured from the DSC traces. The conditions used were 20°C/min heating ramp, and 10 mg sample weight **(See Table 5.12 for DSC results)**.

4.2 STRETCHING EXPERIMENTS ON PET SHEETS

To study the parameters that affect the high temperature dimensional stability of PET bottles, it was necessary to simulate the expansion process using both uniaxial and biaxial stretching experiments on PET sheets. Since uniaxial stretching experiments are a lot easier to perform than biaxial stretching experiments, preliminary work on uniaxial stretching experiments were carried out in order to find out (if existent) the relationship between the two experiments.

4.2.1 Uniaxial Stretching

Dumb-bell shaped specimens were cut from the roll of PET sheets (BS2782 Part 3 Method 302A). The gauge length of these specimens was 30 mm while the width was 4 mm. The thickness of the samples used was 0.8 mm for the thick sheets and 0.4 mm for the thin sheets.

Uniaxial stretching experiments were carried out at a grip separation of 200 mm/min on the J.J. Lloyd machine and at preset temperatures of 60°C, 80°C, 90°C, 100°C, 125°C and 150°C on non-nucleated PET thick (0.8 mm thickness) and thin (0.4 mm) sheets.

Note that prior to stretching a small piece from PET sheet from the roll was observed between cross polars and found to be free of any extrusion orientation.

At 150°C the nucleated samples showed considerable crystallisation, making the samples unstretchable and, therefore, only four drawing temperatures, i.e. 80°C, 90°C, 100°C and 125°C were used in this case.

The specimens were preheated for 3 mins in the heating chamber of the machine, stretched at three different draw ratios i.e. 2:1, 3:1 and 4:1 and then quenched with a wet cloth before being removed from the clamps. To study the effect of stretching rate on high temperature shrinkage, a crosshead speed of 500 mm/min was also studied using samples from non-nucleated PET sheets of 0.8 mm thickness at three different temperatures of 80°C, 90° and 100°C, at various draw ratios up to 6:1.

4.2.2 Biaxial Stretching

Specimens for biaxial stretching experiments were cut into 6 cm squares from the original sheets and the edges shaped at low temperature i.e. at 75°C for 2 mins in an hydraulic press so that they could be effectively gripped in the jaws of the stretching jig.

a) **Biaxial stretching without in plane distortion**

For balanced biaxial drawing experiments the following specimens were used:

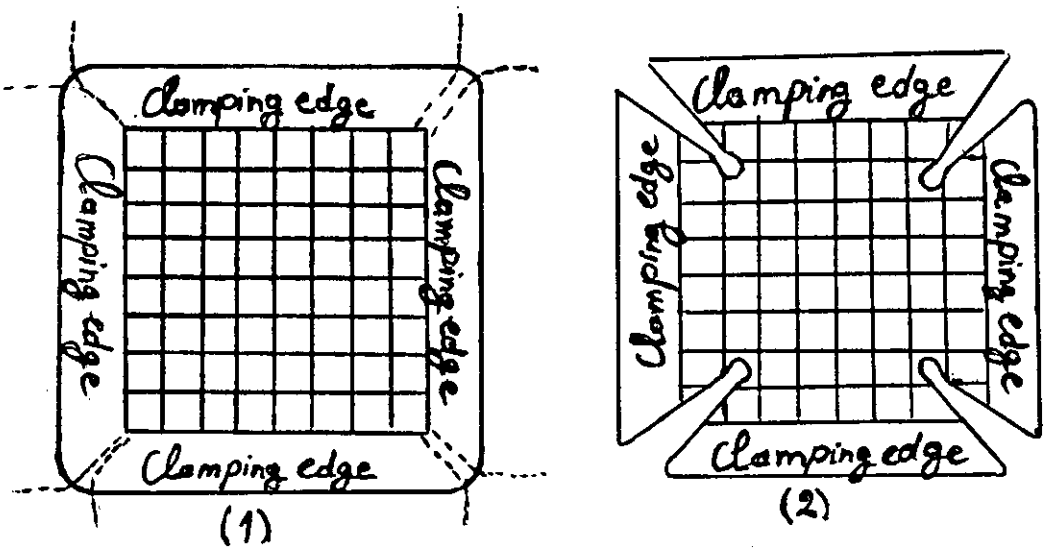

1. Specimens for draw ratio of 2:1.
2. Specimens for draw ratio of 3.5:1.

Biaxial stretching experiments were carried out on the Instron machine at temperatures of 80°C, 90°C, 100°C and 110°C using both nucleated and non-nucleated PET thick sheets (800μm).

Two biaxial draw ratios, 2:1 and 3:1 (equal draw ratios in longitudinal and transverse directions) were used, approximately representing the range of draw ratios in the bottles, i.e. 2:1 at the top and 3.5:1 in the middle.

Each sample was preheated for 3 mins before being stretched at a crosshead speed of 200 mm/min and then cooled with a wet cloth before being removed from the jaws.

Following the same procedure, biaxial stretching experiments were also carried out on all the blends shown in Table 3.4, with an overall draw ratio of 3.5:1 in each direction, and at temperatures of 80°C, 90°C, 100°C, and 125°C for injection moulded plaques.

b) Biaxial stretching with in plane distortion

Following the discovery of lower shrinkage at the edges of the biaxially drawn samples (shear regions), biaxial stretching experiments with varying amounts of in plane distortions were also investigated.

To obtain in plane distortions using the biaxial stretching apparatus in Figure 3.1(b), the following specimen geometries were investigated by stretching the samples along the axes indicated.

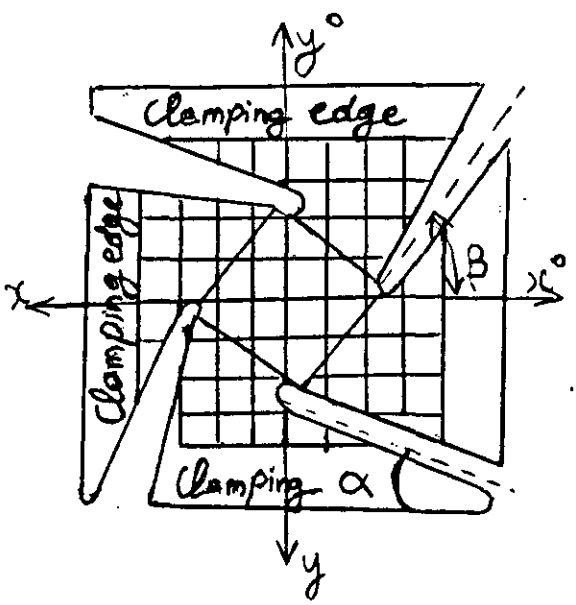

System G1

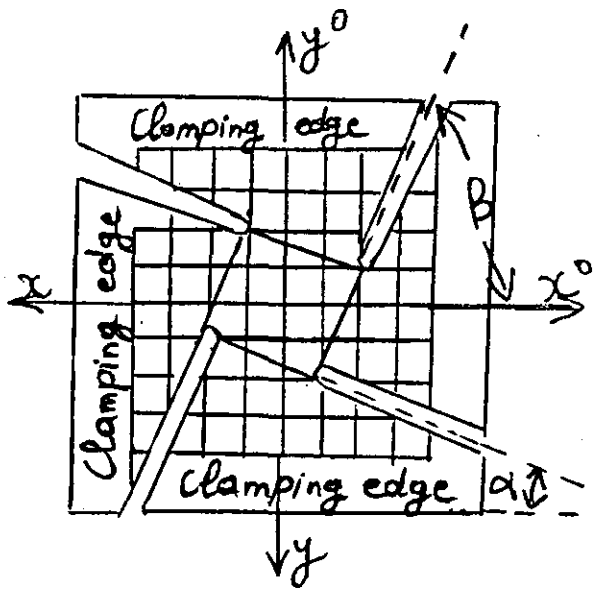

System G2

System G1: High rotations/
small distortions
$\alpha < 45^{\circ}$
$\beta = 45^{\circ}$

System G2: Low rotations/
large distortions
$\alpha < 45^{\circ}$
$\beta > 45^{\circ}$

Experiments by biaxial stretching with in plane distortions were carried out on the Instron machine at three different temperatures of 80°C, 90°C and 100°C, using an axial draw ratio of 2:1 in both directions. Each sample was preheated for 3 mins and then stretched at 200 mm/min.

4.2.3 Theoretical Considerations for Biaxial Drawing with In-plane Distortion (this will be referred to as in plane shear deformations through the remainder of the text).

1. Definition of draw ratios and shear angles in biaxial stretching with in-plane shear, referred to as complex in-plane shear. Applicable to flat (sheet or film) and cylindrical (tubular) products [149].

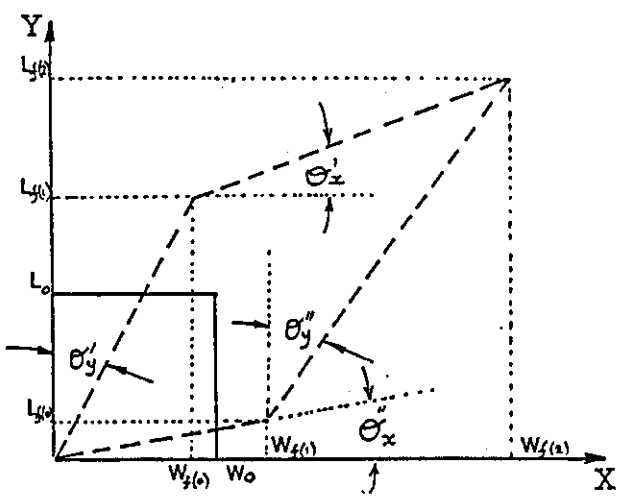

a) Axial draw ratio in the y direction: $\lambda_y^T = \frac{\bar{L}_f}{L_o}$

where $\bar{L}_f = \frac{L_{f(1)} + L_{f(2)} - L_{f(0)}}{2}$

b) Axial draw ratio in the x direction: $\lambda_x^T = \frac{\bar{W}_f}{W_o}$

where $\bar{W}_f = \frac{W_{f(1)} + W_{f(2)} - W_{f(0)}}{2}$

c) Area expansion ratio: $\lambda_A = \frac{\text{Final Area}}{\text{Original Area}} = \lambda_x^T . \lambda_y^T$

d) Average axial draw ratio: $\lambda_{av}^T = \frac{\lambda_x^T + \lambda_y^T}{2} = \sqrt{\lambda_A}$

e) Shear draw ratio relative to the y direction:

$$\lambda_y^S = \sec \bar{\theta}y = \sqrt{1 + \tan^2 \bar{\theta}y}$$

where $\bar{\theta}y = \frac{\theta'y + \theta''y}{2}$ (average angle of shear for the y direction)

f) Shear draw ratio relative to the x direction:

$$\lambda_x^S = \sec \bar{\theta}x = \sqrt{1 + \tan^2 \bar{\theta}x}$$

where $\bar{\theta}x = \frac{\theta'x + \theta''x}{2}$ (average angle of shear for the y direction)

g) Total angle of shear $\bar{\theta} = \bar{\theta}x + \bar{\theta}y$

h) Total shear draw ratio $\lambda^S = \lambda_y^S + \lambda_x^S$

2. Definition of draw ratios and shear angles in biaxial stretching with in-plane shear, referred to as simple in-plane shear.

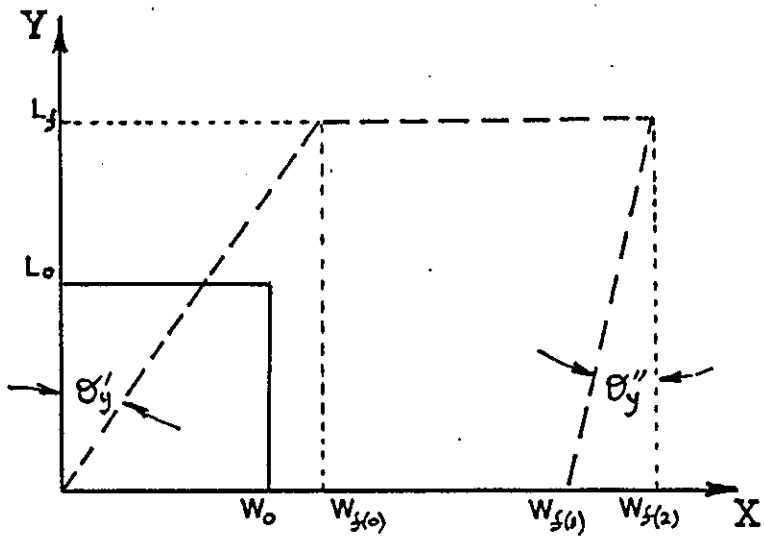

a) Axial draw ratio in the y direction: $\lambda_y^T = \frac{\bar{L}_f}{L_o}$

b) Axial draw ratio in the x direction: $\lambda_x^T = \frac{\bar{W}_f}{W_o}$

where $\bar{W}_f = \frac{W_{f(1)} + W_{f(2)} - W_{f(0)}}{2}$

c) Area expansion ratio: $\lambda_A = \frac{\text{Final Area}}{\text{Original Area}} = \lambda_x^T . \lambda_Y^T$

d) Average axial draw ratio: $\lambda_{av}^T = \frac{\lambda_x^T + \lambda_Y^T}{2} = \sqrt{\lambda_A}$

e) Shear draw ratio relative to the y direction:

$$\lambda_y^S = \sec \bar{\theta}_y = \sqrt{1 + \tan^2 \bar{\theta}_y}$$

where $\bar{\theta}_y = \frac{\theta'_y + \theta''_y}{2}$ (average angle of shear for the y direction)

f) Shear draw ratio relative to the x direction: $\lambda_x^S = 0$

g) Total angle of shear $\bar{\theta} = \bar{\theta}_y$

h) Total shear draw ratio $\lambda^S = \lambda_y^S$

3. Calculation of the draw ratio in the middle and the total extension ratio in the edge (shear region)

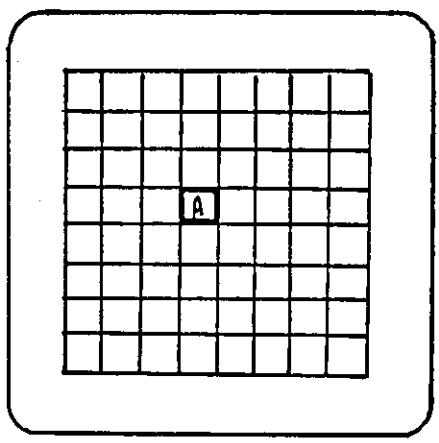

$$\bar{\lambda}^{T}_{\text{(central region)}} = \sqrt{\frac{A'}{A}} \; ; \qquad \bar{\lambda}^{T}_{\text{(corner region)}} = \sqrt{\frac{A''}{A}}$$

$$\lambda_x^S = \sec\left(\frac{\theta'x + \theta''x}{2}\right)$$

$$\lambda_y^S = \sec\left(\frac{\theta'y + \theta''y}{2}\right)$$

$$\bar{\lambda}^{S} = \frac{\lambda_x^S + \lambda_y^S}{2}$$

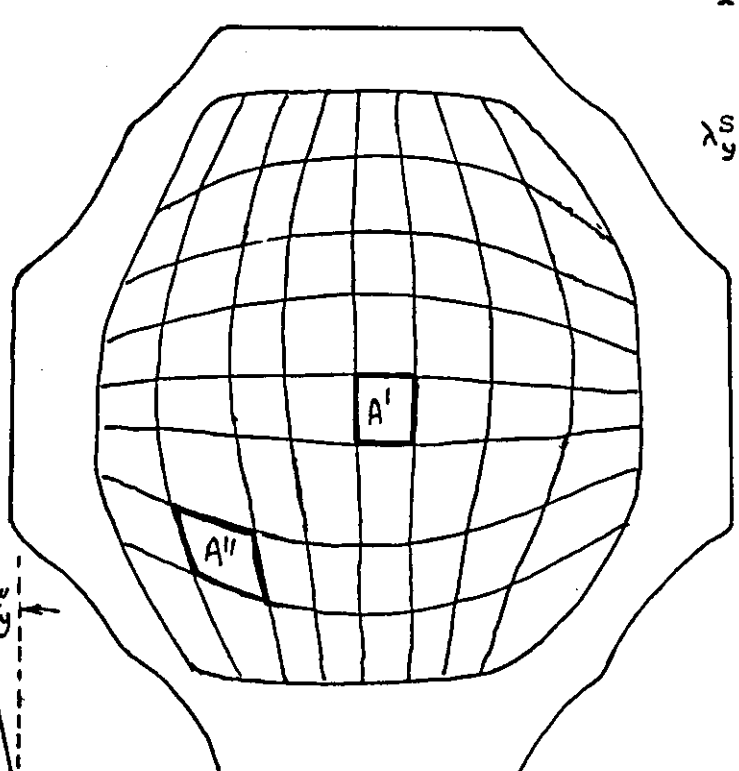

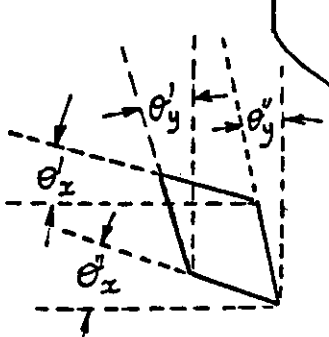

4. Calculation of the draw ratio in the middle and the total shear extension ratio at the edge (shear region)

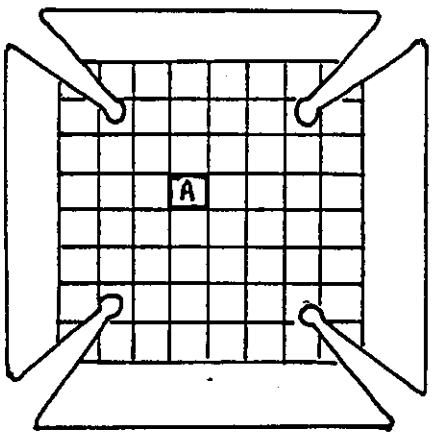

$$\bar{\lambda}^{T}_{\text{(central section)}} = \sqrt{\frac{A'}{A}} \; ; \quad \bar{\lambda}^{T}_{\text{(corner section)}} = \sqrt{\frac{A''}{A}}$$

$$\lambda_x^S = \sec \bar{\theta}x; \text{ where } \bar{\theta}x = \frac{\theta'x + \theta''x}{2} \; ; \quad \lambda_y^S = \sec \bar{\theta}y; \text{ where } \bar{\theta}y = \frac{\theta'y + \theta''y}{2}$$

$$\lambda^S = \frac{\lambda_x^S + \lambda_y^S}{2}$$

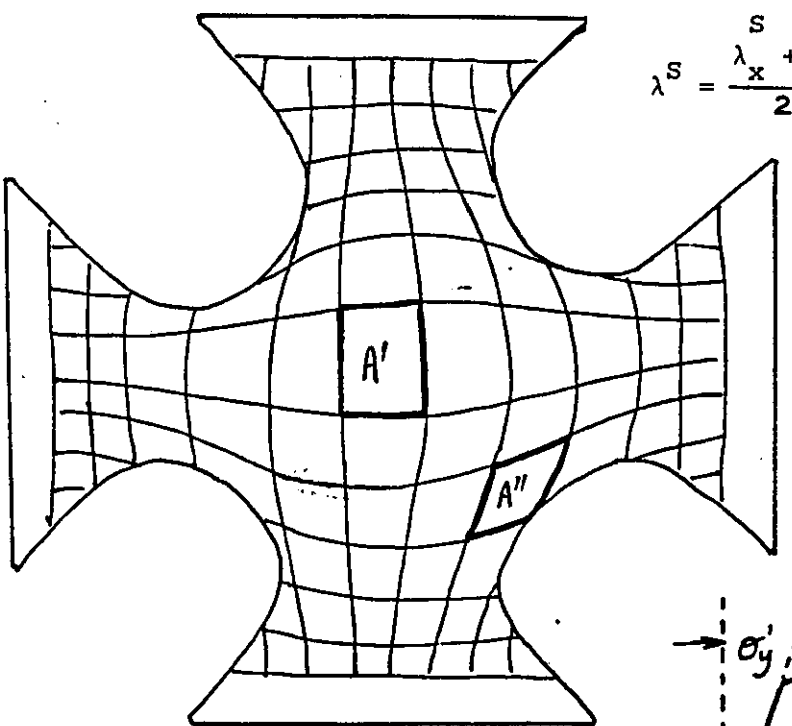

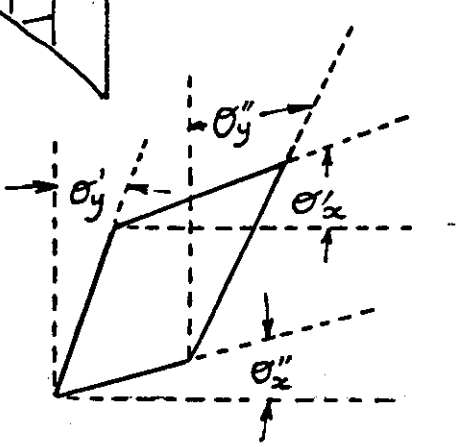

5. Calculation of the shear extension ratio for geometry of G1 jig (high rotations/small distortions)

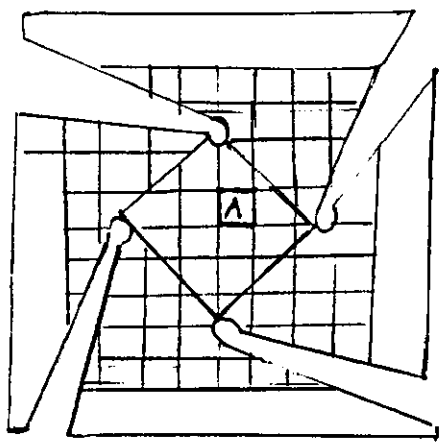

$\bar{\lambda}^T = \sqrt{\frac{A'}{A}}$; $\bar{\lambda}^S = \sec \bar{\sigma}$; where $\bar{\theta} = \frac{\bar{\theta}x + \bar{\theta}y}{2}$

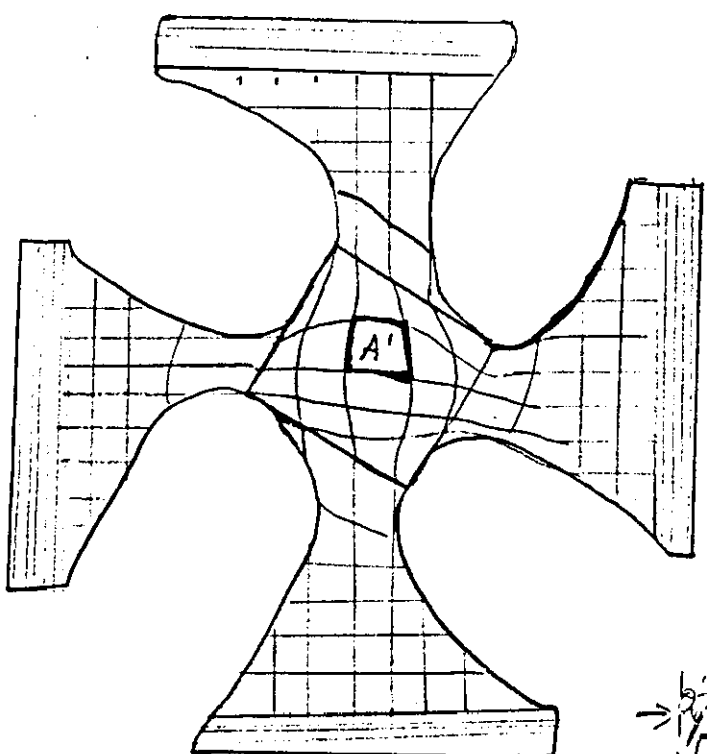

$\bar{\theta}x = \frac{\theta'x + \theta''x}{2}$

$\bar{\theta}y = \frac{\theta'y + \theta''y}{2}$

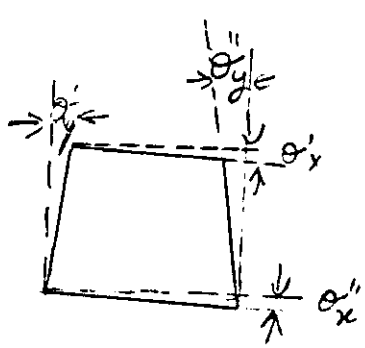

6. Calculation of the shear extension ratio for geometry of G2 jig (low rotations/large distortions)

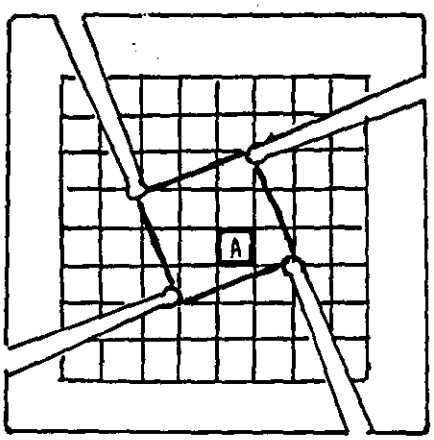

$\bar{\lambda}^T = \sqrt{\frac{A'}{A}}$; $\bar{\lambda}^S = \sec \bar{\theta}$; where $\bar{\theta} = \frac{\bar{\theta}x + \bar{\theta}y}{2}$

$$\bar{\theta}x = \frac{\theta'x + \theta''x}{2}$$

$$\bar{\theta}y = \frac{\theta'y + \theta''y}{2}$$

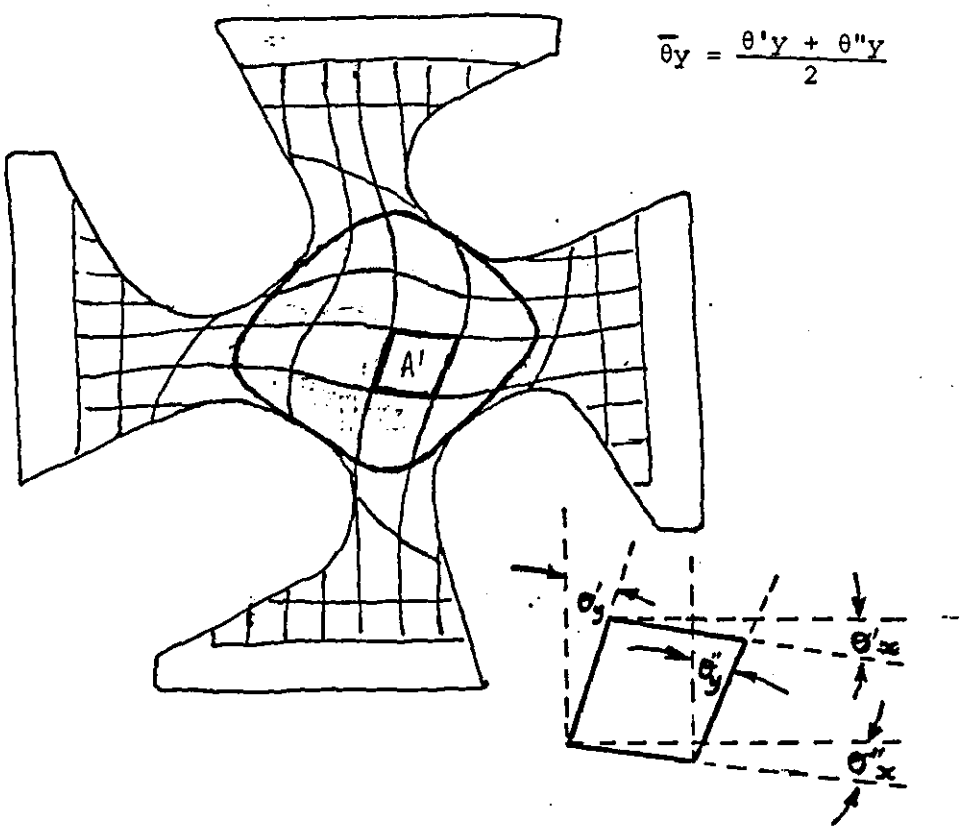

4.2.4 Considerations of Biaxial Drawing Stresses

Balanced Biaxial Extension

Biaxial extension with in-plane distortions(G_2 jig)

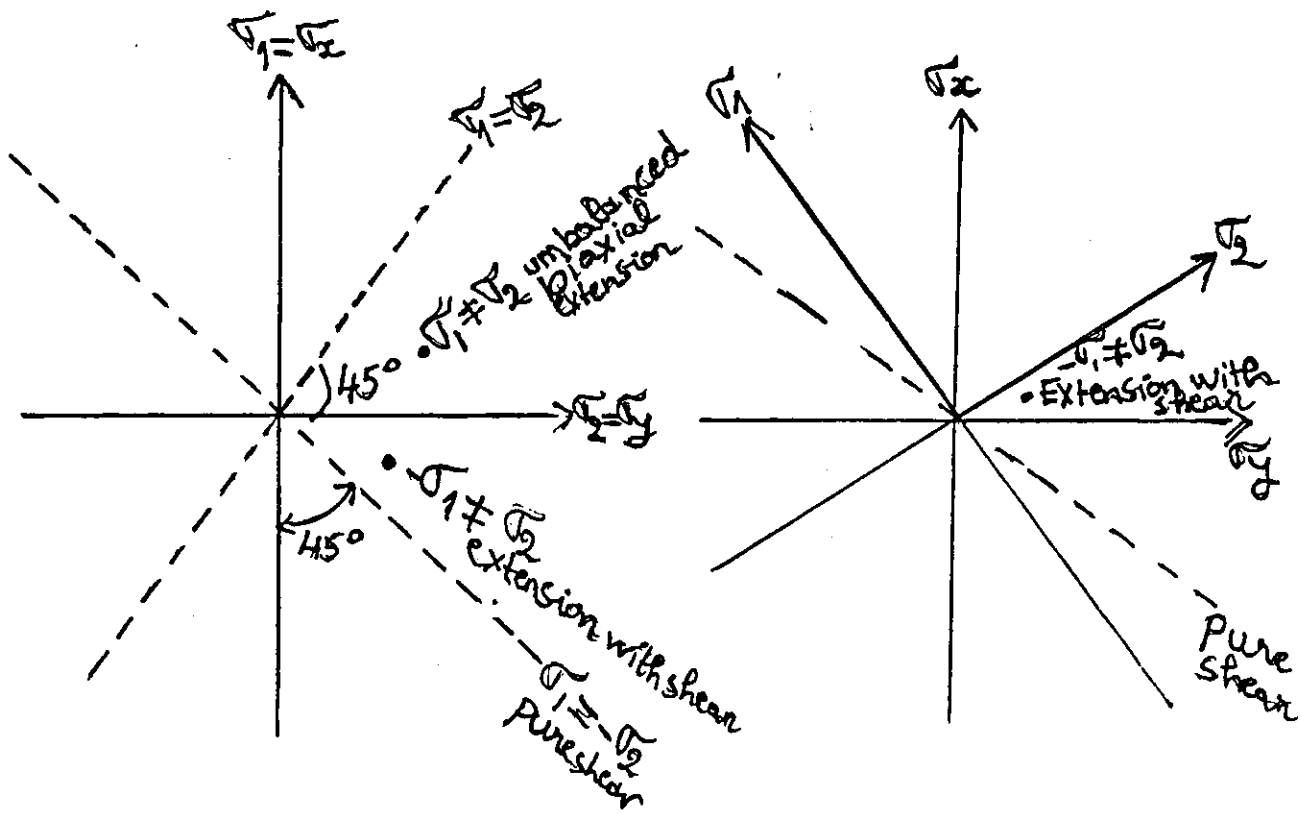

x and y are drawing direction, 1 and 2 are directions of principal stresses[149].

For balanced biaxial extension the direction of the principal stresses in the plane of the sheet coincide with the direction of drawing operation. When samples of the sheet are drawn in the G2 jig, the axes of the principal stresses rotate and no longer coincide with the drawing direction and, therefore, a square section in the original sheet becomes distorted. Since distortions are normally associated with shear, for identification purposes, this type of drawing process has been referred to as biaxial stretching with in-plane shear.

In the case of large deformations Hooke's law no longer applies and strains have to be redefined in terms of extension ratios. While the relationships between stresses and strains are well understood for the case of highly elastic deformations (linear types), this is not so for the case in question. The deformations are, in fact, nearer to plastic deformations which, depending on temperature, may have strain softening or strain hardening features

The relationships between stresses and extension ratios for these types of deformations are not clearly understood. Hence it is difficult to describe accurately the deformations in terms of principal strains and shear strains. The fact that these types of deformations result in drawn samples exhibiting very low shrinkage, which has been associated with the development of a higher level of crystallinity (see later), it is more important to consider the molecular dynamics of the process than the stresses/strains relationships which are based on the assumption that the material is a continuum.

The mechanism which is responsible for the increased level of crystallinity in the samples as a result of distortions on a macroscale cannot be deduced from the tests carried out and is considered to be outside the scope of this study.

4.3 PREPARATION OF BLENDS

Blending PET with the glassy and semi-crystalline polymers listed in Table 3.2, was the second approach used as a possible means of decreasing the shrinkage of drawn PET based products.

4.3.1 Drying Method

All the materials used in the specified blends, are hygroscopic, hence any water absorbed has to be removed before melt processing in order to prevent hydrolytic degradation.

Drying the materials is relatively simple but virgin polymers or reground blends must be dried to less than 0.02% moisture and kept below this level for processing. In this study the drying conditions for each polymer were as follows:

PET, PA, PC and MXD6 were dried in an oven at 120°C for 8 hrs and then stored in the oven at 95°C until ready for processing. After tumbling the granules together, each blend was left for 1 hr at 120°C in the dehumidifier of the twin screw extruder.

The phenoxy polymer was dried under vacuum at 60°C for 12 hrs, i.e. below the Tg of the polymer to prevent the granules sticking together.

4.3.2 Melt Blending Operating Procedure

All the blends were prepared by melt mixing in the twin screw extruder using the following conditions. Dried pellets of PET and the other materials were tumble blended to the desired composition before being

mixed in the extruder and each blend was extruded as laces in a water bath and pelletised. The temperature profile was: feed zone 245°C, mixing zone 270°C, metering zone 285°C and die temperature 290°C. The speed was 250 rpm.

The screw configuration used was as follows:

Die	Camel Back Discharge	2.5D Feed Screws	Thin Orifice Plugs	4 x 90° Mixing Paddles	6 x 60° Mixing Paddles	6D Feed Screw	Feed

The formulations prepared are shown in Table 4.1.

TABLE 4.1: Detailed formulations of PET blends

Materials / Formulations	PET	PC	Par	PH	MXD6	NaB_z	Irganox B561
F1	100	-	-	-	-	-	-
F2	95	4	-	1	-	-	-
F3	95	-	4	1	-	-	-
F4	95	-	-	4.9	-	0.1	-
F5	80	16	-	4	-	-	-
F6	80	20	-	-	-	-	-
F7	80	-	20	-	-	-	-
F8	80	-	16	4	-	-	-
F9	80	10	10	-	-	-	-
F10	80	8	8	4	-	-	-
F11	80	-	18	2	-	-	-
F12	80	-	18	2	-	0.2	1
F13	70	-	30	-	-	-	-
F14	70	30	-	-	-	-	-
F15	70	-	30	-	-	0.2	1
F16	70	-	28	2	-	-	-
F17	90	-	28	2	-	0.2	1
F18	80	-	-	2	18	-	-
F19	80	-	-	-	20	-	-
F20	70	-	-	-	30	-	-
F21		-	-	-	100	-	-

The hypotheses behind the choice of these formulations are as follows:

a) The Tg of PET is increased by using high Tg amorphous materials such as PC and Par which are compatible with PET.

b) Phenoxy can react with both PET, PC and PA, however it could increase the compatibility of PET/PC and PET/Par blends, or

c) In order to maintain the crystalline nature of PET in PET/Par blends, it was necessary to inhibit the ester-exchange reaction. For that purpose 1% of stabiliser (organophosphate) B561 and 0.2% NaB were incorporated into the blends).

The crystalline (MXD6) polymer has been chosen to maintain a high level of crystallinity in the product. (See Chapter 5, Section 5.3, for the details of why compositions were selected).

4.4 PREPARATION OF SPECIMENS FROM BLENDS

4.4.1 Injection Moulding of Plaques

Dried pellets of the different blends were injection moulded into nominally 1 mm thick, 75 mm wide and 125 mm long plaques (see Figure 4.3) using the Bipel injection moulder at a barrel temperature of 285°C. To prevent PET in the blend crystallising during moulding a chiller was used to keep the mould at very low temperature (i.e. 5°C), using a cycle time of 60s.

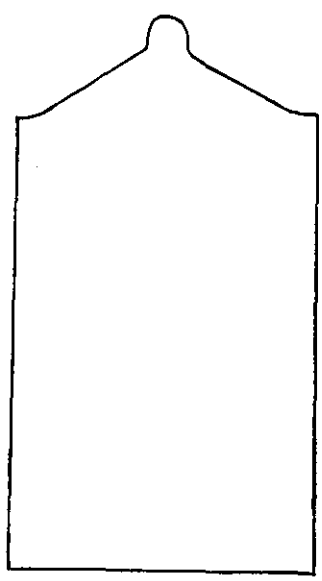

FIGURE 4.3: Injection Moulded Plaque

4.4.2 Preparation of Specimens for Biaxial Stretching Experiments

Before the preparation of specimens for biaxial stretching experiments, the injection moulded plaques were examined optically using polarised light in order to determine whether any substantial amount of orientation is present in the moulded samples. These observations have proved that there is some orientation in the flow direction but based on shrinkage measurements done on the samples, these were proved to have zero shrinkage.

From the injection moulded plaque samples for biaxial stretching were prepared by pressing 6 cm square sections at 75°C for 2 min in the hydraulic press to produce the required shape in the gripping areas and prevent slippage. Due to a problem of stress concentration at the edge of the sample, the corners were then cut off as shown in Figure 4.4. Grids 5 mm square were then scribed on the specimens with a permanent ink pen.

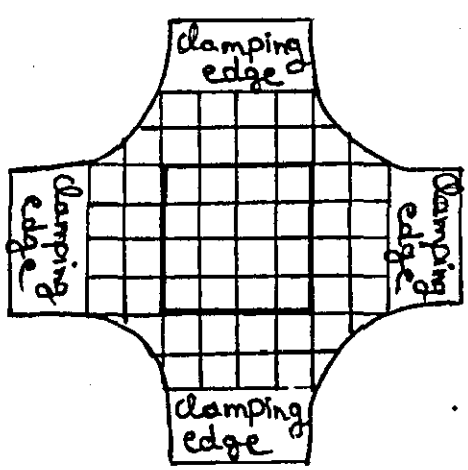

FIGURE 4.4

4.5 EVALUATION OF DRAWN SPECIMENS

4.5.1 Shrinkage Tests

Knowing that for hot filling applications and sterilisation purposes PET bottles will be exposed to high temperatures, particularly in the range of 85°C-100°C, shrinkage tests were carried out at these two particular temperatures for 2 mins. This was considered to be the longest time the bottles would be exposed in the applications mentioned above.

From the uniaxially stretched samples, 40 mm length strips were cut off and then immersed in water at 85°C and 100°C respectively for a period of 2 mins. High shrinkage temperatures (i.e. 120°C and 150°C) were also used in order to understand the relationship between drawing temperature and shrinkage temperature and how these affect the percentage shrinkage for monoaxially drawn specimens. In the latter case, samples were immersed in an oil bath of 120°C and 150°C for 2 mins.

The percentage shrinkage for monoaxially drawn specimens was calculated as follows:

$$\% \text{ Shrinkage} = \frac{L_i - L_f}{L_i} \times 100$$

where L_i = length before shrinkage

L_f = length after shrinkage.

For the biaxially stretched samples shrinkage tests were carried out also in boiling water and in water at 85°C for 2 mins. The samples were taken from the middle (2 cm x 2 cm square) and the shear region (see Section 4.2.3 (3 and 4)) of the of the biaxial stretched specimens and the percentage shrinkage was calculated as follows.

$$\% \text{ Area Shrinkage} = \frac{A_I - A_f}{A_I} \times 100$$

$$= (1 - \frac{A_f}{A_I}) \times 100$$

where A_I = area before shrinkage

A_f = area after shrinkage.

Therefore % linear shrinkage $(1 - \sqrt{\lambda_A}) \times 100$.

where $\lambda_A = \frac{Af}{A_i}$

4.5.2 DSC Analysis

DSC measurements were carried out on the Du Pont 2000 Thermal Analysis Instruments machine taking (a) unaxially stretched samples showing respectively maximum and minimum shrinkage, (b) biaxially drawn samples, (c) samples from the shear regions of the biaxially drawn samples, and (d) those obtained from combined extension and shear experiments. The temperature range used was 40°C-280°C with a nitrogen atmosphere and an empty capsule as reference. Sample weights were varied from 6 to 15 mg and the heating rate was kept constant at 20°C/min.

In most cases, however, in order to determine the effect of heating rate ΔH (crystallisation) and on the crystallisation temperature (T_c), some experiments were also carried out at heating rates of 5°C/min, 10°C/min and 15°C/min using the uniaxial stretched samples drawn at 80°C (minimum shrinkage) and 100°C (maximum shrinkage) for DR = 4:1.

DSC tests were also carried out on all the blends at a heating rate of 20°C using samples from the extruded pellets, injection moulded plaques, and biaxial stretched specimens.

The thermal analysis data such as T_c, T_m, ΔH_c and ΔH_m were measured and a typical trace of the thermogram obtained is illustrated in Figure 4.5.

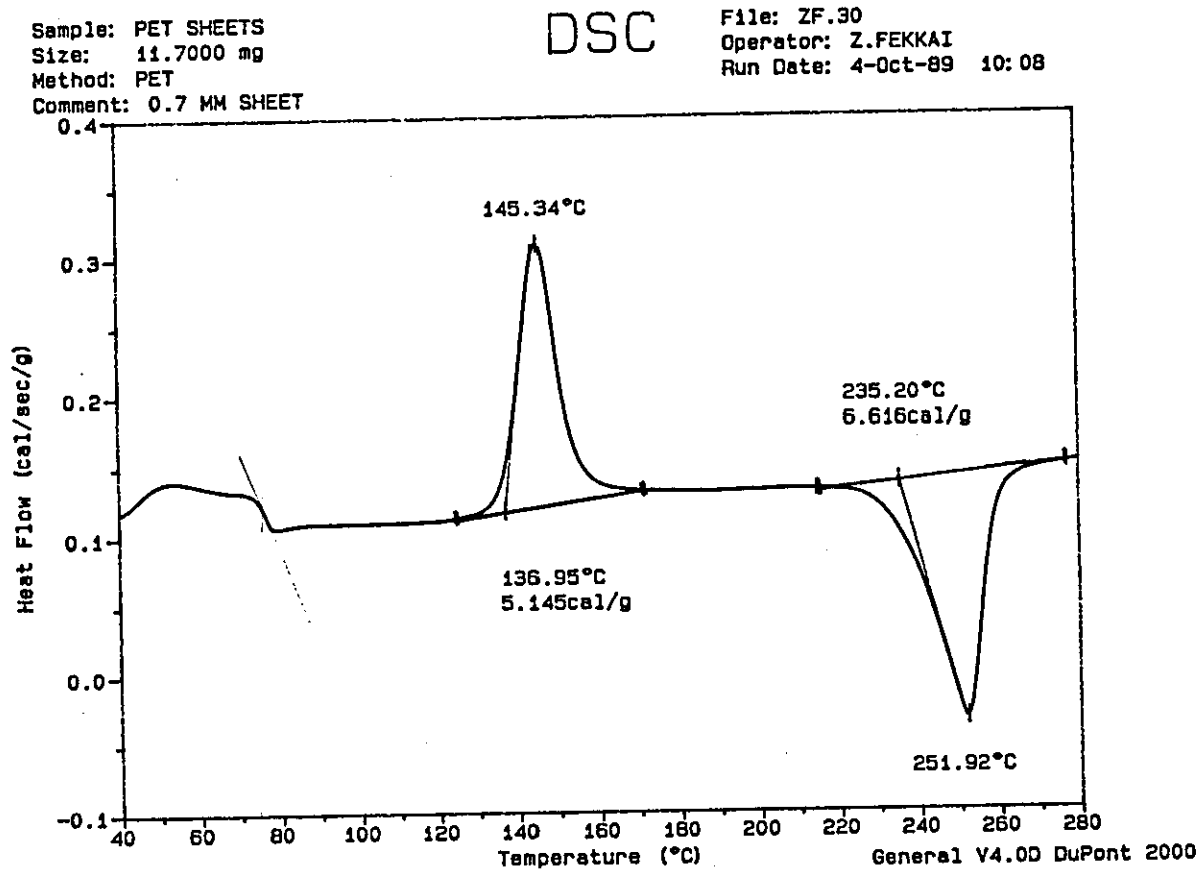

FIGURE 4.5: DSC Trace of PET Amorphous Sheet

To assess the effect of the level of crystallinity before and after stretching on the resulting shrinkage, the percentage of crystallinity initially present in the sample was calculated for all the samples, assuming ΔH_f = 32.5 cal/g for the pure PET crystal [61].

$$\% \text{ crystallinity in the sample} = \frac{\Delta H_f - \Delta H_c}{32.5} \times 100$$

where ΔH_f = heat of fusion

ΔH_c = heat of crystallisation from cold

4.5.3 Density Measurements

Density measurements were carried out at 25°C using a Davenport density gradient column filled with an aqueous solution of calcium nitrate. Known density floats were used to calibrate the column; the calibration graphs are given in Appendix A, Figures A_1 and A_2.

Density measurements were carried out on samples taken from uniaxially drawn PET using a density range of 1.3400-1.390 and also on PET/MXD6 (70/30) blends (i.e. the blend exhibiting very low shrinkage) using a density range of 1.290-1.3420.

Five mm strips were cut off from the monoaxially drawn PET samples and 2.5 mm squares were cut off from the biaxially drawn PET/MXD6 (70/30) blends samples. The chosen floats and samples were cleaned with soapy water and then with acetone to remove any dirt or grease contamination. After that these were wetted with a little of the high density solution before being placed in the basket of the sweep and then in the column (see Chapter 2, Section 2.1.4 for the equations used to calculate the percentage of crystallinity from density).

4.5.4 Scanning Electron Microscopy

To study the morphology of the different blends prepared, SEM tests were carried out on the Cambridge Stereoscan 360 electron microscope, using fractured specimens in liquid nitrogen taken from the injection moulded plaques as well as from the extruded pellets. Each specimen was gold coated and images of the fractured surfaces were obtained (after gold evaporation coating) on the scanning electron microscope.

4.5.5 Optical Microscopy

Optical microscopy studies were carried out on the samples showing very low shrinkage (e.g. samples drawn uniaxially at 80°C for DR = 4:1) and on the samples of very high shrinkage (e.g. samples drawn uniaxially at 100°C for DR = 4:1).

Samples Preparation

Due to the fact that the uniaxially stretched samples were flexible, the techniques used for microtoming thin sections was the CO_2 freezing technique.

A small specimen 5 x 10 sq mm was cut from the middle of the uniaxially stretched samples, and then placed on the CO_2 freezing stage and temporarily held in place with a suitable water based adhesive. The CO_2 valve was opened as soon as freezing commenced, water was dripped round the specimen until it was totally embedded in ice. CO_2 was not used continuously, but in bursts lasting about 15 seconds as soon as the temperature rises significantly. Microtome sections of about 10 μm through the thickness were cut using a glass knife and then photographed in an optical microscope between crossed polars.

4.5.6 Annealing Tests

Annealing experiments were carried out in an oven at preset temperatures of 100°C, 125°C, 150°C and 180°C for 30s, on the uniaxially and biaxially drawn PET samples. A 4 cm long specimen and a square piece (2 x 2 cm) were taken from the middle of the uniaxial and biaxial drawn samples respectively and clamped in a special jig to

avoid shrinkage during annealing.

4.5.7 Dynamic Mechanical Spectra

Dynamic mechanical tests were carried out on the Du Pont 2000 apparatus to determine the relaxation spectrum corresponding to the glass-transition (Tg) of the injection moulded plaques of all the blends. The measurements were made from -50°C to 150°C, at a constant heating rate of 2°C/min and at constant frequency of 1 Hz. The samples were cut into a rectangle of about 18 mm long and 12 mm wide using an electrical saw. The thickness was kept constant and equal to 1 mm thickness of the injection moulded plaques.

4.5.8 Birefringence Measurements

Birefringence measurements were carried out using a UV spectrophotometer on those uniaxially drawn samples at 80°C, 90°C, 100°C and 125°C for DR = 4:1. (Note that the samples with DR = 4:1, the birefringence could not be calculated by the UV spectrometer).

The basic principle of this method was to measure the distribution of intensity versus wavelength with a spectrophotometer, and compute the optical retardation of the stretched samples. The experimental arrangement was as follows[24]A sample was cut from the uniaxially drawn PET specimens and placed between crossed polars in the sample chamber of a Beckman Acta MVII ultra-violet spectrophotometer. With the h-lamp switched on, a wavelength scan was made between 450-800 nm. A trace is obtained which has a series of peaks. The peak number was plotted as a function of the reciprocal of the peak wavelength. A tangent was drawn at a wavelength of 546 nm, the gradient of the

tangent is equal to the optical retardation. Equation 4.1 shows that the optical retardation divided by the sample thickness is equal to the average through-thickness birefringence

$$\Delta\bar{n} = [m \div (1/\lambda_m] \div h \qquad (4.1)$$

where m is the peak number, λ_m is the peak wavelength and h is the sample thickness. (See fig 3.2)

4.5.9 Evaluation of Stresses Developed During Drawing

During uniaxial and biaxial stretching experiments force vs extension curves were recorded. It was noticed that in some cases a strain hardening behaviour was observed especially for uniaxially drawn samples. However calculation of the yield stress and final stress have been carried out to quantify the relationship between force and extensions involved in the drawing process.

CHAPTER 5
RESULTS

The main results of this study are presented in this section primarily in the form of figures and tables, and in accordance with the outline given in the experimental section. More detailed results are shown in the Appendix.

5.1 UNIAXIAL STRETCHING EXPERIMENTS

5.1.1 Shrinkage Results

The shrinkage data in boiling water for non-nucleated PET thick sheets (0.8 mm) are presented in Figure 5.1. These show that shrinkage is very dependent on draw ratio in stretching experiments performed below 100°C, showing a minimum at draw ratios (DR) around 4:1. At a drawing temperature (DT) of 100°C shrinkage results are intermediate between those obtained at DT's of 125°C and 90°C. In this temperature range there is an inverse correlation between draw ratio and shrinkage, which is the inverse of the results obtained with draw temperatures of 80°C and 90°C.

At high draw temperatures, i.e. between 125°C and 150°C shrinkage is low and almost independent of draw ratio. This could be explained by the fact that thermal crystallisation proceeds at a fairly high rate at these temperatures.

At drawing temperatures below the Tg of PET (i.e. DT = 60°C) higher shrinkage is obtained at all draw ratios.

The shrinkage results in boiling water for the nucleated PET thick sheets (0.8 mm) are presented in Figure 5.2. These sheets were drawn only at temperatures below 130°C (i.e. at 80°C, 90°C, 100°C, 110°C and 125°C), in order to avoid thermal crystallisation taking place prior to stretching. The results show that the highest level of shrinkage is obtained at the lowest draw ratio (i.e. 2:1).

For all drawing temperatures used (i.e. 80°C, 90°C, 100°C, 110°C and 125°C), it was found, however, that when the samples were drawn at draw ratios greater than 3:1 a slight haze in the drawn samples is obtained but shrinkage is quite low. This correlation suggests that stress-induced crystallisation that has taken place during drawing may be the main reasons for the observations made above.

The shrinkage results for samples stretched at 500 mm/min are presented in Figure 5.3. The data show that the lowest shrinkage is obtained at DT = 90°C and DR = 4:1. For samples drawn at 200 mm/min, on the other hand, the lowest shrinkage was obtained at DT = 80°C and DR = 4:1. This means that by increasing the stretching rate, the minimum in the shrinkage curve has been shifted to a higher draw temperature.

The shrinkage results in boiling water for both nucleated and non-nucleated PET thin sheets (0.4 mm) are presented in Figures 5.4 and 5.5 respectively. These show that a lower shrinkage is obtained for sheets nucleated with Ca Montanate (0.5%). The lowest shrinkage is always obtained, however, with the thick sheets (0.8 mm) suggesting the existence of an inverse correlation between shrinkage and original

thickness of the sheet used, possibly through the crystallinity level developed during manufacture of the sheet and subsequent heating in the tensometer chamber prior to stretching.

The same behaviour was observed for non-nucleated PET drawn samples (see Figure 5.5), confirming that the highest shrinkage is always observed on the thinner samples. Moreover as shown in Figure 5.5, the lowest shrinkage for the thin PET sheet is obtained at a higher temperature compared to the thick one.

The percentage shrinkage obtained at temperatures 85°C, 120°C and 150°C for non-nucleated PET thick sheets (0.8 mm) is shown in Figure 5.6. At temperatures of 85°C shrinkage is not at its minimum, as expected, but it seems that at 100°C the maximum shrinkage is obtained and as the shrinkage temperature increases to 120°C and 150°C shrinkage decreases. This could be due to further crystallisation taking place during shrinkage tests at these high temperatures.

The shrinkage results on annealed samples are presented in Figure 5.7. Shrinkage is reduced considerably when drawn samples are annealed at 100°C under constrained length conditions. At annealing temperatures of 125°C and above the percentage shrinkage is reduced to zero, even at high ambient temperatures up to 120°C, for the samples drawn at 80°C and 90°C. Shrinkage is still appreciable, however, for samples drawn at 60°C, 100°C and 125°C.

Zero shrinkage is obtained on all drawn samples when the annealing temperature is greater than 150°C (see Figure 5.7), but only the samples drawn at 80°C and 90°C for draw ratios greater than 3:1 remain transparent after annealing. Thermal crystallisation occurs in other samples. Note that all shrinkage results were an average of 10 specimens measured with accuracy with $\pm$ 0.5%.

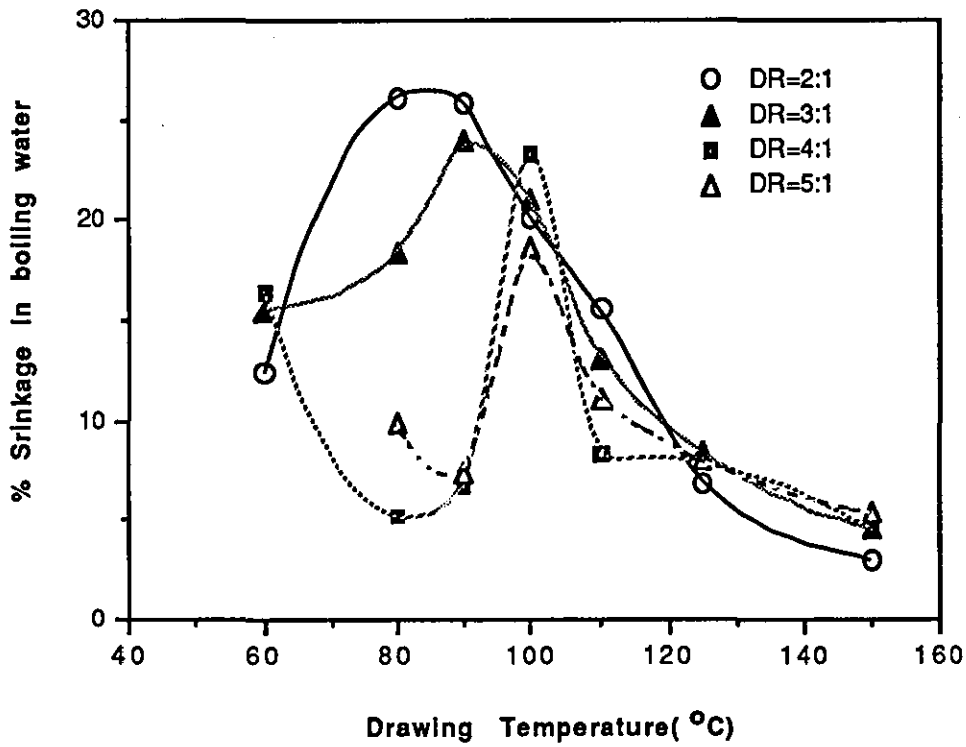

Figure5.1: Relationship between drawing conditions and shrinkage in boiling water for uniaxially drawn non-nucleated thick PET samples(0.8mm)

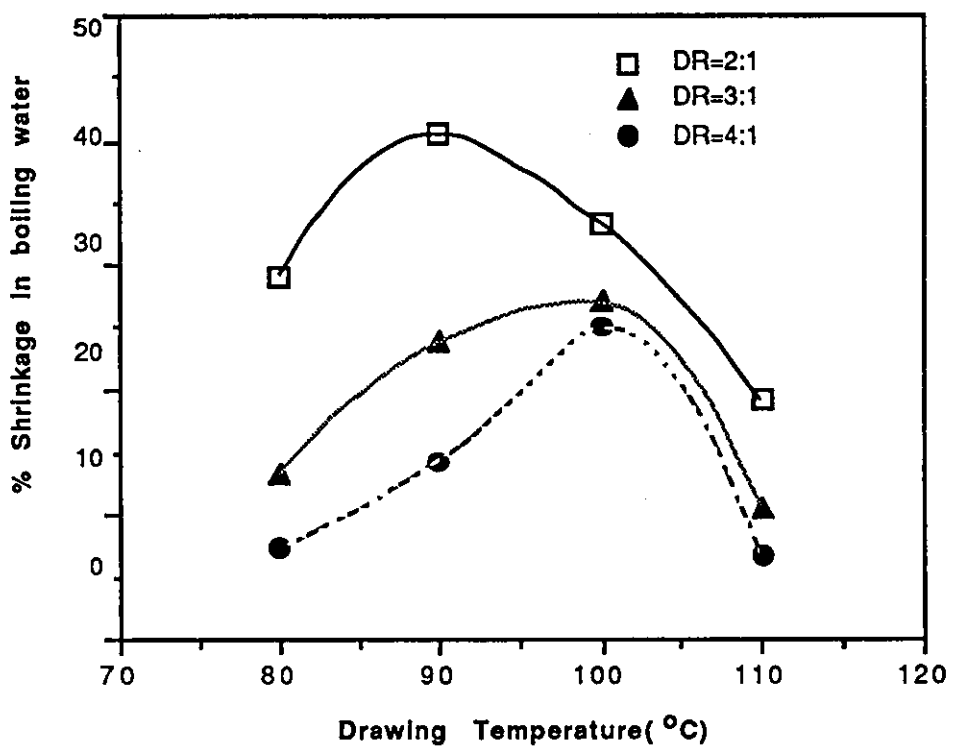

Figure 5.2: Relationship between drawing conditions and shrinkage in boiling water for uniaxially drawn nucleated thick PET samples(0.8mm)

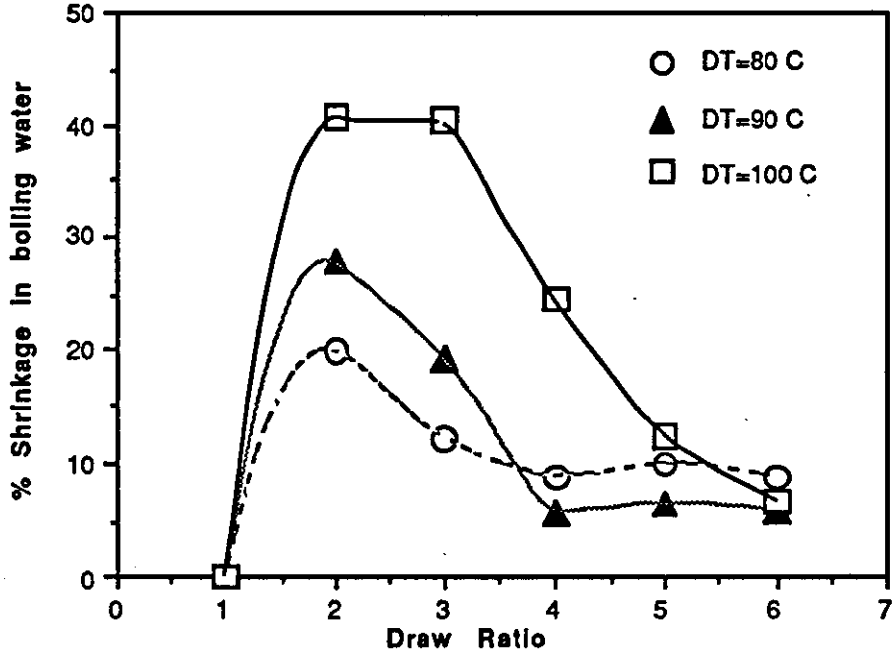

Figure5.3: Effect of Drawing Conditions on % Shrinkage for non-nucleated PET thick samples (0.8mm) uniaxially drawn at 500mm/min

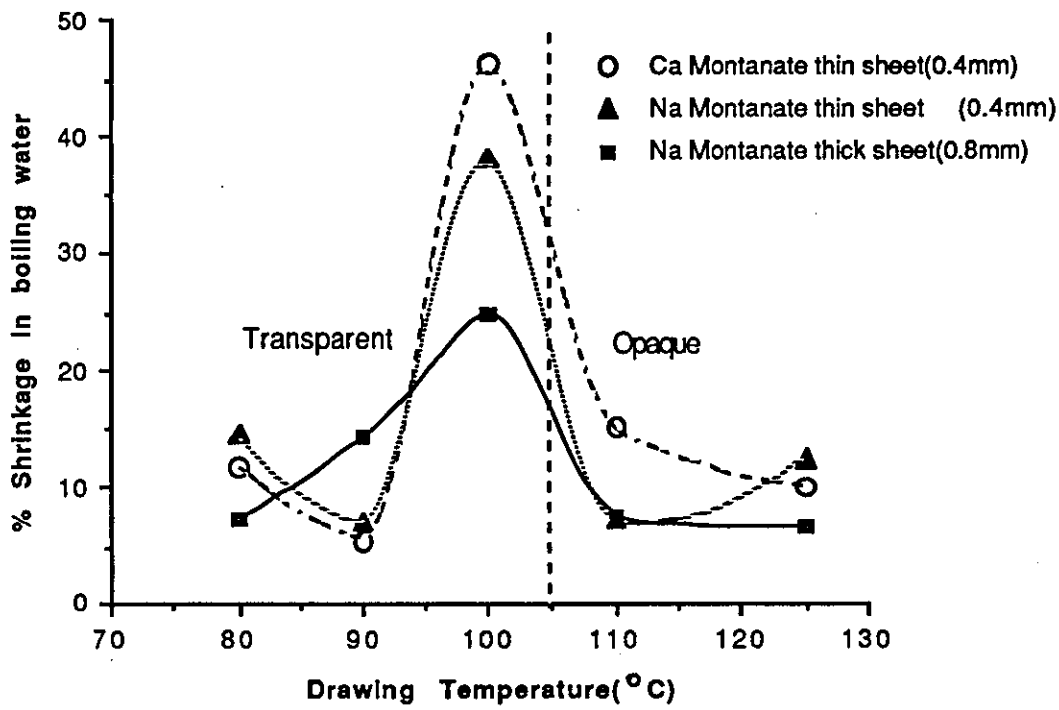

Figure5.4: Effect of thickness on shrinkage for nucleated PET uniaxially drawn at draw ratio=4:1

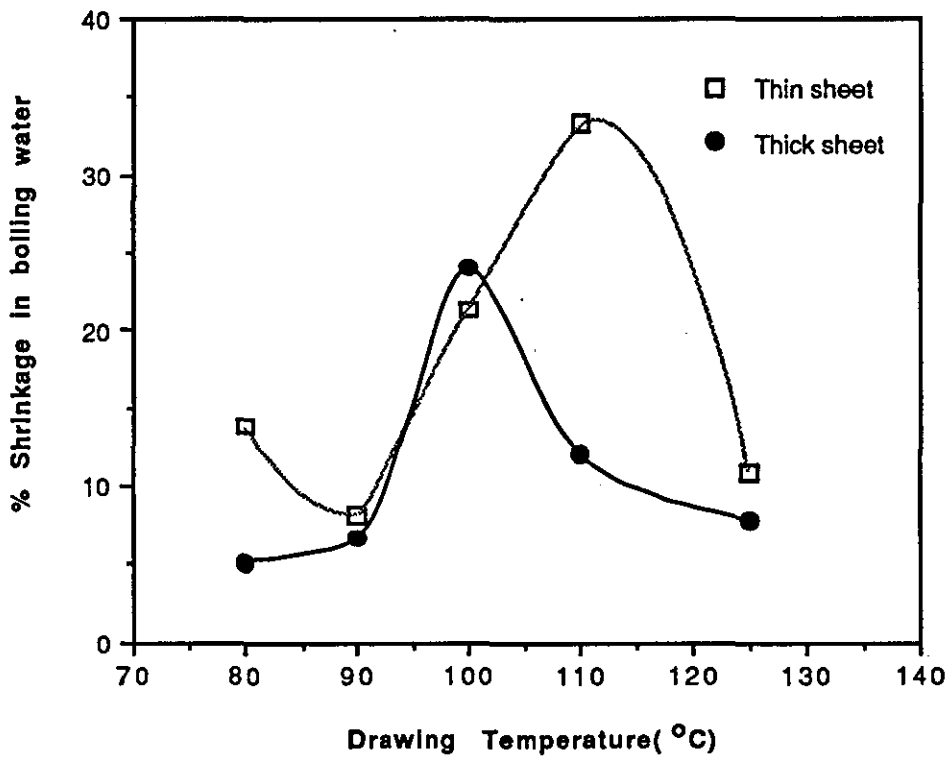

Figure5.5: Effect of thickness on shrinkage for uniaxially drawn non-nucleated PET (Draw Ratio=4:1)

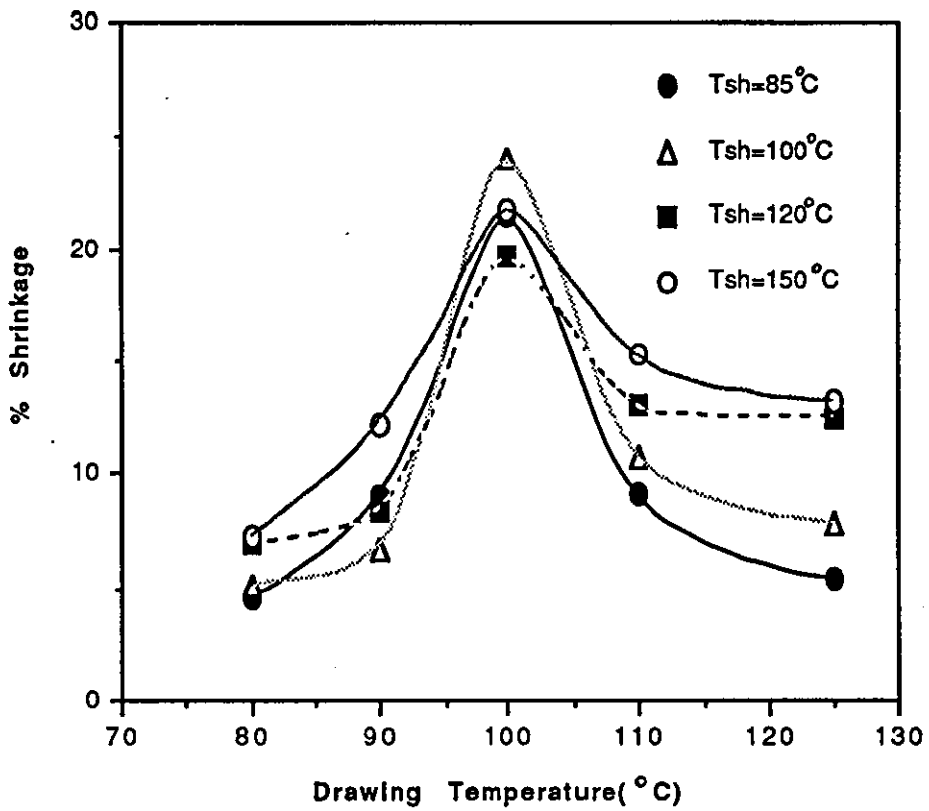

Figure 5.6: Relationship between shrinkage temperature and drawing temperature for the PET thick samples (0.8mm) uniaxially drawn at draw ratio=4:1

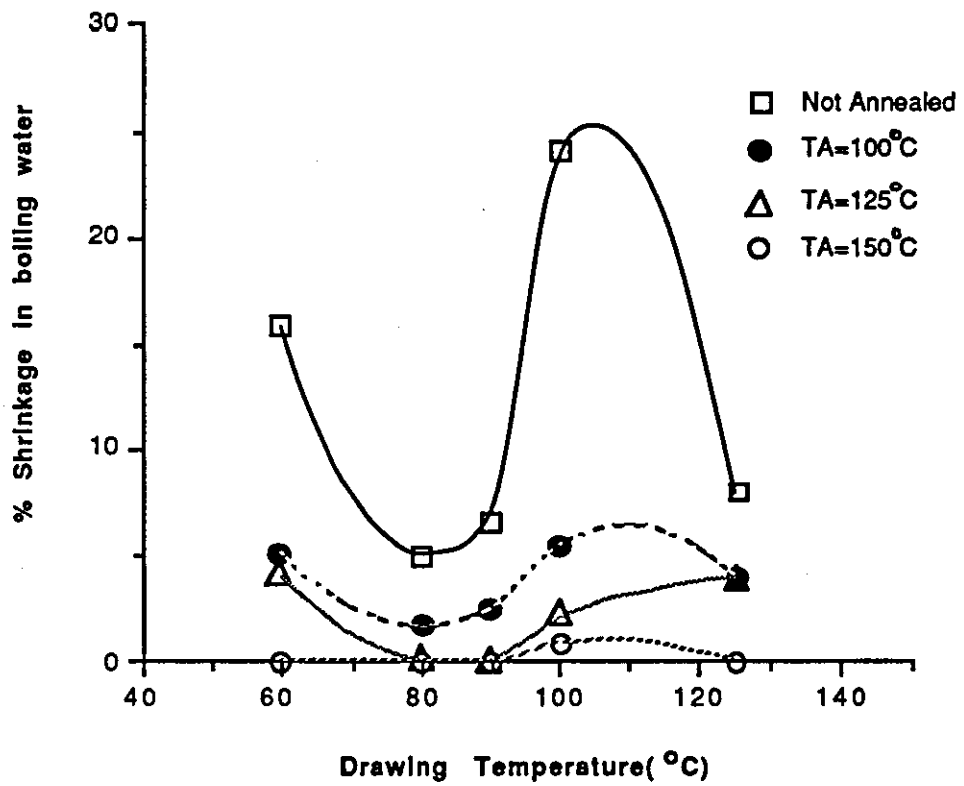

Figure 5.7: Relationship between shrinkage and annealing temperature for non-nucleated PET thick sheets (0.8mm) uniaxally drawn at draw ratio=4:1

5.1.2 DSC Data

The DSC results for samples drawn from non-nucleated and nucleated PET thick samples (0.80 mm) are shown in Figures 5.8-5.13 and in Table 5.1.

Figures 5.8 (a and b) show the DSC traces at 20°C/min heating rate for all the samples exhibiting maximum shrinkage (i.e. DT = 100°C, DR = 4:1 and DT = 80°C, DR = 2:1). The DSC traces show that a crystallisation peak is exhibited at Tc = 125°C, i.e. at about 10°C to 15°C below the crystallisation peak temperature for the corresponding PET sheets before being drawn. The Tg of the drawn samples, however, remain constant at 75°C, irrespective of draw ratio and thermal history of the sample. The melting temperature also remains unchanged at 254°C.

Figure 5.8(c) shows the DSC trace of the samples exhibiting stress hardening behaviour during stretching (i.e. TD = 80°C, DR = 4:1), but remaining transparent (i.e. not exhibiting thermal crystallisation).

The DSC data on these samples, show that only a small crystallisation peak is observed, indicating the occurrence of extensive stress-induced crystallisation has taken place during stretching, which is responsible for the strain hardening behaviour (as shown later in the mechanical properties results) and for the low residual crystallisability of the drawn samples and, in turn, to the low shrinkage observed.

Figure 5.8 (d and c) show the DSC traces of samples uniaxially drawn

at 125°C and 150°C respectively which were opaque i.e. a substantial amount of thermal crystallisation has taken place during drawing. The DSC traces of Figure 5.8(e) do not have a crystallisation peak confirming that the material has crystallised thermally during stretching due to the high temperature.

Figure 5.9 shows the DSC traces of annealed samples which also exhibit zero shrinkage. Once more no crystallisation peak is observed, confirming that the material undergoes thermal crystallisation during annealing and that the crystallites so formed may be responsible for suppressing the shrinkage in the samples. In addition to the original melting endotherm (T_m = 254°C), a small melting endotherm is seen at temperatures over the temperature range 20° to 50°C above the annealing temperature used. In the case of annealed samples therefore, shrinkage does not occur because no further crystallisation can take place.

The DSC results for the nucleated PET samples are presented in Figure 5.10 (a and b). Figure 5.10(a) shows the DSC trace for the nucleated samples after stretching at 80°C for DR = 4:1. Since a small crystallisation peak is observed, complete crystallisation has not occurred, despite the fact that the samples after stretching are not transparent. The crystallisation peak temperature (Tc) occurs at 95°C while the melting remains unchanged at 254°C.

Figures 5.11 (a1,b1) show the DSC traces at 5°C/min scan rate of samples uniaxially stretched at 80°C (i.e. exhibiting minimum shrinkage) and 100°C (i.e. exhibiting maximum shrinkage) for DR = 4:1,

while Figures 5.11 (a2,b2) show the DSC results on the same samples using 10°C/min heating rate, and Figures 5.11 (a3,b3) show the DSC results at 15°C/min heating rate, also for the same samples. More detailed DSC results are shown in Appendix B, Figures B3 to B5.

TABLE 5.1: DSC DATA AT 20°C/MIN SCAN RATE

Material	DT (°C)	DR	Tc (°C)	ΔHc (cal/g)	Tm (°C)	ΔHf (cal/g)
Non-nucleated PET sheets (0.8 mm)	-	-	145.34	5.15	251.92	6.62
Non-nucleated PET sheets (0.4 mm)	-	-	140.39	6.57	247.55	8.75
Monoaxially Drawn Samples	80	2:1	126.95	5.87	251.44	9.35
	80	4:1	99.79	0.98	249.83	12.52
	90	4:1	103.34	1.54	252.63	9.35
	100	4:1	124.78	4.69	249.66	9.674

In every case the percentage initial and total crystallinity was calculated from the heat of crystallisation (ΔH_c) and heat of fusion (ΔH_f) i.e.

$$\% \text{ crystallinity initial} = \frac{\Delta H_f - \Delta H_c}{32.5} \times 100$$

$$\% \text{ crystallinity total} = \frac{\Delta H_f}{32.5} \times 100$$

TABLE 5.2: CRYSTALLINITY AND SHRINKAGE DATA FOR MONOAXIALLY DRAWN SAMPLES

Materials	DT (°C)	DR	% Linear shrinkage in boiling water	% Crystallinity (initial)	% Crystallinity (total)	Δ* Residual heat of crystallisation
Non-nucleated PET sheets (0.8 mm)	-	-	-	4.52	20.35	15.83
Non-nucleated PET sheets (0.4 mm)	-	-	-	6.71	26.92	20.21
Non-nucleated PET sheets (0.8 mm)	80	2:1	26.08	10.70	28.76	18.06
Non-nucleated PET sheets (0.8 mm)	80	4:1	5.10	35.49	38.52	3.03
Non-nucleated PET sheets (0.8 mm)	90	4:1	6.67	24.04	28.76	4.72
Non-nucleated PET sheets (0.8 mm)	100	4:1	24.07	15.33	29.76	14.43

* Δ is the difference between the total crystallinity achievable for a particular sample and the initial crystallinity.

The results in Tables 5.1 and 5.2 show that shrinkage is directly proportional to the residual heat of crystallisation, irrespective of the drawing temperature (see Figure 5.8).

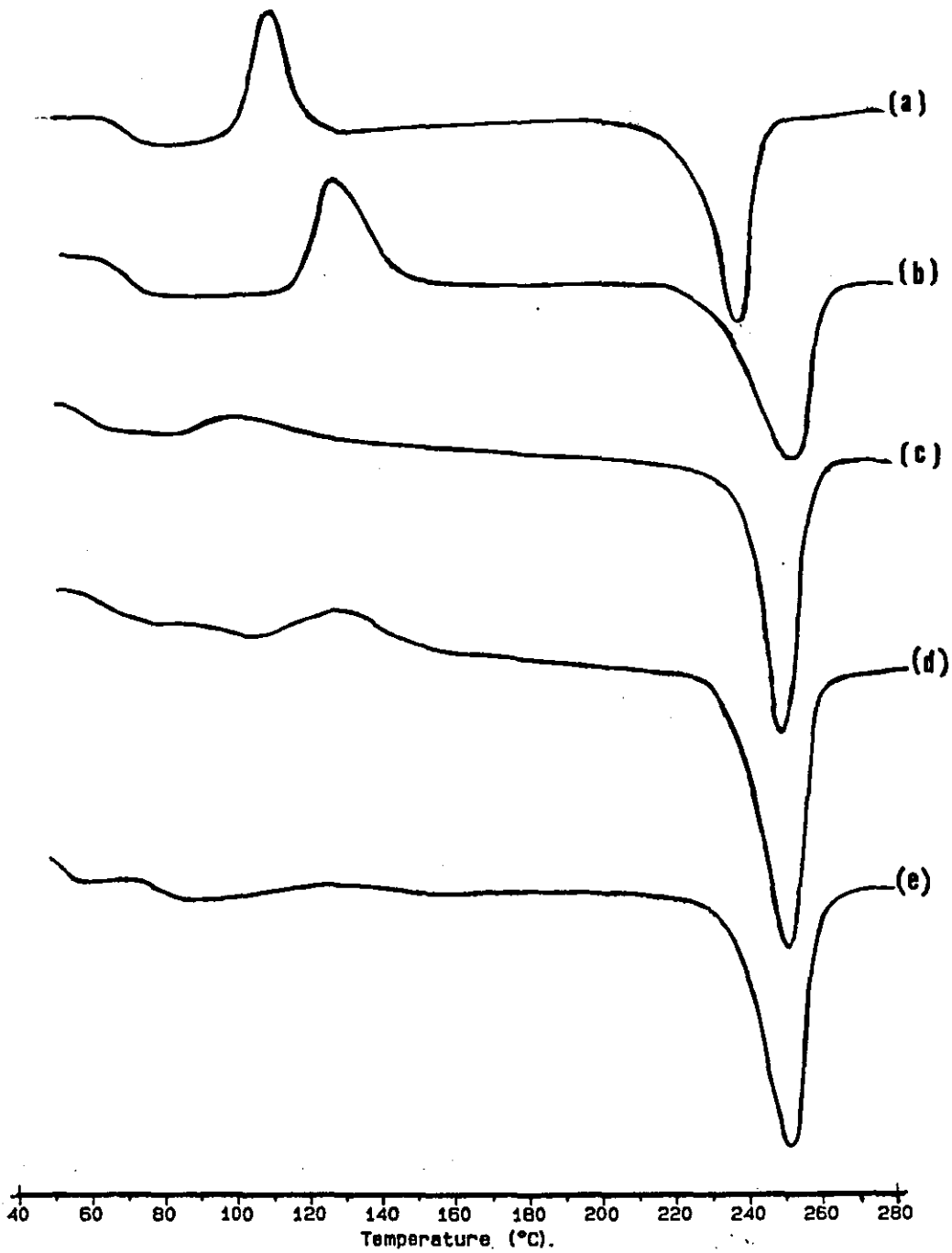

FIGURE 5.8: DSC traces at 20°C/min heating rate of uniaxially drawn non-nucleated thick PET samples (0.8 mm): (a) DT = 100°C, DR = 4:1; (b) DT = 80°C, DR = 2:1; (c) DT = 80°C, DR = 4:1; (d) DT = 125°C, DR = 4:1; (e) DT = 150°C, DR = 4:1

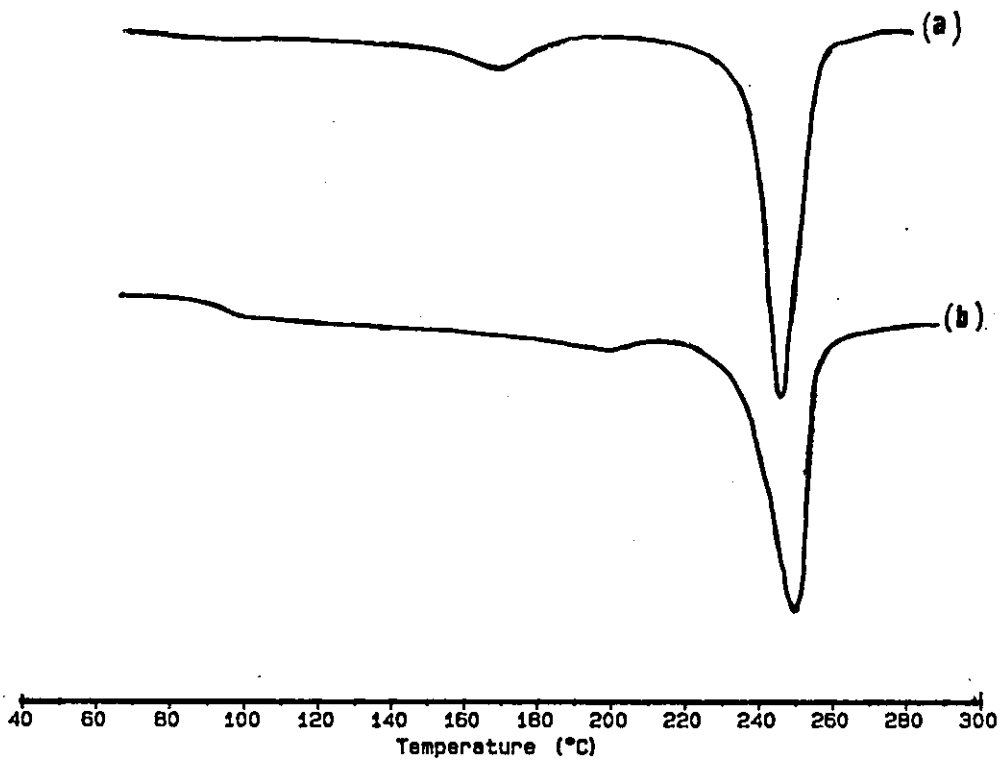

FIGURE 5.9: DSC traces at 20°C/min heating rate of annealed samples with zero shrinkage: (a) TD = 80°C, DR = 4:1, TA = 125°C; (b) TD = 100°C, DR = 2:1, TA = 180°C

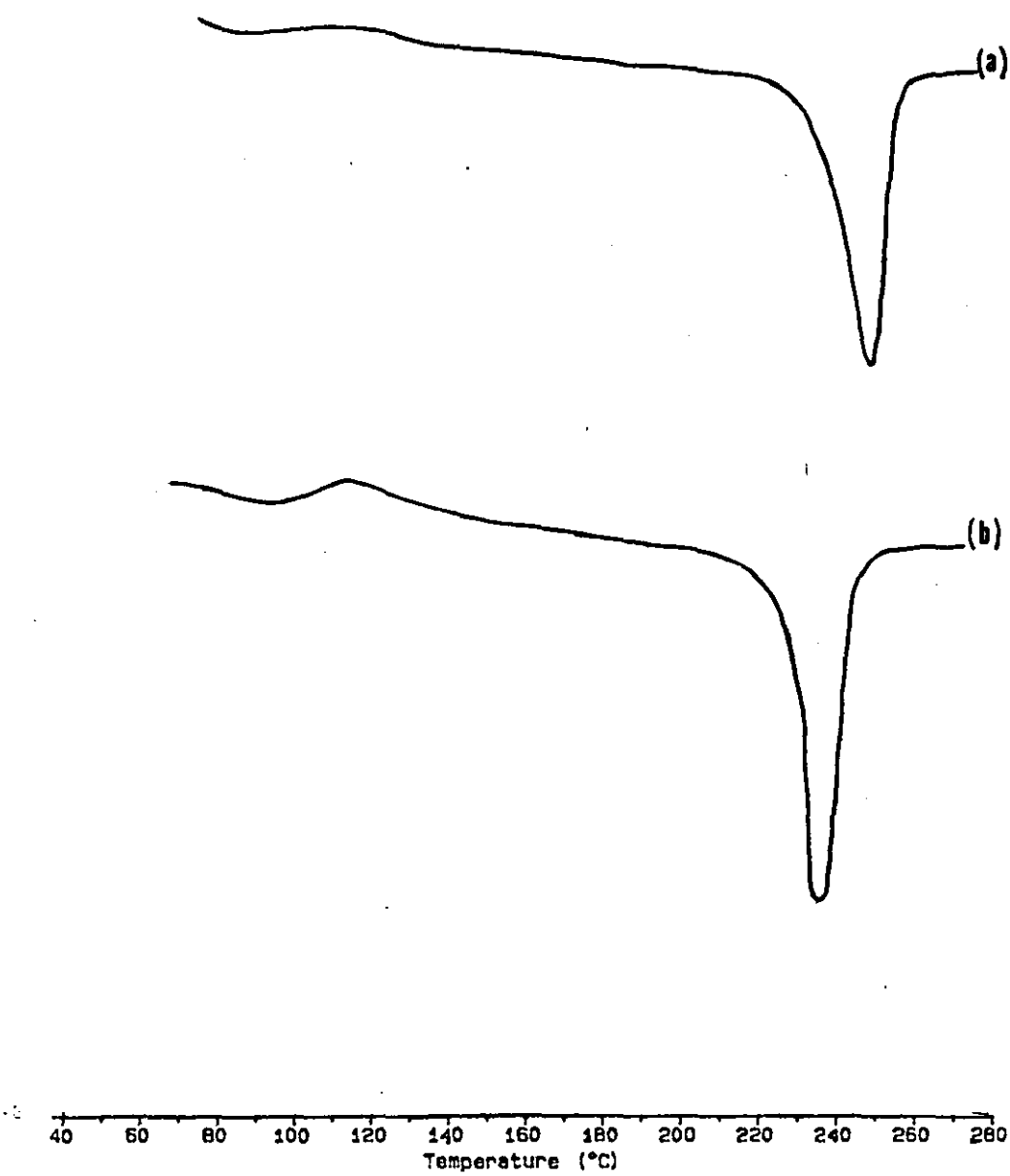

FIGURE 5.10: DSC traces at 20°C/min heating rate of uniaxially drawn nucleated thick PET samples (0.8 mm): (a) Ca Montanate (0.5%); (b) Na Montanate (0.5%)

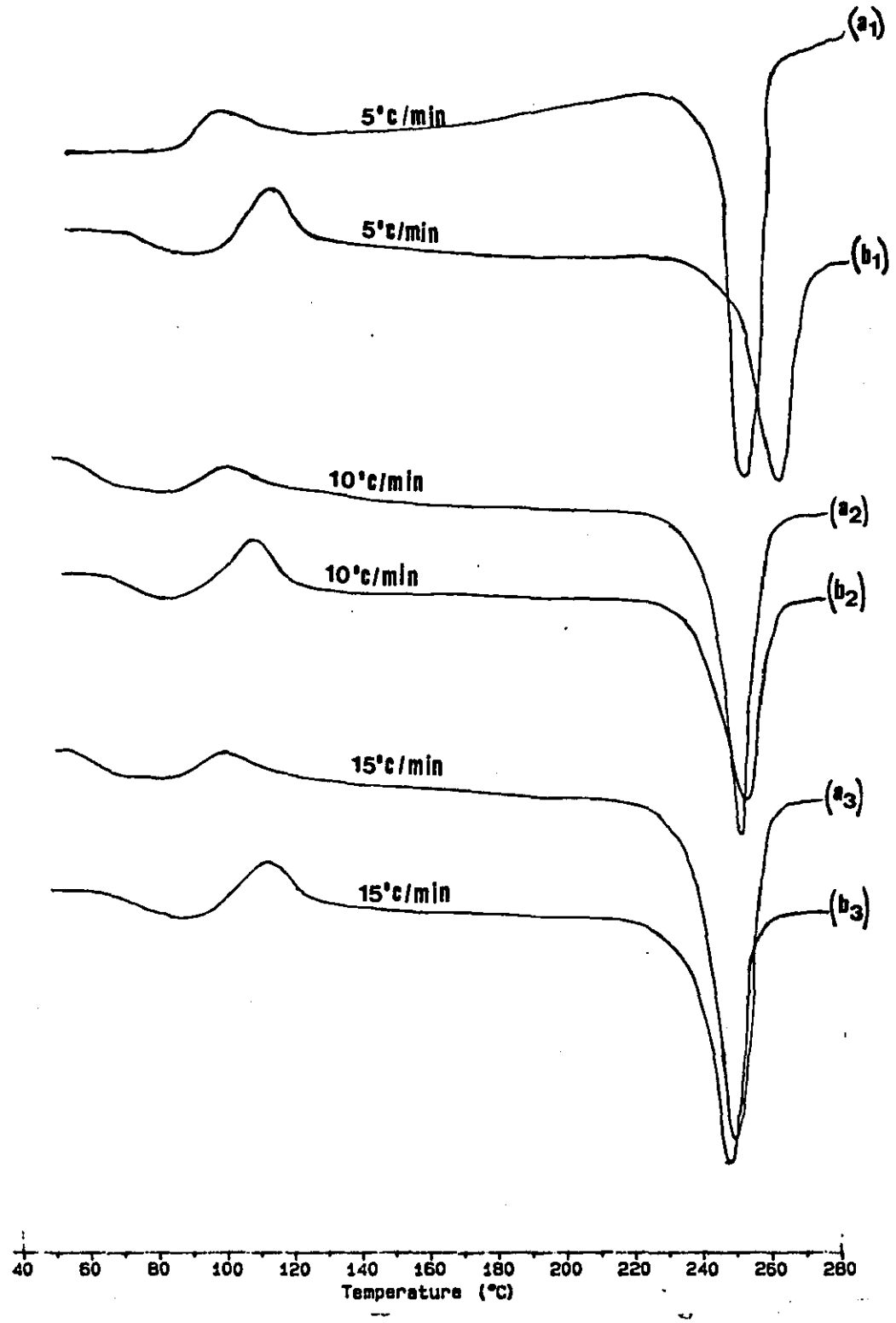

FIGURE 5.11: DSC traces of uniaxially drawn non-nucleated thick PET samples (0.8 mm): (a) TD = 80°C, DR = 4:1; (b) TD = 100°C, DR = 4:1

5.1.3 Density of Drawn Samples

The density results of the uniaxially drawn PET thick sheets (0.8 mm) are presented in Figures 5.12 and 5.13.

Figure 5.13 shows the relationship between shrinkage and the density at different draw ratios. The results show that for the same drawing temperature shrinkage is related to density and that the lowest shrinkage is obtained for samples exhibiting the highest density. More density results are presented in Appendix A (Tables A1 and A2). Note that the density results were calculated with an accuracy within $\pm$ 0.03 g/cm^3.

5.1.4 Birefringence Results

The birefringence results for the uniaxially drawn PET thick sheets (0.8 mm) before annealing are presented in Table 5.3. These show that the shrinkage for samples drawn below 125^{o}C is very dependent on the birefringence, and very high birefringence is observed for samples showing very low level of shrinkage, however the two variables are not directly proportional.

TABLE 5.3: BIREFRINGENCE RESULTS FOR UNIAXIALLY DRAWN NON-NUCLEATED PET SHEETS OF 0.8 mm THICKNESS BEFORE ANNEALING

DT (^{o}C)	DR	% Shrinkage in boiling water	D_n (Birefringence)
80	4:1	5.1	0.0863
90	4:1	7.33	0.0645
100	4:1	24.07	0.0495
125	4:1	7.87	0.0930

Note that each value was an average of 5 and the accuracy of the results was within $\pm$ 0.001.

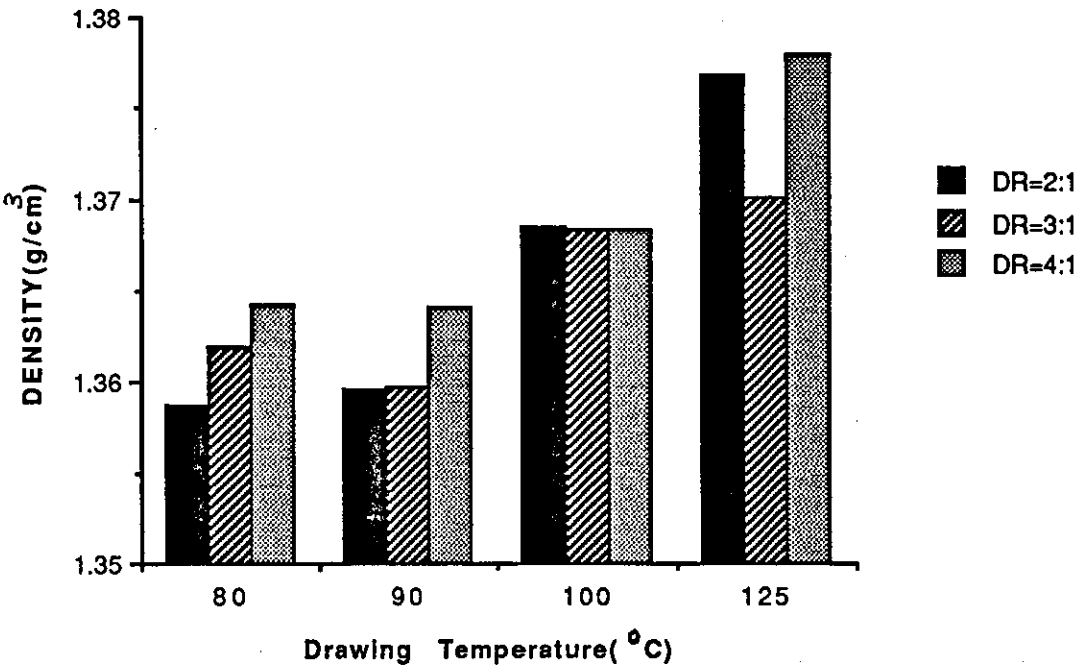

FIGURE 5.12: Relationship between drawing conditions and density for the uniaxially drawn non-nucleated PET thick samples(0.8mm)

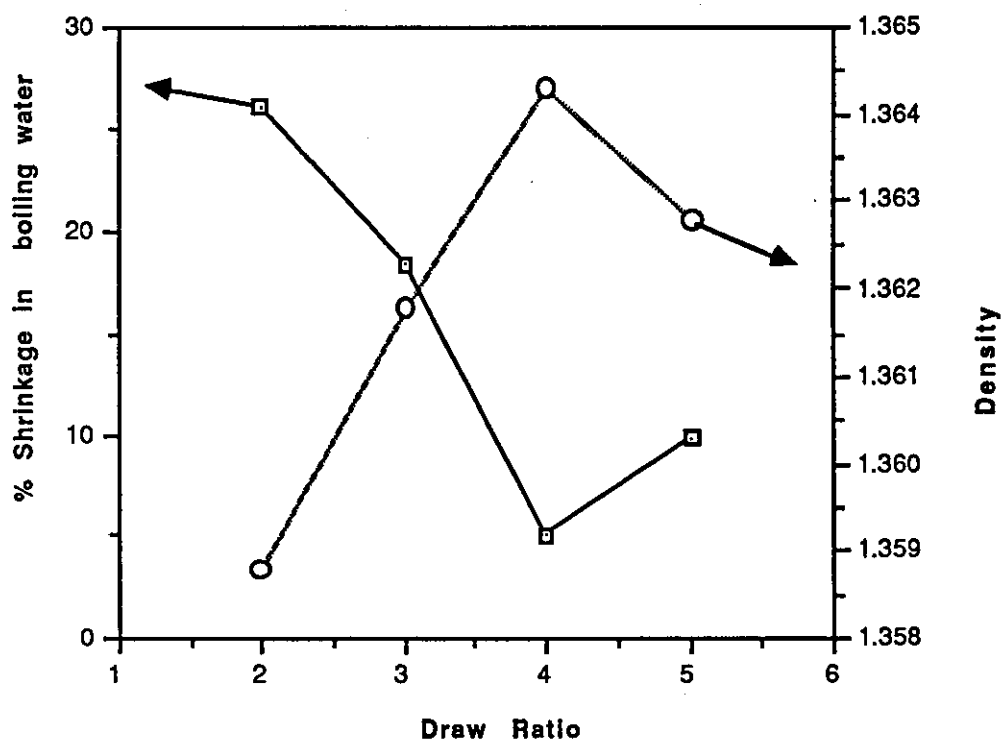

Figure 5.13 :Relationship between density and shrinkage at different draw ratios for uniaxially drawn non-nucleated thick PET samples(0.8mm) at DT=80°C

(a)

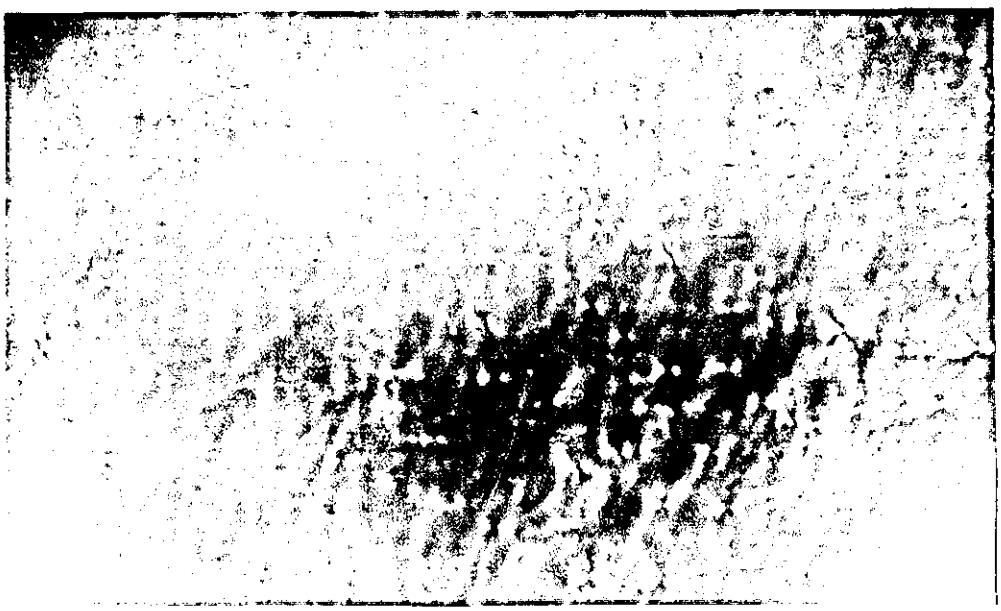

25×10

(b)

25×10

FIGURE 5.14: Optical microscopy results of uniaxially drawn non-nucleated thick PET samples
(a) TD = 80°C, DR = 4:1; (b) TD = 100°C, DR = 4:1

(Picture taken perpendicular to the cross-sectional surface and flow direction)

5.1.5 Optical Microscopy Results

Optical microscopy results are presented in Figure 5.14 in the form of micrographs.

For the samples before drawing no spherulites were observed, while the samples drawn uniaxially at 80°C for DR = 4:1 (i.e. samples exhibiting minimum shrinkage) it was revealed the presence of a quite large number of small spherulites, confirming that these spherulites were formed during drawing and that they play an important role in reducing shrinkage.

On the other hand, only very few spherulites were observed, in samples drawn at 100°C for DR = 4:1 (i.e. samples showing maximum shrinkage).

5.1.6 Results of Stresses Developed During Uniaxial Stretching

The stress results of uniaxially drawn non-nucleated thick PET samples (0.8 mm) are presented in Table 5.4.

Note that each value was an average of 10 and the accuracy of the results was within $\pm$ 0.1 N/m^2.

TABLE 5.4: STRESSES RECORDED FOR UNIAXIAL DRAWING EXPERIMENTS ON PET SAMPLES (0.8 mm)

Drawing Temp T(°C)	Properties σ_y N/m^2 (x 10^6)	σ_f N/m^2 (x 10^6)
80	0.17	0.22
90	0.15	0.14
100	0.16	0.13
110	0.23	0.17
125	0.77	1.27

These show that at a drawing temperature of 125°C, the final stress is greater than the yield stress, possibly due to the crystallisation rate being quite high at this temperature. However, the same behaviour is observed also at a drawing temperature of 80°C which may result from stress-induced crystallisation. This could be once more the reason for having a low shrinkage for samples drawn at 80°C and DR = 4:1.

5.2 BIAXIAL STRETCHING EXPERIMENTS

5.2.1 Shrinkage Results

Shrinkage data for PET bottles obtained for experiments carried out in boiling water and in water at 85°C are presented in Tables 5.5 and 5.6.

Table 5.5 shows the shrinkage results for samples taken from the waist of the bottles, while in Table 5.6 are shown the shrinkage results for samples taken at the top around the neck regions of the bottles. In both cases the data were obtained before and after annealing under constrained conditions at 100°C and 180°C for 30s. These results show that the percentage shrinkage in the two perpendicular directions, i.e. axial and hoop directions, is quite high, while a near-zero shrinkage is obtained when the samples are annealed at 180°C for 30s.

The shrinkage results in boiling water for PET samples biaxially stretched without shear are presented in Figures 5.15-5.19.

Figures 5.15 and 5.16 show the shrinkage results for the samples taken from the middle of the biaxial stretched specimens. These show that for the two biaxial drawn ratios 2:1 and 3.5:1 the highest percentage shrinkage is obtained at a draw temperature (DT) of 80°C for specimens produced from both nucleated and non-nucleated PET thick sheet samples (0.8 mm). The shrinkage data for bottles correspond to those for sheets drawn at 100°C.

TABLE 5.5: SHRINKAGE RESULTS FOR SAMPLES TAKEN FROM THE WAIST REGIONS OF THE BOTTLES (DR_L = 3:1, DR_h = 3.5:1)

Annealing Temperature (°C)	% Linear Shrinkage (Average at 85°C)		% Linear Shrinkage (Average at 100°C)	
	HD	LD	HD	LD
Not annealed	10.00	8.57	14.28	13.33
100	5.15	3.25	7.5	5.0
180	0	0	2.5	1.25

HD = hoop direction
LD = longitudinal direction
DR_l = draw ratio in the longitudinal direction
DR_h = draw ratio in the hoop direction

TABLE 5.6: SHRINKAGE RESULTS FOR SAMPLES TAKEN FROM THE TOP REGIONS OF THE BOTTLES (i.e. NEAR THE NECK DR_L = 2:1, DR_h = 2:1)

Annealing Temperature (°C)	% Linear Shrinkage (Average at 85°C)		% Linear Shrinkage (Average at 100°C)	
	HD	LD	HD	LD
Not annealed	18.35	12.00	25.0	15.0
100	6.95	5.30	9.8	6.5
180	1.70	0.69	3.6	2.7

HD = hoop direction
LD = longitudinal direction

On the other hand Figures 5.17 and 5.18 show the shrinkage data for the same samples, but the specimens were taken from the shear region of the biaxial stretched samples.

The results show that shrinkage is always lower in the shear region than in the middle. The lowest shrinkage being obtained in the shear regions for specimens produced at 110°C drawing temperature.

Figures 5.17 and 5.18 show that the higher the shear extension ratio the lower the shrinkage. Note that in these regions the axial draw ratio is much smaller than for samples taken in the middle revealing the very predominant role played by in-plane shear deformations (see Section 4.2.3, for the definition and calculation of the total extension ratio in the shear region).

The shrinkage results at 85°C for both nucleated and non-nucleated PET thick samples (0.8 mm) taken from the middle and shear region are presented in Figures 5.15-5.18.

The results of the samples taken from the middle show that for both biaxial draw ratio 2:1 and 3.5:1 the shrinkage decreases with increasing the drawing temperature, reaching a minimum at about 110°C. This is contrary to monoaxially drawn samples which showed a minimum at 80°c (see Figures 5.15-5.16). The results for samples taken from the shear region, on the other hand, show the same trend but lower shrinkage in relation to specimens taken in the middle regions and that zero shrinkage is obtained for the non-nucleated PET samples produced at 110°C drawing temperature and for draw ratio = 3.5:1. In

all cases no measurable change in angle of shear was observed as a result of shrinkage.

The shrinkage results on annealed samples taken from the middle of the biaxially drawn PET thick sheet (0.8 mm) are presented in Figure 5.19. These show that zero percent shrinkage can only be obtained at very high annealing temperature (TA = 180°C). However, only the samples drawn at 80°C and 90°C, remain transparent, while drawing the specimens above 110°C produces opacity and reduces the drawability.

The shrinkage results in boiling water for samples stretched under combined biaxial drawing and shear deformation are presented in Table 5.7 (see Figure 3.1, Section 3.2.2 for illustration of the jigs used).

These show that a lower shrinkage is obtained for samples biaxially drawn with superimposed shear deformations than for the samples drawn biaxially with pure biaxial extension. Furthermore the lowest shrinkage is obtained for samples with higher amounts of shear deformations, i.e. samples drawn with configurations G_2 (see Section 4.2.2(b) for illustration of the geometries G_1 and G_2).

See Section 4.2.3 for the calculation of the shear extension ratio for each geometry.

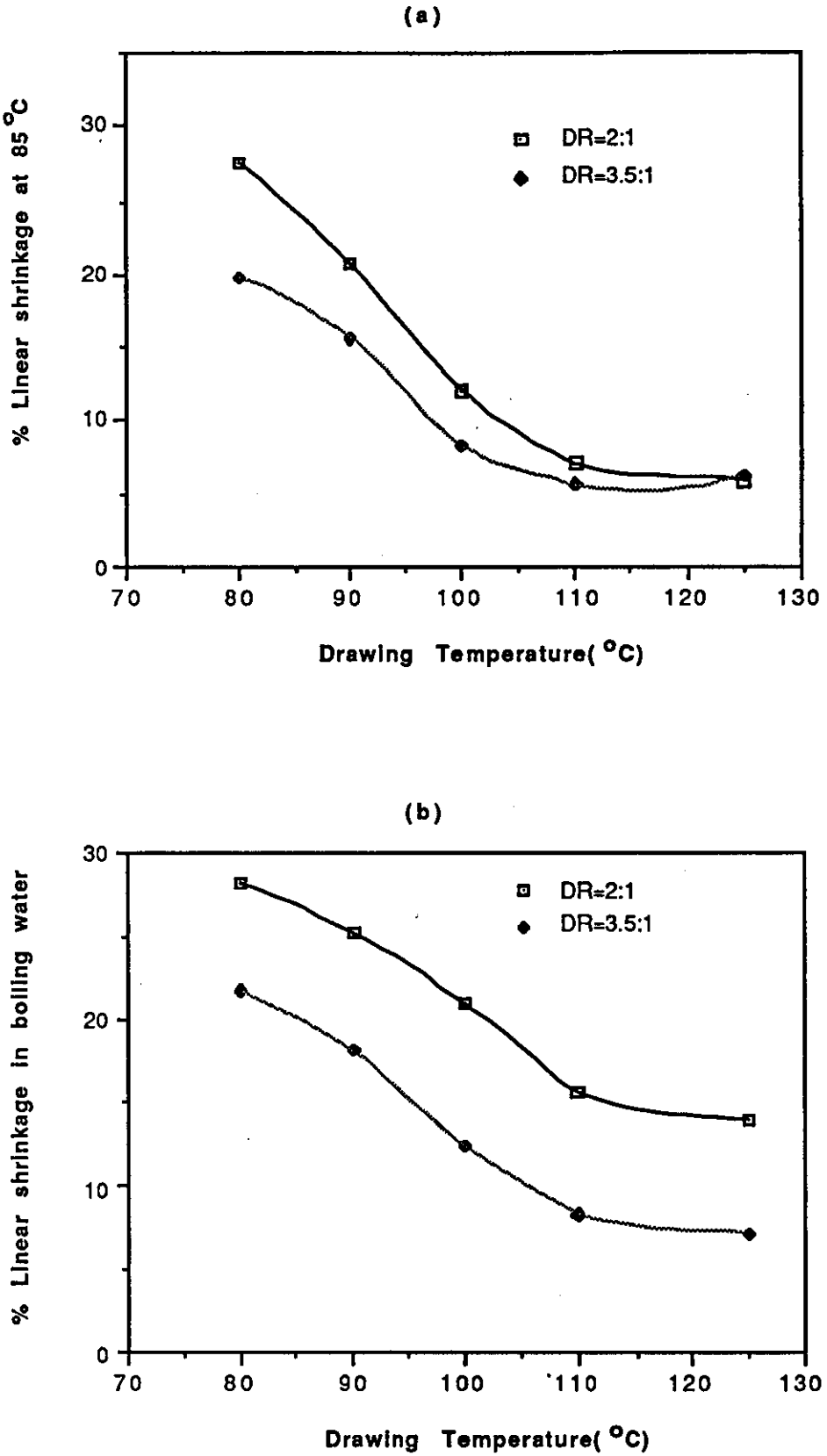

Figure5.15: Relationship between linear shrinkage and drawing conditions for biaxially drawn non-nucleated PET samples(0.8mm thick)

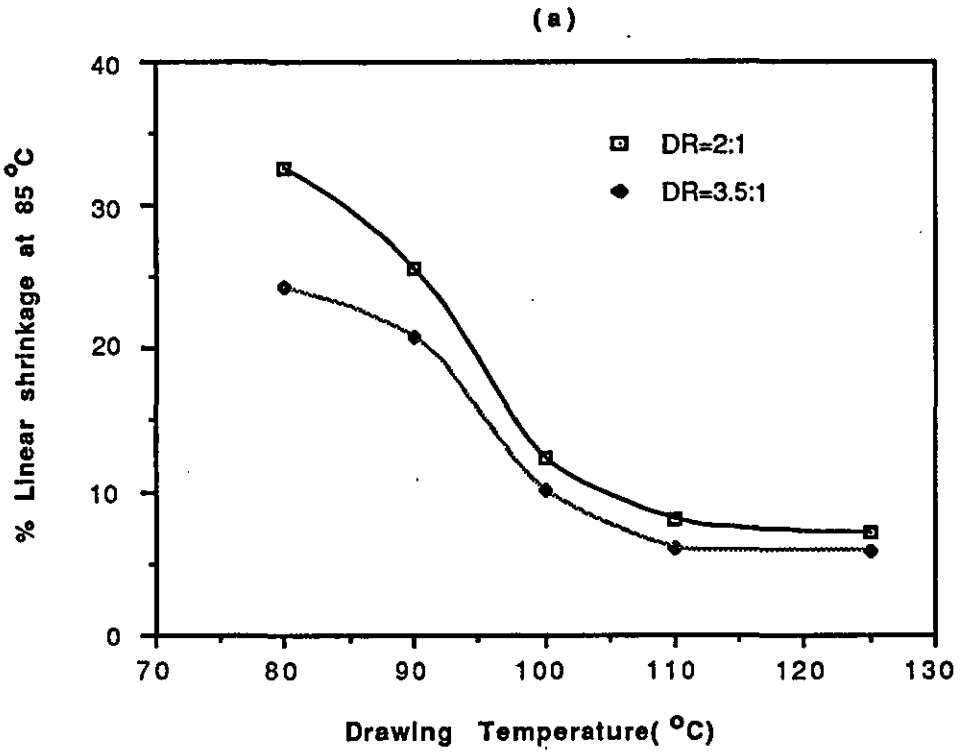

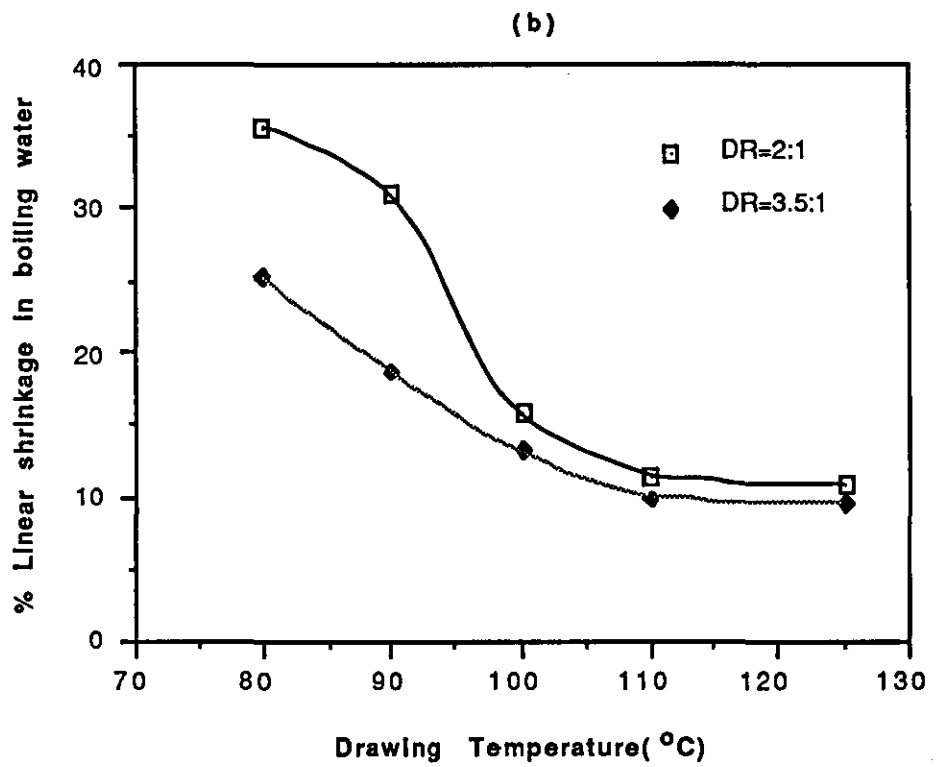

Figure5.16: Relationship between linear shrinkage and drawing conditions for samples taken from the middle of the biaxially drawn nucleated PET thick samples (0.8mm)

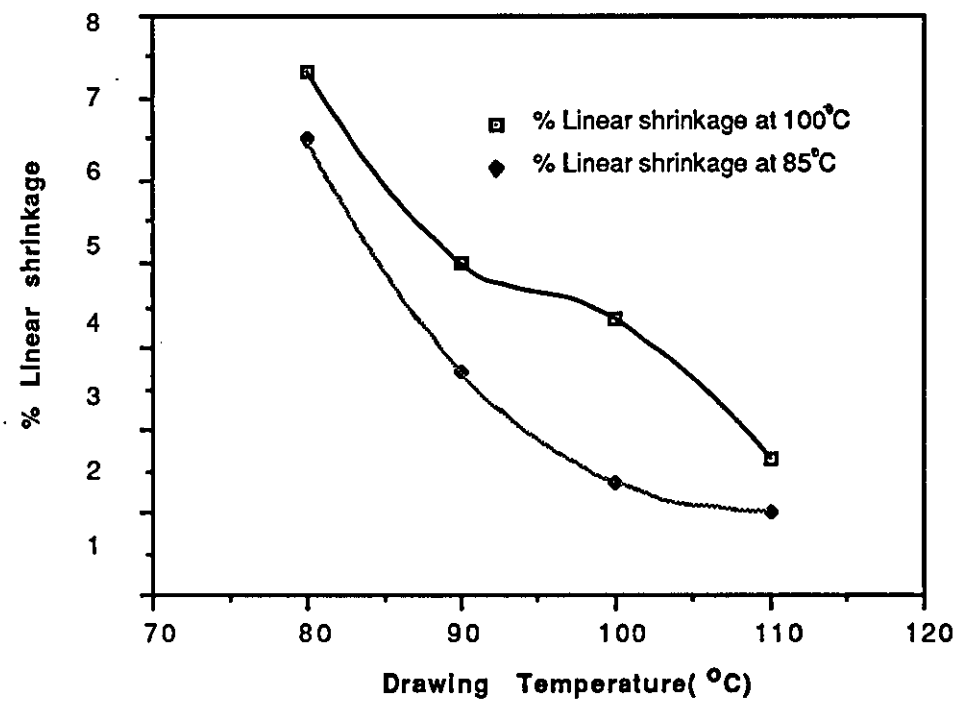

Figure5.17: Relationship between drawing conditions and linear shrinkage for samples taken from the shear region of the biaxially drawn non-nucleated PET thick sheets (biaxial draw ratio=2:1, average axial draw ratio in the shear region=1.44, shear extension ratio=1.09 and total extension ratio=1.56)

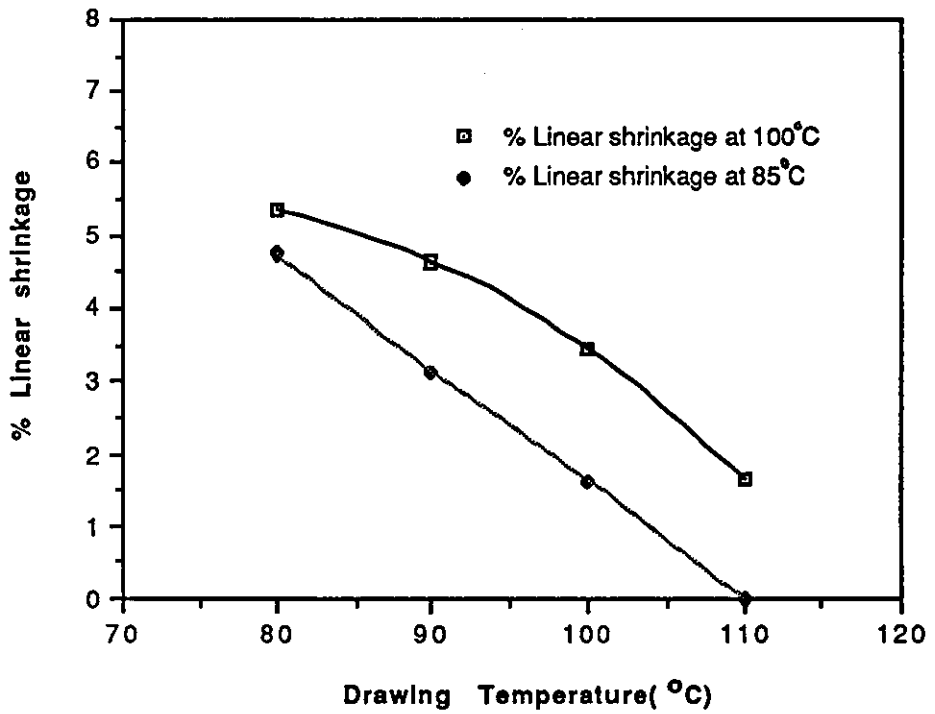

Figure5.18: Relationship between drawing conditions and linear shrinkage for samples taken from the shear region of the biaxially drawn non-nucleated PET thick sheets (biaxial draw ratio=3.5:1, average axial draw ratio in the shear region=1.67, shear extension ratio=1.16 and total extension ratio=1.93)

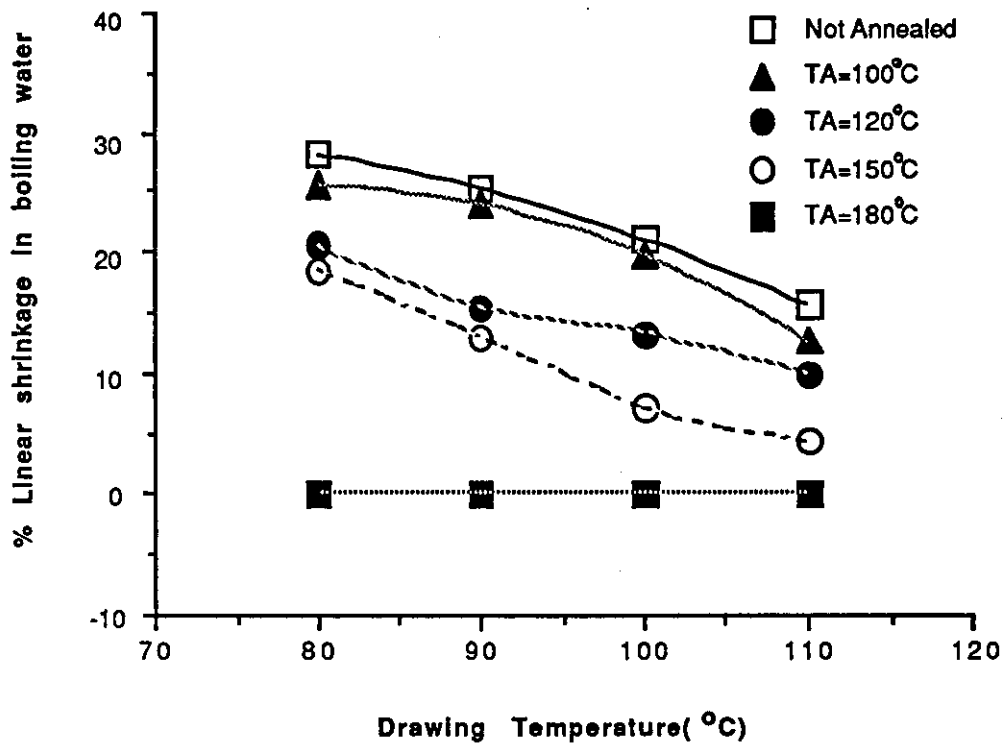

Figure 5.19: Relationship between drawing temperature and linear shrinkage for the samples taken from the middle of the biaxially drawn non-nucleated PET thick sheets(0.8mm, biaxial draw ratio=2:1), after annealing at different temperature

TABLE 5.7: SHRINKAGE DATA FOR THE NON-NUCLEATED PET THICK SAMPLES (0.8 mm) BIAXIALLY DRAWN WITH IN-PLANE SHEAR DEFORMATION

	Shear Deformation (G_1)			Shear Deformation (G_2)		
Drawing Temperature (^{o}C)	80	90	100	80	90	100
% Linear shrinkage in boiling water	12.54	11.54	7.94	8.0	5.75	3.4

See Chapter 4, Section 4.2.3 (5 and 6) for calculation of the shear extension ratio for each geometry.

5.2.2 DSC Data

The DSC results for the biaxially drawn samples from non-nucleated and nucleated PET thick samples (0.80 mm) are shown in Figures 5.20-5.22 and in Tables 5.8-5.11. Figures 5.20 and 5.21 show the DSC traces for all the samples biaxially drawn without shear taken from the middle and shear region of DR = 2:1 and 3.5:1 respectively.

Figure 5.22 shows the DSC traces for the biaxially drawn nucleated PET thick samples (0.8 mm) at DR = 2:1.

The DSC results show that a very small heat of crystallisation, ΔH_c, is observed for the samples taken from the shear part of the biaxially drawn samples (these samples exhibit low shrinkage), whereas high H_c values are observed for samples in the middle (these samples exhibit high shrinkage). Figure 5.23 shows the DSC traces for all the samples biaxially drawn with superimposed shear deformation using both jigs G_1 and G_2.

TABLE 5.8: DSC DATA FOR THE NON-NUCLEATED PET THICK SHEETS (SAMPLES DRAWN BIAXIALLY WITH DR = 2:1)

	DT (°C)	ΔH_c (cal/g)	Tc (°C)	ΔH_f (cal/g)	Tm (°C)
Middle part	80	5.59	124.88	9.85	248.15
Shear part	80	2.13	106.10	10.90	248.15
Middle part	100	5.09	125.56	8.68	250.50
Shear part	100	2.98	115.19	10.55	249.18

TABLE 5.9: CRYSTALLINITY AND SHRINKAGE DATA FOR THE NON-NUCLEATED PET THICK SHEETS
(samples drawn biaxially with DR = 2:1)

	DT (°C)	% Linear shrinkage in boiling water	% Crystallinity (initial)	% Crystallinity (total)	Δ* Residual heat of crystallisation
Middle part	80	28.08	13.10	30.30	17.20
Shear part	80	7.33	26.98	33.54	6.55
Middle part	100	21.01	11.03	26.70	15.67
Shear part	100	4.33	23.27	32.46	9.19

Δ* is the difference between the total crystallinity achievable for a particular sample and the initial crystallinity.

% initial crystallinity is the crystallinity present in the drawn sample:

$$\% \text{ crystallinity initial} = \frac{\Delta H_f - \Delta H_c}{32.5} \times 100$$

where 32.5 is ΔH_f in cal/g for the pure crystal.

TABLE 5.10: DSC DATA FOR THE NUCLEATED PET THICK SHEET (SAMPLES DRAWN BIAXIALLY WITH DR = 2:1)

	DT (°C)	ΔH_c (cal/g)	Tc (°C)	ΔH_f (cal/g)	Tm (°C)
Middle part	80	4.98	121.88	8.78	250.00
Shear part		0.64	120.10	9.52	250.51
Middle part	90	6.03	128.05	9.58	250.32
Shear part		2.25	117.94	9.84	251.29

Note: Nucleated specimens could not be drawn at 100°C and above due to thermal crystallisation occurring during drawing

TABLE 5.11: CRYSTALLINITY AND SHRINKAGE DATA FOR THE NUCLEATED PET THICK SHEET (samples drawn biaxially with DR = 2:1)

	DT (°c)	% Linear shrinkage in boiling water	% crystal-linity (initial)	% crystal-linity (total)	Δ^* residual heat of crystal-lisation
Middle part	80	35.7	11.68	27.01	15.33
Shear part		18.35	27.33	29.29	1.96
Middle part	90	31.00	10.94	29.48	18.54
Shear part		16.35	23.35	30.28	6.93

Δ^* is the difference between the total crystallinity achievable for a particular sample and the initial crystallinity

TABLE5.12: DSC DATA FOR ENICHEM BOTTLES

	T_g (^oC)	T_c (^oC)	ΔH_c (cal/g)	T_m (^oC)	ΔH_m (cal/g)
Preform	80	144.93	4.774	254.38	9.562
Top region (B)	78	148.00	6.583	252.10	10.113
Middle region (A)	78	100.12	2.354	256.56	11.17

See Figure 4.1 for regions A and B.

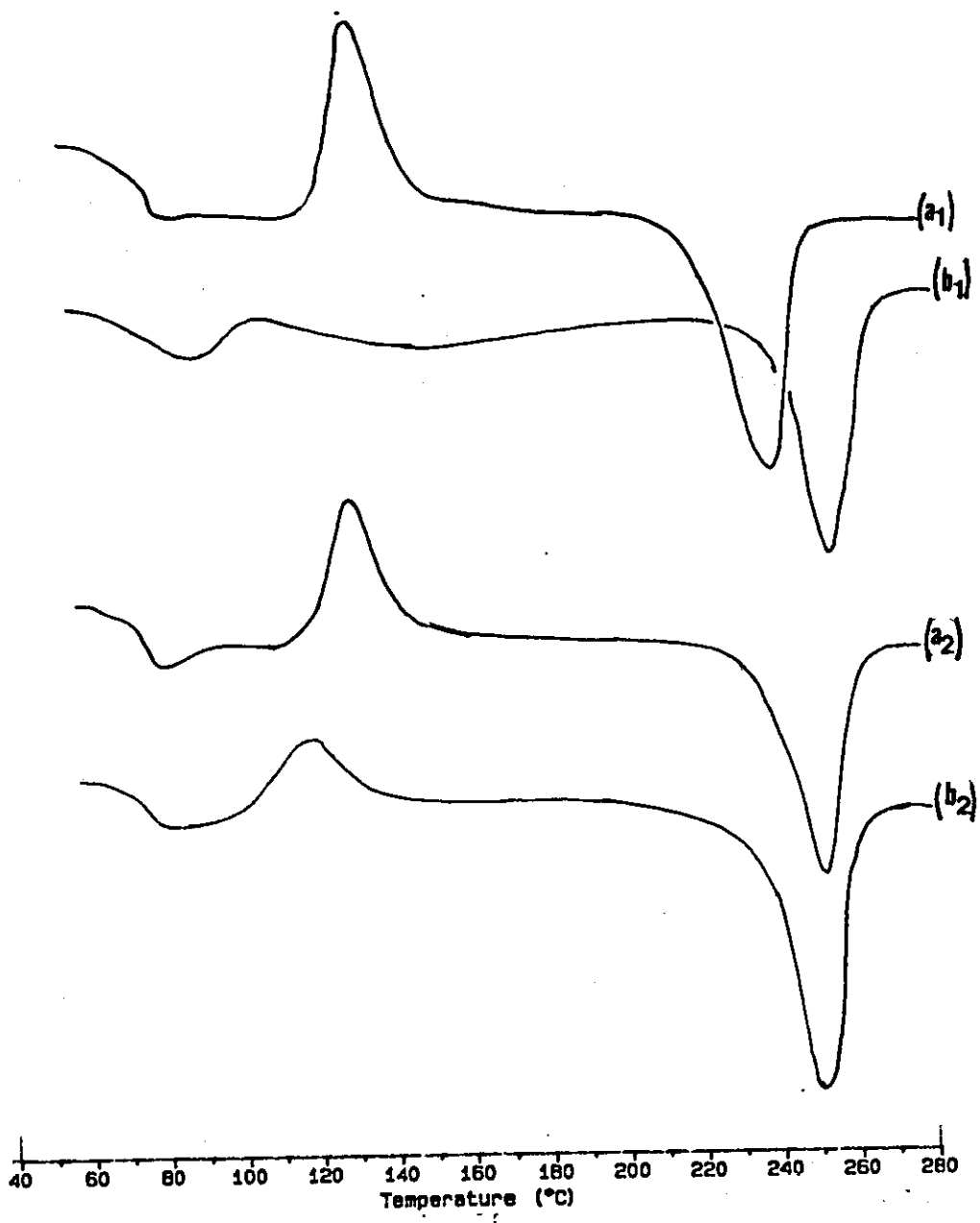

FIGURE 5.20: DSC traces at 20°C/min heating rate of non-nucleated thick PET samples (0.8 mm) biaxially drawn for DR = 2:1 at 80°C (a_1, a_2); and 90°C (b_1, b_2)
a) samples taken from the middle region
b: samples taken from the shear region

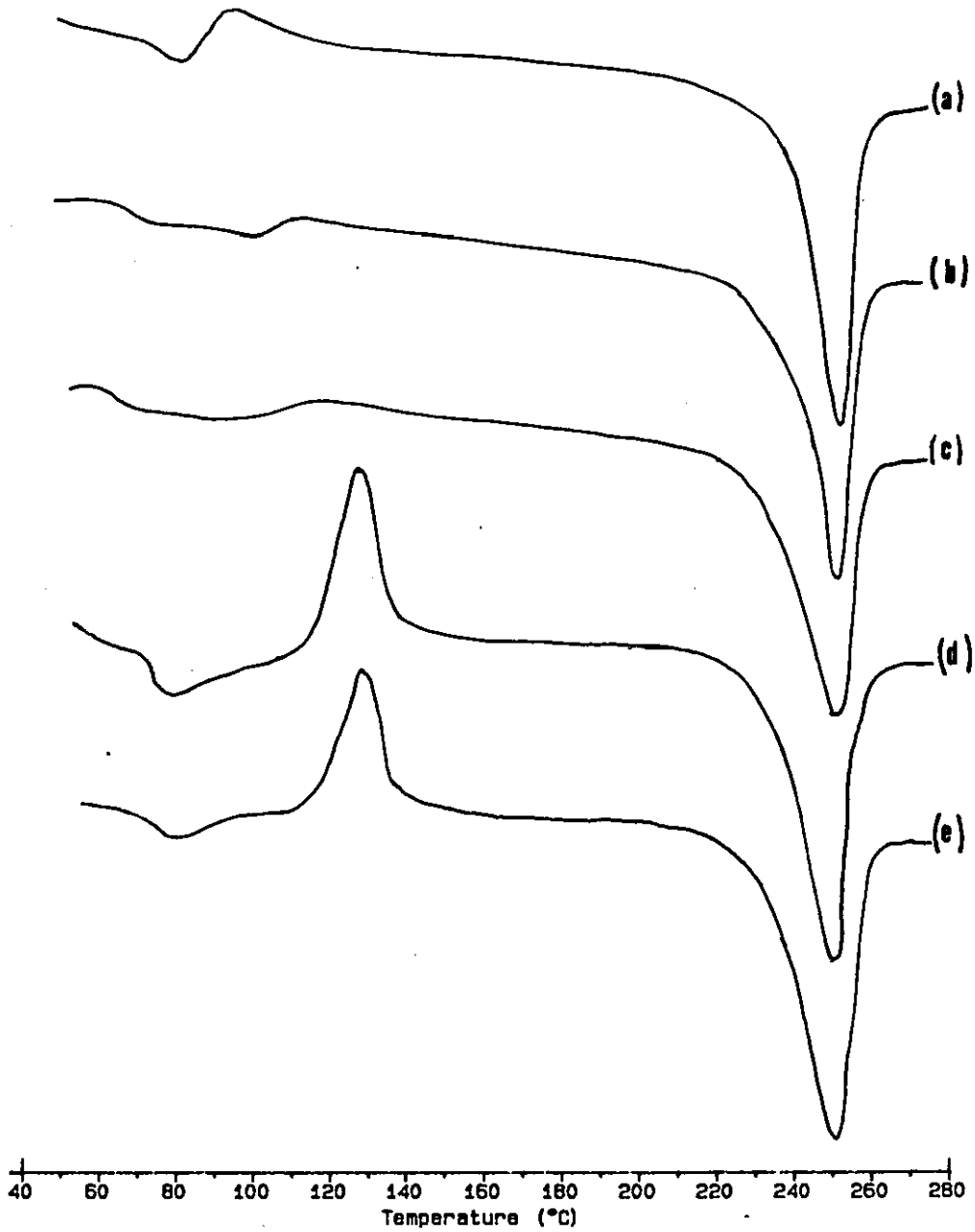

FIGURE 5.21: DSC traces at 20°C/min heating rate of the samples taken from the middle of non-nucleated thick PET samples (0.8 mm) biaxially drawn at DR = 3.5:1
a) TD = 80°C; (b) TD = 90°C; (c) TD = 100°C; (d) TD = 110°C; (e) TD = 125°C

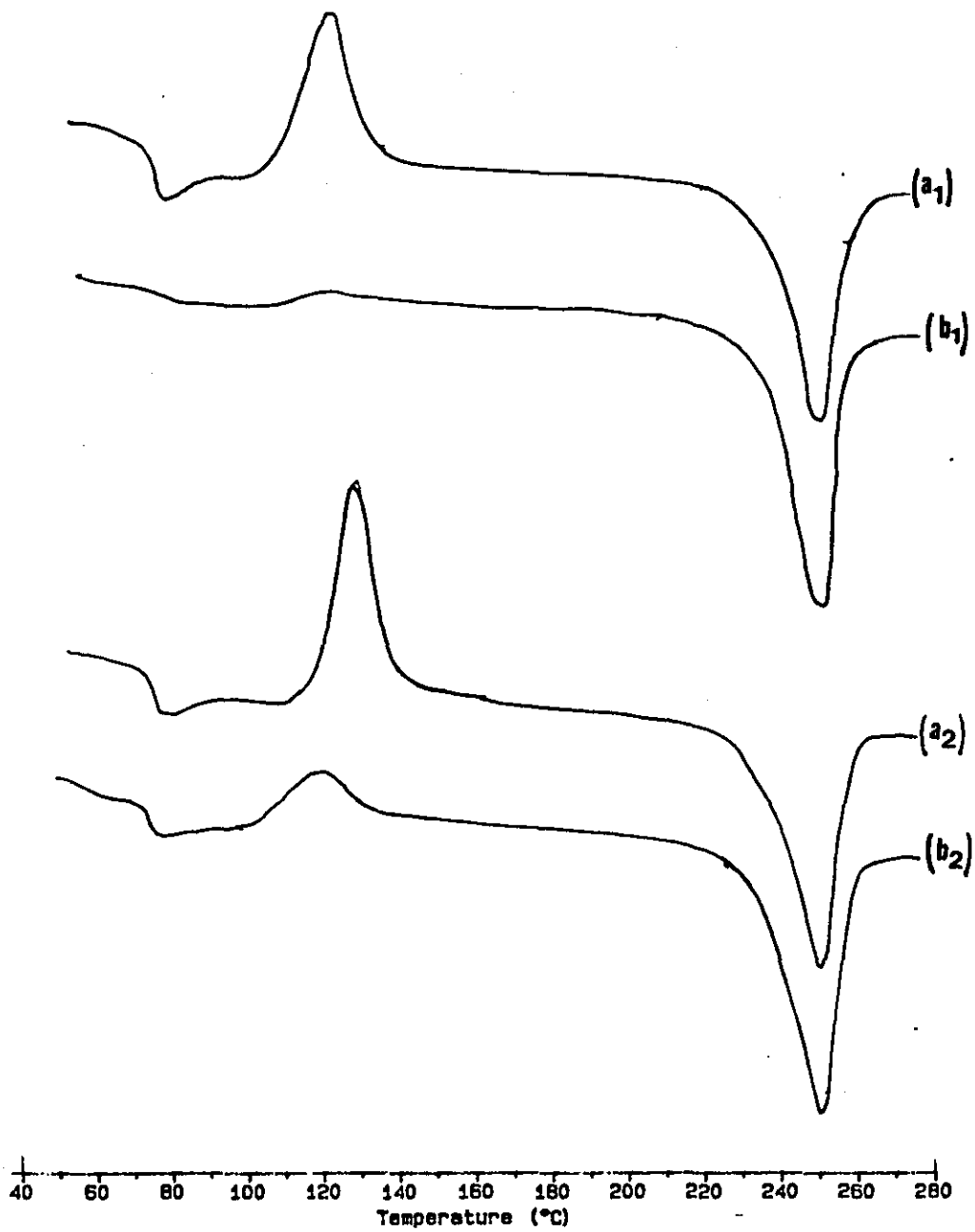

FIGURE 5.22: DSC traces at 20°C/min heating rate of nucleated thick PET samples (0.8 mm) biaxially drawn for DR = 2:1 at 80°C (a_1, a_2) and 90°C (b_1, b_2).
a) samples taken from the middle region
b) samples taken from the shear region

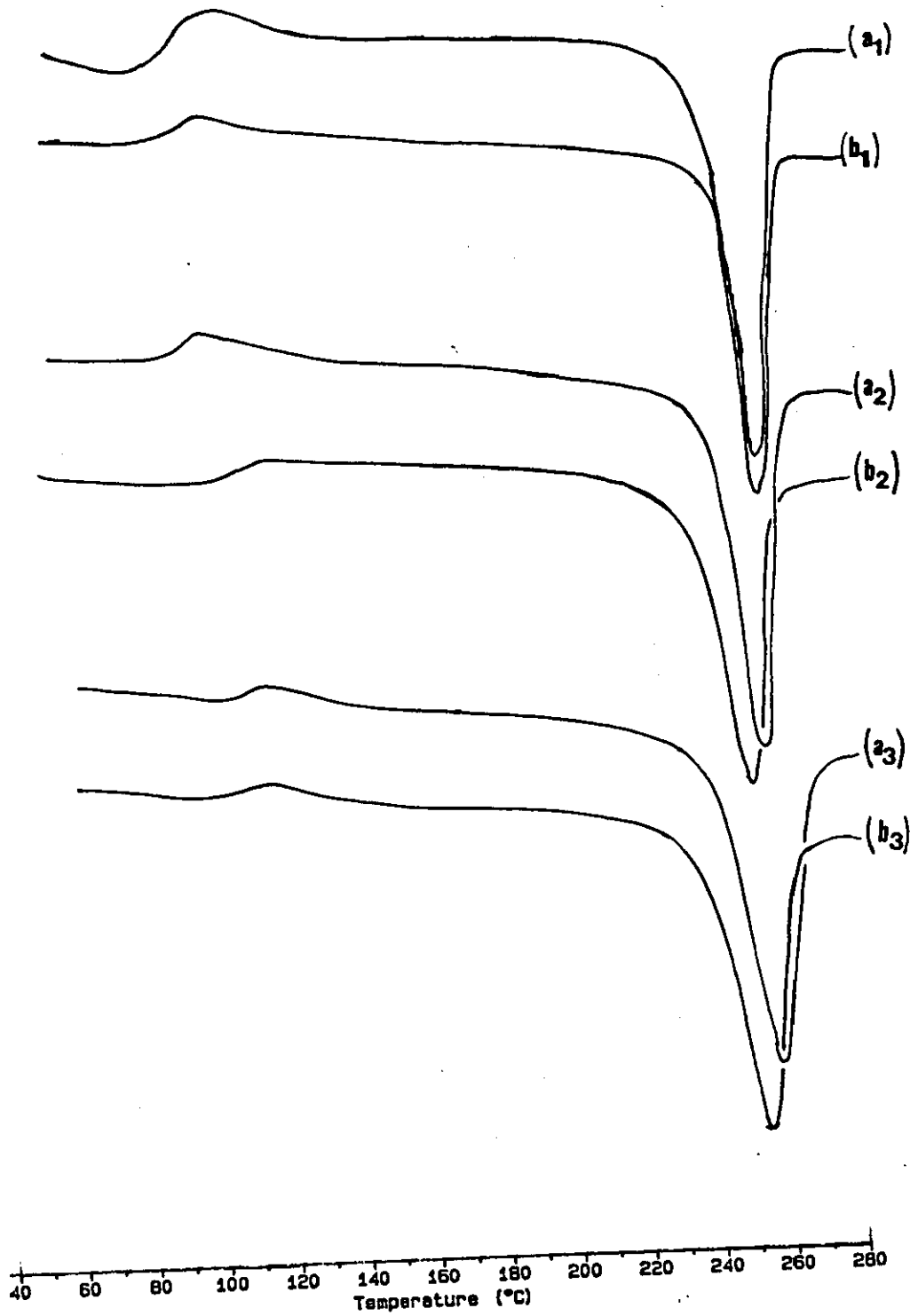

FIGURE 5.23: DSC traces at 20°C/min heating rate for non-nucleated thick PET samples (0.8 mm) biaxially drawn with superimposed shear deformations at (1) 80°C; (2) 90°C; (3) 100°C; (a) G_1 samples; (b) G_2 samples

5.3 EVALUATION OF BLENDS

5.3.1 Shrinkage at High Temperatures

To increase the Tg of PET, which was hypothesised as a possible way of increasing dimensional stability in the range 85-100°C, a small amount of polycarbonate (PC) and polyarylate (PA) (i.e. 4%) were blended with PET, adding 1% phenoxy as a possible compatibiliser as it can react easily with both polymers. The shrinkage results in boiling water for the blends listed below, which were biaxially drawn at DR = 2:1 and 3.5:1 are presented in Figures 5.24 (a) and (b) respectively.

F_1 poly(ethylene terephthalate) (PET) (100)

F_2 poly(ethylene terephthalate)/polycarbonate/phenoxy (PET/PC/PH) (95/4/1)

F_3 Poly(ethylene terephthalate)/polyarylate/phenoxy (PET/PA/PH) (95/4/1)

F_4 poly(ethylene terephthalate)/phenoxy/sodium benzoate (PET/PH/NaB) (95/4/0.1).

The addition of 5% masterbatch (i.e. PC/PH or Par/PH, 4%/1%) in PET was not sufficient to increase the Tg of the blend, which was believed to be the reason for not observing a reduction in shrinkage as shown in Figure 5.24(a) and (b). Consequently 20% masterbatch was blended with PET as for the formulations listed below:

(F_5) poly(ethylene terephthalate)/polycarbonate/phenoxy (PET/PC/PH) (80/16/4)

(F_6) poly(ethylene terephthalate)/polycarbonate (PET/PC) (80/20)

(F_7) poly(ethylene terephthalate)/polyarylate (PET/PA) (80/20)

(F_8) poly(ethylene terephthalate/polyarylate/phenoxy (PET/PA/PH) (80/16/4)

(F_9) poly(ethylene terephthalate/polyarylate/polycarbonate (PET/PA/PC) (80/10/10).

(F_{10}) poly(ethylene terephthalate/polycarbonate/polyacrylate/phenoxy (PET/PC/PA/PH) (80/8/8/4).

The shrinkage results in boiling water for these formulations biaxially drawn with DR = 2:1 and 3.5:1 are presented in Figure 5.25(a) and (b) respectively.

Figures 5.25(a) and (b) show that the percentage shrinkage follows the same trend as that in Figure 5.24 and in some cases even higher than that of PET. It is worth noting however, that by using phenoxy with PA and PC the samples achieve greater extensibility, especially at 100°C where samples of binary blends PET/PC and PET/PA (80/20) were not stretchable at DR = 3.5:1.

By increasing the amount of PC and PA in PET blends a high Tg was obtained but the amount of crystallinity was lower than for PET alone. Therefore to minimise the reduction in crystallinity of PET in PET/PA blends it was thought to be necessary to inhibit the ester-exchange reaction by using 1% stabiliser (organophosphite) and 0.2% of nucleating agent (NaB) in subsequent formulations.

The shrinkage results in boiling water for these blends, (see list below), which were biaxially drawn at DR = 3.5:1 are presented in Figure 5.26:

(F_{11}) poly(ethylene terephthalate)/polyarylate/phenoxy (PET/Par/PH) (80/18/2)

(F_{12}) poly(ethylene terephthalate)/polyarylate/phenoxy (PET/Par/PH (80/18/2) + 0.2% NaB + 1% S

(F_{13}) poly(ethylene terephthalate)/polyarylate (PET/Par) (70/30)

(F_{14}) poly(ethylene terephthalate)/polycarbonate (PET/PC) (70/30)

(F_{15}) poly(ethylene terephthalate)/polyarylate (PET/Par) (70/30) + 0.2% NaB + 1% S

(F_{16}) poly(ethylene terephthalate)/polyarylate/phenoxy (PET/Par/PH) (70/28/2)

(F_{17}) poly(ethylene terephthalate)/polyarylate/phenoxy (PET/Par/PH) (70/28/2) + 0.2% NaB + 1% S

Note that only formulations F_{13} and F_{15} could be stretched to 3.5:1, all the other blends exhibited a very low stretchability.

Shrinkage results in boiling water for these two formulations (i.e. PET/Par (70/30) are shown in Figure 5.26.

It is interesting to note that the stabilised blend F_{15} shows a shrinkage behaviour very similar to that of PET (although a little higher), whereas for the unstabilised sample shrinkage is almost double at both draw ratios. Moreover, these samples could not be drawn even to 2:1 at 80°C, while when stretched at 90°C they became hazy showing signs of microvoiding. On the other hand at 100°C, 110°C, 120°C and 130°C, the samples remained transparent. The haziness of the samples drawn at 90°C is due to the fact that they have been drawn below the Tg, and is different from the opacity observed when samples crystallise thermally.

Hypothesising that if the shrinkage temperature is lower than the Tg of the drawn sample the level of shrinkage can be considerably reduced, shrinkage tests were subsequently carried out at 85°C.

The results presented in Figure 5.26(a) show a lower shrinkage which is in fact obtained at 85°C rather than in boiling water, but it is still high, confirming once more that the important factor to decrease shrinkage is to reduce the amount of residual crystallisability of the polymer after drawing and not to increase the Tg.

To test further this last hypothesis, PET was blended with polymetaxylene adipamide (MXD6), which is a crystalline and incompatible polymer but produces transparent blends in combination with PET.

Shrinkage results in boiling water for the MXD6 based formulations (listed below), biaxially drawn at draw ratios = 3.5:1 are presented in Figure 5.27.

(F_{18}) poly(ethylene terephthalate)/polymetaxylene adipate/phenoxy (PET/MXD6/PH) (80/18/2)
(F_{19}) poly(ethylene terephthalate)/polymetaxylene adipate (PET/MXD6) (80/20)
(F_{20}) poly(ethylene terephthalate)/polymetaxylene adipate (PET/MXD6) (70/30)
(F_{21}) polymetaxylene adipate (MXD6) (100) control.

By adding 30% MXD6 to PET shrinkage decreases drastically at all drawing temperatures and a much lower shrinkage than for PET alone is

obtained at drawing temperatures in the range 100°C-120°C.
Possibly the dispersed MXD6 phase nucleates the stress-induced crystallisation in the surrounding PET matrix.

At 20% addition of MXD6 shrinkage becomes lower than that of PET only at drawing temperatures above 100°C.

For MXD6 alone the shrinkage reaches a minimum at 90-100°C, but above 100°C increases very rapidly whereas for PET shrinkage continues to decrease up to a draw temperature of 120°C.

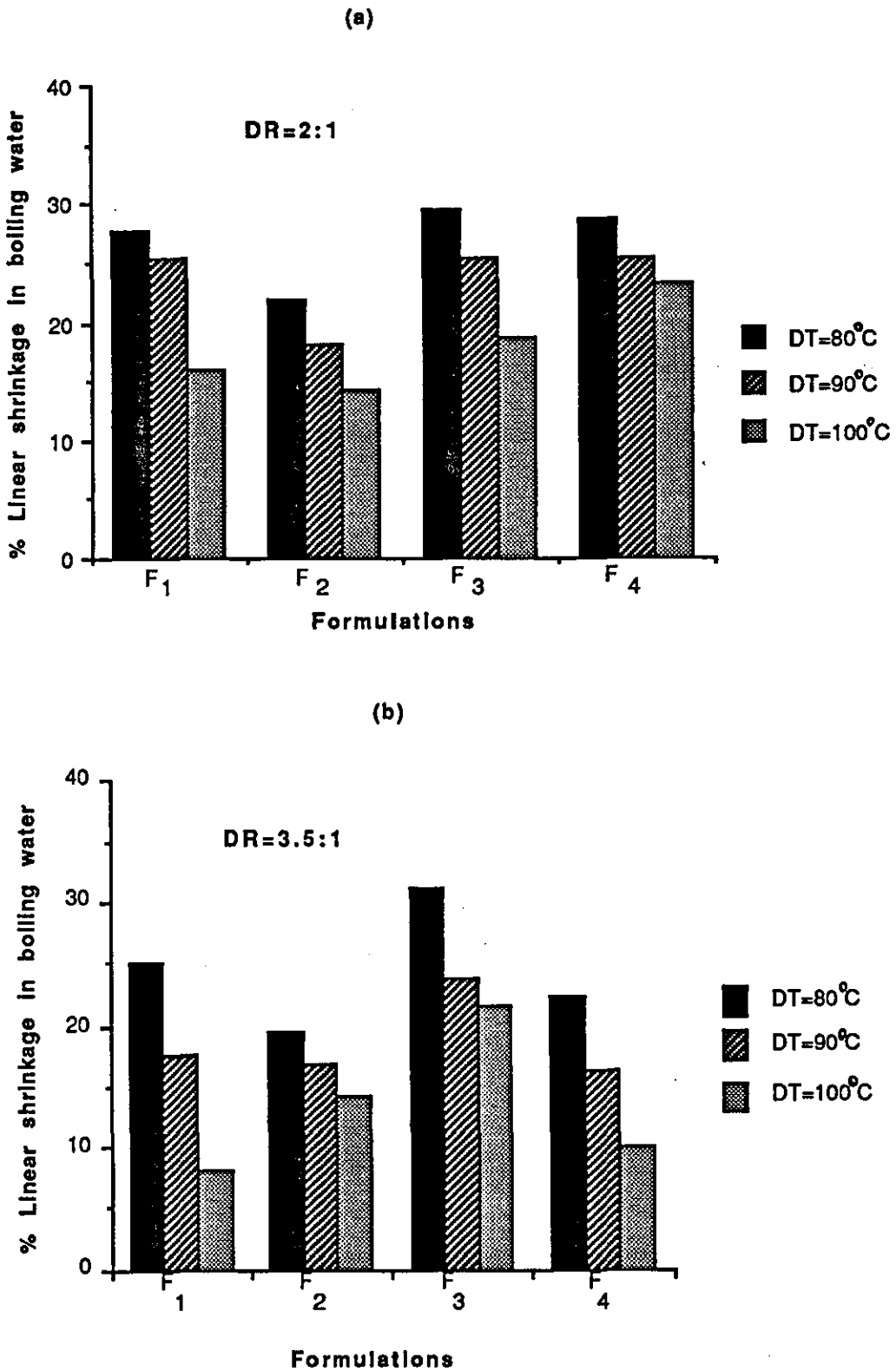

Figure5.24: Relationship between drawing conditions and shrinkage for the biaxially drawn F1(PET),F2(PET/PC/PH)(95/4/1), F3(PET/PA/PH)(95/4/1),F4(PET/PH/Nab)(95/4.9/0.1)

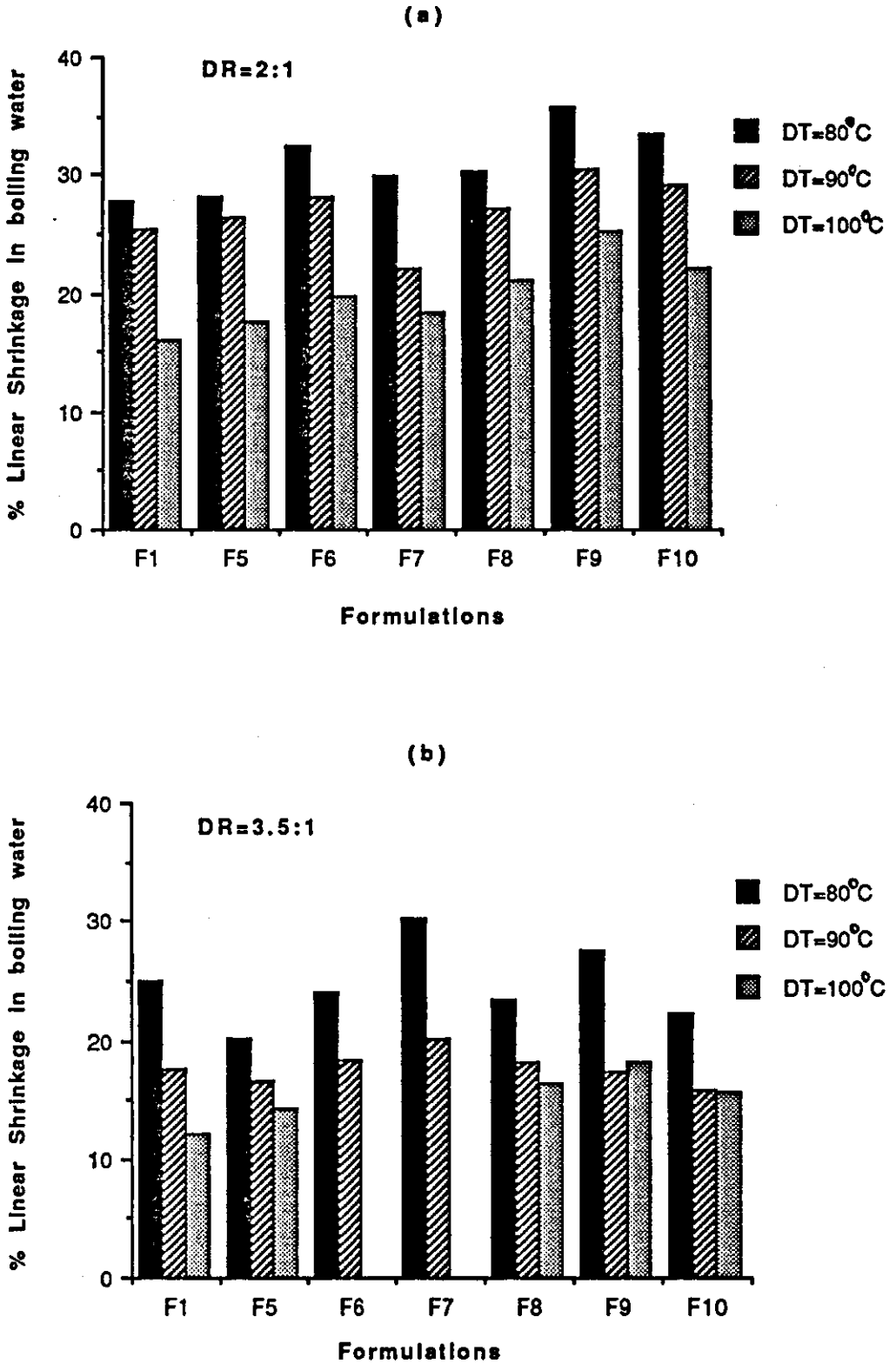

Figure5.25: Relationship between drawing conditions and linear shrinkage of biaxially drawn F1(PET), F5(PET/PC/PH)(80/16/4), F6(PET/PC)(80/20),F7(PET/PA)(80/20), F8(PET/PA/PH)(80/16/4), F9(PET/PC/PA)(80/10/10/),F10(PET/PC/PA/PH)(80/8/8/4)

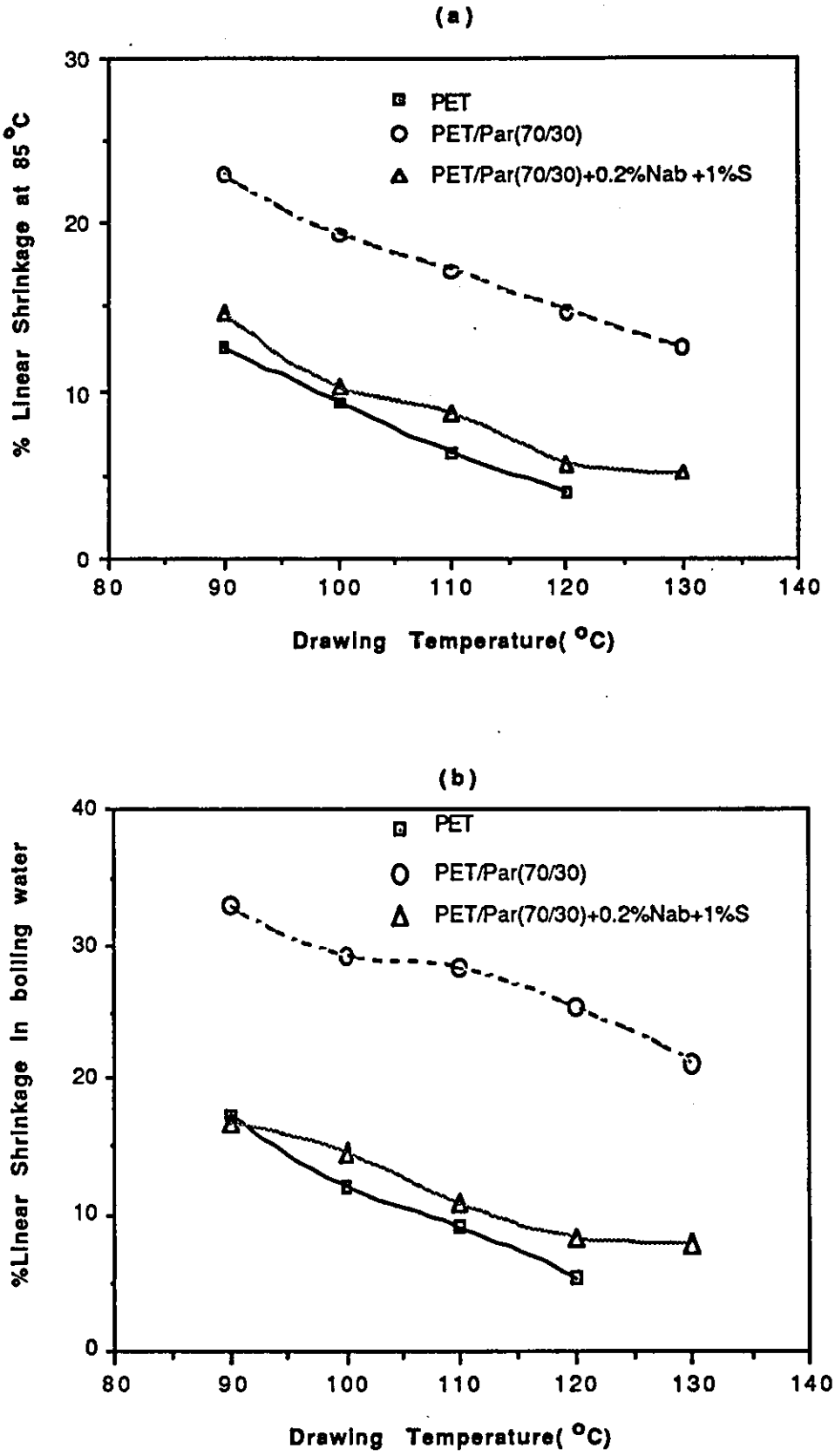

Figure5.26: Relationship between drawing conditions and linear shrinkage of biaxially drawn PET/Par blends at a draw ratio 3.5:1 (samples taken from the middle of the specimens)

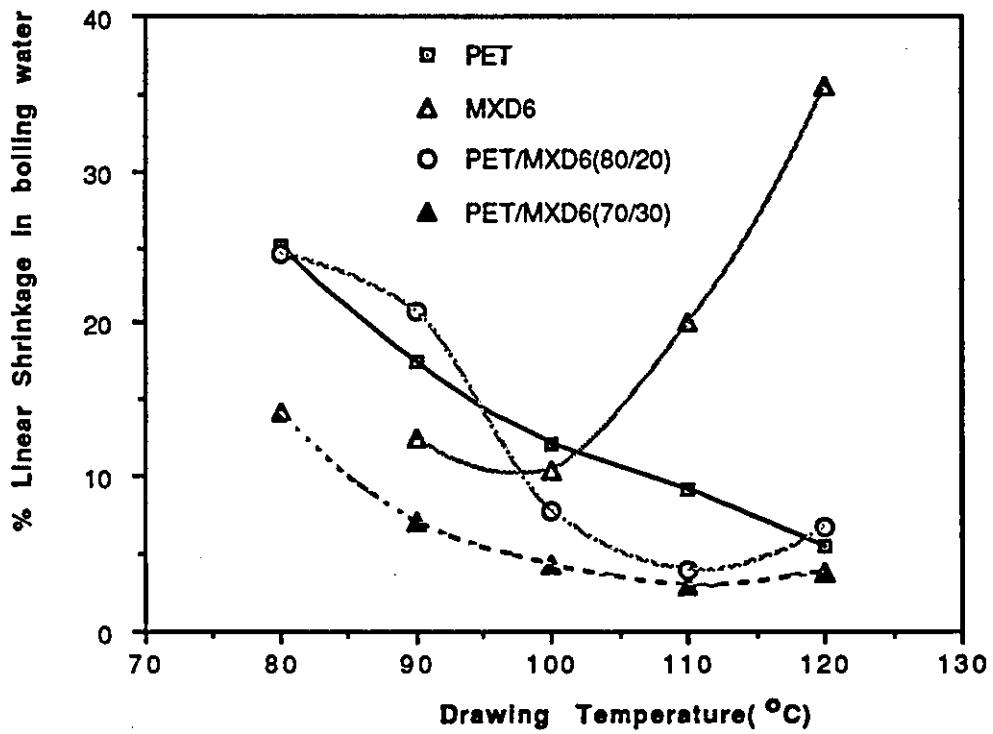

Figure5.27: Effect of drawing conditions on linear shrinkage of biaxially drawn PET/MXD6 blends at draw ratio 3.5:1 (samples taken from the middle of the specimens)

5.3.2 DSC Data

The DSC results of the injection moulded plaques for the blends containing small amounts of PC and PA (i.e. F_2, F_3, F_4) are shown in Figure 5.28 and Table 5.13.

These results show that very little change in the Tg of the PET has occurred, with the exception of formulation F_2 (i.e. PET/PC/PH, 95/4/1) for which Tg is increased to 85°C. One notes that this particular formulation has a lower crystallinity than the others. Surprisingly the other blends have similar crystallinity as pure PET and the melting point for all the blends is the same as that of PET (i.e. 254°C) indicating that the soluble amorphous polymer is being excluded from the crystallisation of PET.

TABLE 5.13: DSC DATA FOR INJECTION MOULDED PLAQUES OF PET BLENDS

Formulations		DSC data				
No	Type	Tg (°C)	Tc (°C)	ΔH_c (cal/g)	Tm (°C)	ΔH_f (cal/g)
F_1	PET (100)	75	133.10	7.06	254.82	11.29
F_2	PET/PC/PH (95/4/1)	85	133.48	4.62	254.64	7.21
F_3	PET/Par/PH (95/4/1)	78	128.83	7.75	254.24	12.19
F_4	PET/PH/NaB (95/4.9)/ 0.1)	76	124.09	6.85	253.44	11.22

The DSC results for the injection moulded plaques of the blends containing larger amounts of amorphous compatible polymer blends (i.e. F_5, F_6, F_7, F_8, F_9, F_{10}) are presented in Figure 5.29 and Table 5.14.

The DSC traces show that the cold crystallisation temperature (Tc) of all these blends increases slightly in comparison to that of the pure PET, except for blends of formulations F_9 (PET/PC/PA = 80/10/10) and F_{10} (PET/PC/PA/PH = 80/8/8/4) where a slight decrease of Tc is observed (see Table 5.13). The glass transition temperature (Tg) for all the blends, however, is somewhat higher than for PET, while the heat of fusion is much lower.

Note that more precise values of Tg (albeit higher) have been obtained by DMA tests than by DSC analysis. Moreover the heat of fusion (ΔH_f) for the PET/PA/PH (80/16/4) blend is very low compared to all the other blends and to PET, which exhibits the highest heat of fusion.

TABLE 5.14: DSC AND DMA DATA FOR INJECTION MOULDED PLAQUES FOR PET BLENDS

Formulations		DMA Data	DSC Data			
No	Type	Tg (°C)	Tc (°C)	ΔH_c (cal/g)	Tm (°C)	ΔH_f (cal/g)
F_1	PET (100)	85	133.10	7.06	254.82	11.29
F_5	PET/PC/PH (80/16/4)	87	137.25	5.16	251.94	7.05
F_6	PET/PC (80/20)	88	139.09	4.95	248.67	7.84
F_7	PET/Par (80/20)	92	149.42	5.17	249.66	6.87
F_8	PET/Par/PH (80/16/4)	90	142.66	1.45	247.88	2.54
F_9	PET/PC/Par (80/10/10)	97	131.88	5.56	250.13	8.01
F_{10}	PET/PC/Par/PH (80/8/8/4)	90	130.17	3.29	247.73	4.61

The DSC results of the extruded pellets and the injection moulded plaques for the blends containing even larger amounts of amorphous

polymer (i.e. F_{12}, F_{13}, F_{14}, F_{15}, F_{16}) are presented in Figure 5.30 (a and b) and in Tables 5.15-5.16. The DSC traces of the extruded pellets show that for all the blends only one Tg is obtained, which is higher than the Tg of PET, while the cold crystallisation temperature (Tc) of all the blends increases and the heat of fusion (ΔH_f) decreases substantially in comparison to that of pure PET.

Unlike the case of previous blends the melting temperature (Tm) decreases by about 5°C to 10°C (see Table 5.15). These high levels of compatible glassy polymer are found to affect considerably the crystallisation behaviour of PET.

Moreover after injection moulding the crystallisation and melting peaks for formulations F_{13} (PET/PA = 70/30) and F_{15} (PET/PA = (70/30) + 0.2% NaB + 1% S) disappear completely, suggesting that these blends become amorphous (or exhibit a very low crystallisation rate) as a result of chemical reactions between the various components during injection moulding. These formulations also showed the highest Tg.

TABLE 5.15: DSC DATA OF EXTRUDED PELLETS

Formulations		Tg (°C)	Tc (°C)	ΔH_c (cal/g)	Tm (°C)	ΔH_f (cal/g)
F_1	PET (100)	75	125.88	6.31	251.54	9.19
F_{12}	PET/Par/PH (80/18/2)+0.2%NaB+1%S	83	140.54	5.72	249.06	7.81
F_{13}	PET/Par (70/30)	92	178.98	5.50	247.55	4.87
F_{14}	PET/PC (70/30)	80	153.99	4.93	253.81	6.85
F_{15}	PET/Par (70/30)+0.2%NaB+1%S	88	152.07	3.92	247.62	4.23
F_{16}	PET/Par/PH (70/28/2)	85	149.84	4.90	147.19	5.81

TABLE 5.16: DSC AND DMA DATA OF INJECTION MOULDED PLAQUES

Formulations		DMA Data	DSC data			
No	Type	Tg (°C)	Tc (°C)	ΔH_c (cal/g)	Tm (°C)	ΔH_f (cal/g)
F_1	PET (100)	85	133.10	7.06	254.82	11.29
F_{12}	PET/Par/PH (80/18/2)+ 0.2% NaB+1%S	97	160.92	5.23	231.14	5.27
F_{13}	PET/Par (70/30)	105	N.A.	0	N.A.	0
F_{14}	PET/PC (70/30)	95	178.29	5.23	242.15	6.00
F_{15}	PET/Par (70/30)+ 0.2% NaB+1%S	100	N.A.	0	N.A.	0
F_{16}	PET/Par/PH (70/28/2)	99	178.44	1.16	225.16	3.60

The DSC results for the blends containing MXD6 are presented in Figure 5.31 and Table 5.17.

The DSC traces of the injection moulded plaques do not reveal any difference in Tg values for PET and PET/MXD6 blends but a slight decrease in ΔH_c values and ΔH_f is observed with the blends. By adding 2% phenoxy to PET/MXD6 containing 80% PET (F_{17}) the Tg as well as the Tc value decreased relative to the values for PET/MXD6 (80/20) blend. Two melting temperatures (Tms) are observed, however, for all PET/MXD6 blends; the lower melting temperature being associated with the MXD6 phase, whilst the higher peak is associated with PET. Moreover a very low crystallisation temperature is observed for MXD6 injection moulded plaques, which confirm the possibility of MXD6 having a stress induced nucleating effect on PET, in PET/MXD6 blends.

TABLE 5.17: DSC DATA OF THE INJECTION MOULDED PLAQUES

Formulations	Tg (°C)	Tc (°C)	ΔH_c (cal/g)	Tm (°C)	ΔH_f (cal/g)
F_1 PET (100)	75	133.10	7.06	254.82	11.29
F_{17} PET/MXD6/PH (80/18/2)	78	134.30	6.27	253.47	9.71
F_{19} PET/MXD6 (80/20)	80	137.32	6.71	255.95	9.94
F_{20} PET/MXD6 (70/30)	80	133.13	6.83	252.30	11.41
F_{21} MXD6 (100)	70	114.26	7.41	243.83	18.44

For the biaxially drawn PET/MXD6 (70/30) blends the DSC results are presented in Figure 5.32 and Table 5.18. These show that the Tg has been decreased considerably over the values of the samples before drawing, and that two crystallisation temperatures (Tcs) are observed; the lower crystallisation temperature being associated with MXD6 phase, and the higher Tc being the one associated with PET.

TABLE 5.18: DSC DATA OF THE BIAXIALLY DRAWN PET/MXD6 (70/30) BLEND AT DR = 3.5:1

Drawing Temp (°C)	Tg (°C)	Tc (°C)	ΔH_c (cal/g)	Tm (°C)	ΔH_f (cal/g)	% Crystal-linity
90	58	70.05 98.61	0.26 1.24	252.01	8.72	22.22
100	58	70.74 111.87	0.46 5.39	251.91	14.17	25.6
110	58	72.10 119.29	0.32 5.57	252.64	14.73	27.2
120	58	71.93 122.51	0.26 5.29	251.70	15.21	29.72

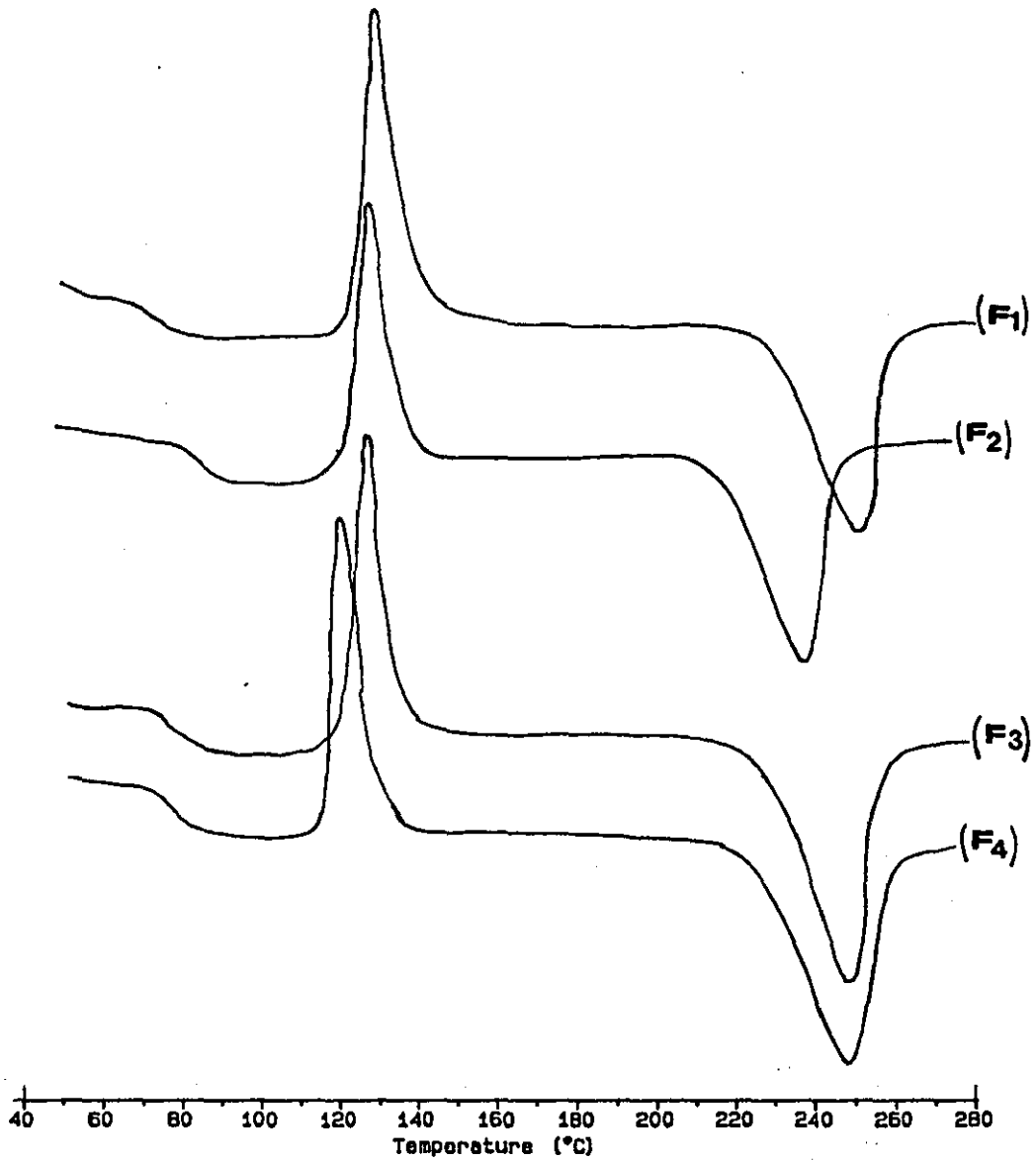

FIGURE 5.28: DSC traces at 20°C/min heating rate of formulations F_1 (PET); F_2 (PET/PC/PH) (95/4/1); F_3 (PET/PA/PH) (95/4/1); F_4 (PET/PH/NaB) (95/4.9/0.1)

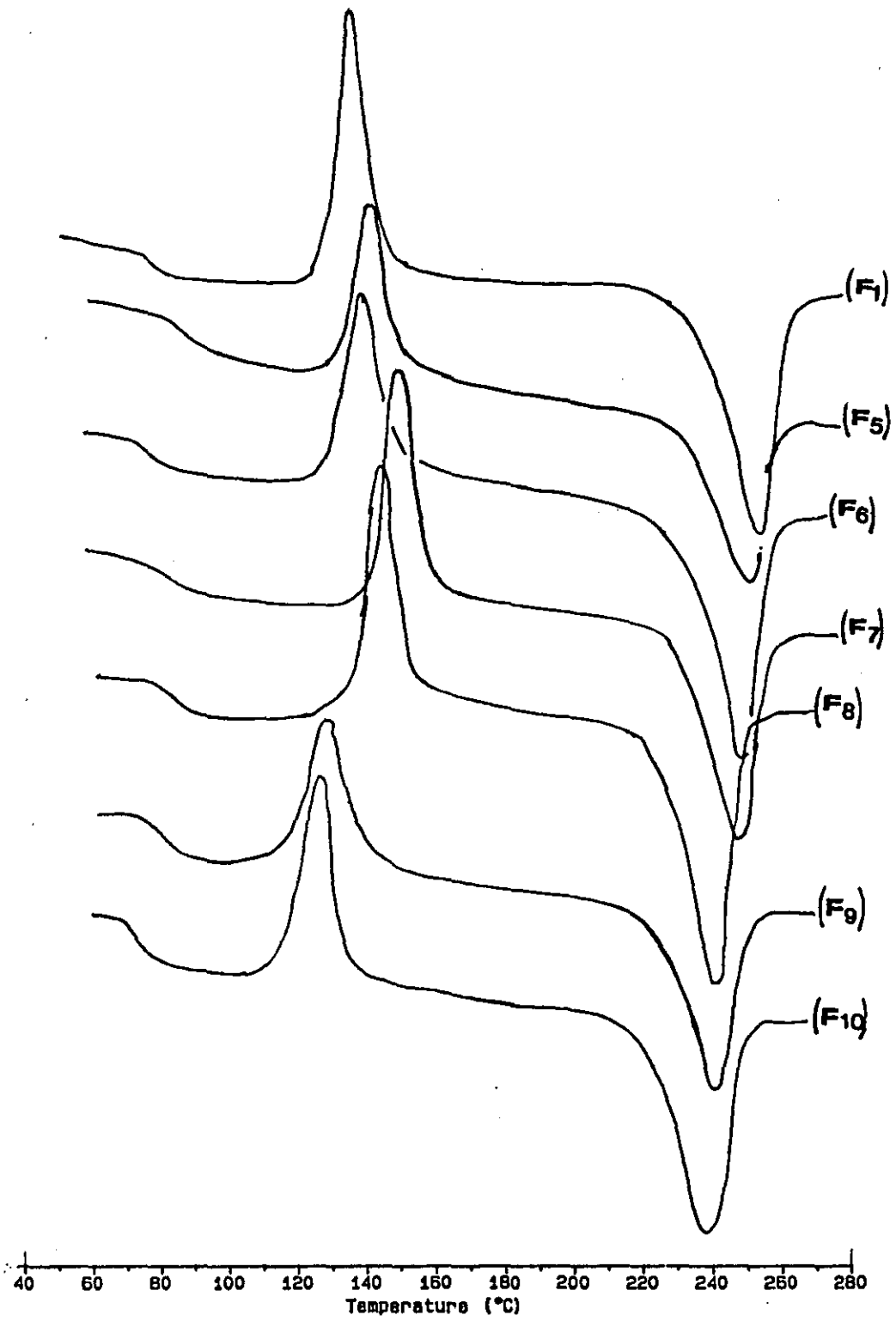

FIGURE 5.29: DSC traces at 20°C/min heating rate of formulations F_1 (PET); F_5 (PET/PC/PH) (80/16/4); F_6 (PET/PC) (80/20); F_7 (PET/PA) (80/20); F_8 (PET/PA/PH) (80/16/4); F_9 (PET/PC/PA (80/10/10); F_{10} (PET/PC/PA/PH) (80/8/8/4)

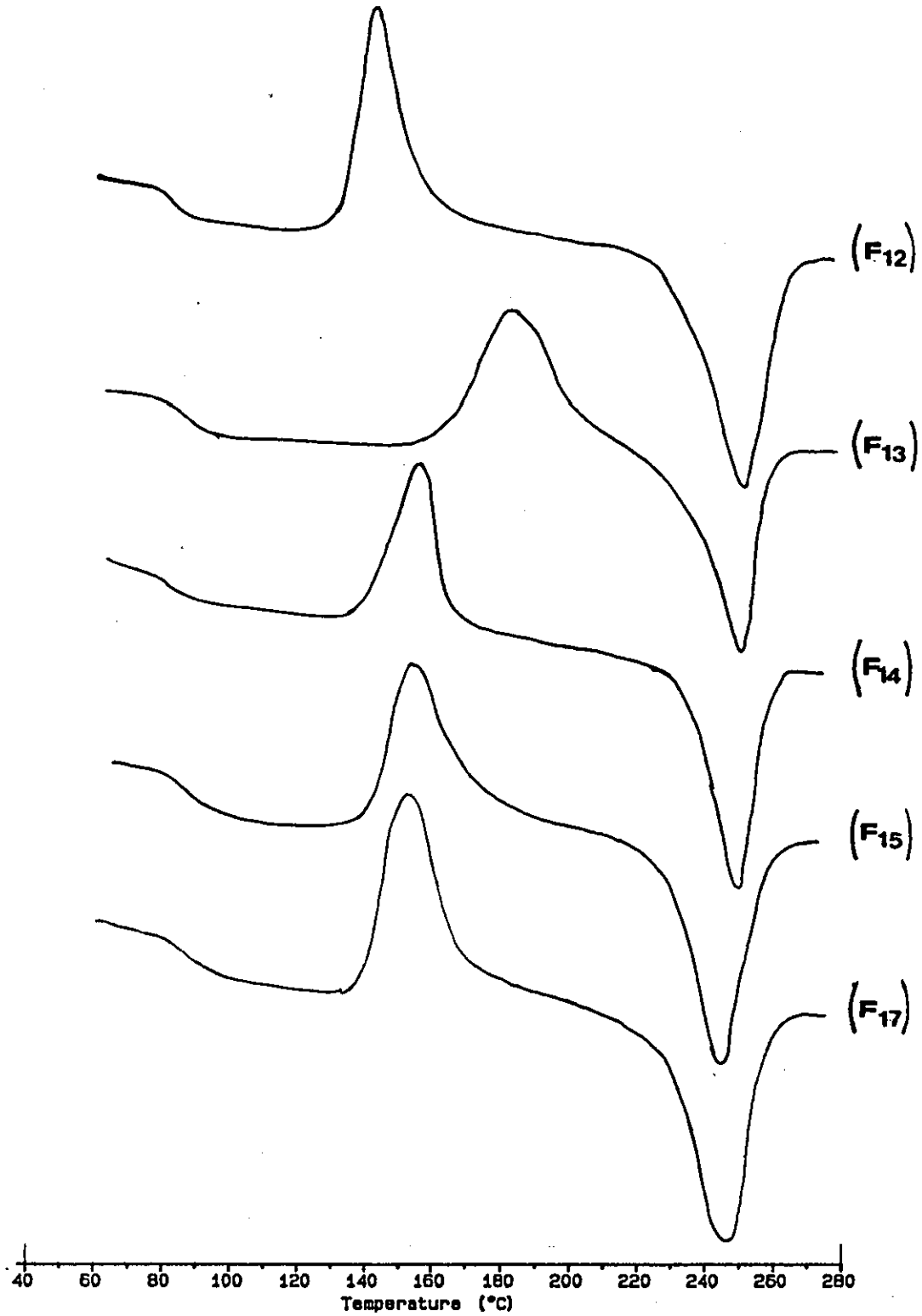

FIGURE 5.30(a): DSC traces at 20°C/min heating rate of the extruded pellets of formulations F_{12} (PET/PA/PH) (80/18/2) + 0.2% NaB + 1%S; F_{13} (PET/PA) (70/30); F_{14} (PET/PC) (70/30); F_{15} (PET/PA) (70/30) + 0.2% NaB + 1%S; F_{11} (PET/PA/PH) (70/28/2) + 0.2% NaB + 1%S

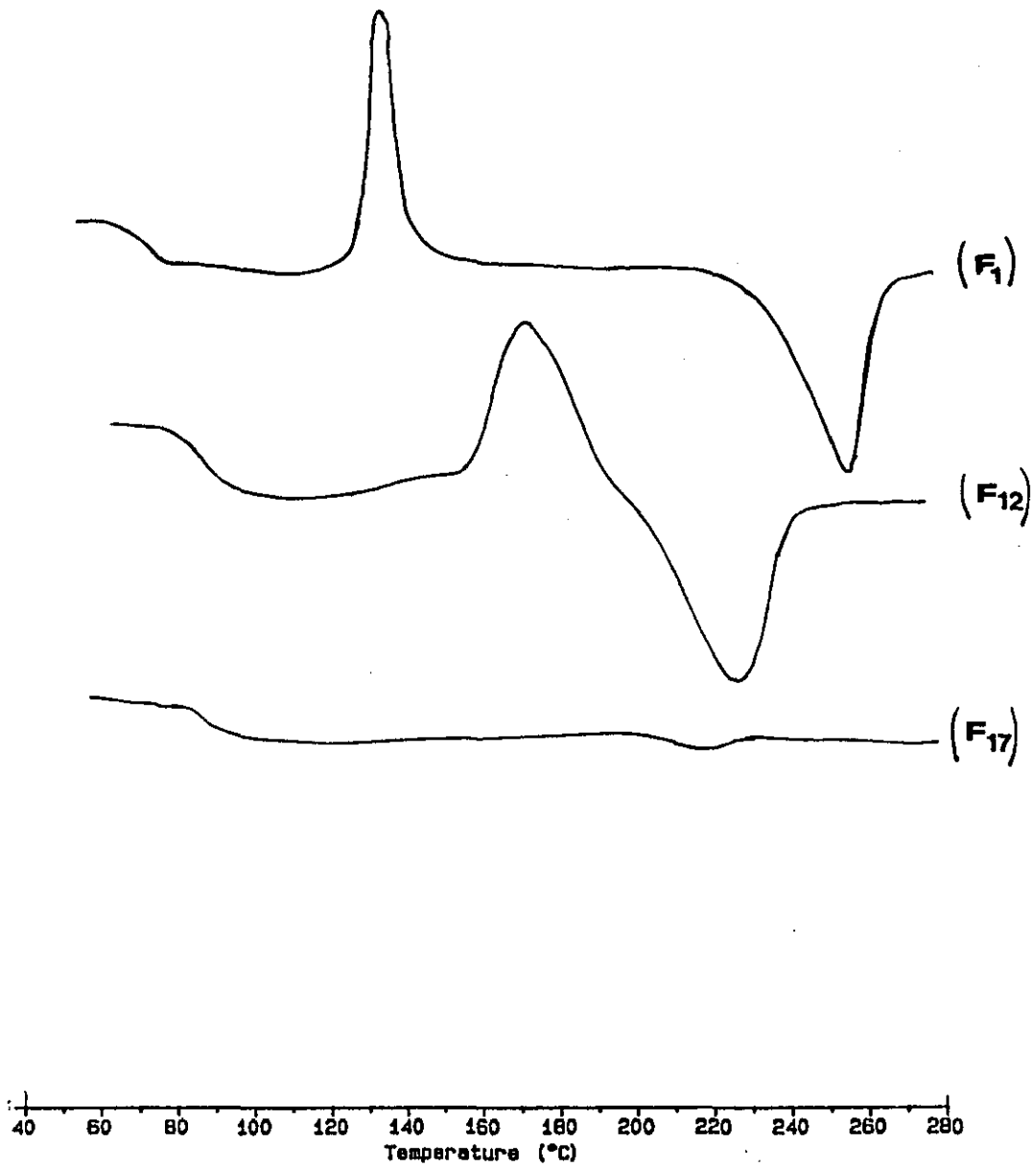

FIGURE 5.30(b): DSC traces at 20°/min heating rate of the injection moulded plaques of formulations: F_1 (PET); F_{12} (PET/PA/PH) (80/18/2) + 0.2% NaB + 1%S; F_{17} PET/PA/PH) (70/28/2) + 0.2% NaB + 1%S

Note that the Tg value of this drawn blend is much lower than that of drawn PET.

5.3.3 Morphology

The microstructure of the different blends (fractured in liquid nitrogen) was studied by scanning electron microscopy (SEM) and the results are presented in Figures 5.33-5.39. Figures 5.33, 5.36 and 5.35 show the SEM micrographs of the injection moulded plaques of PET, PET/PA/PH (80/16/4), PET/Par (80/20), PET/PC (80/20), PET/PC/PH (80/16/4), PET/PC/PA (80/10/10) and PET/PA/PC/PH (80/8/8/4) blends.

One one phase is observed for the binary blends, PET/PC and PET/PA (80/20). These blends were transparent and only one Tg value was recorded by the DMA tests. Moreover crazing marks over the fracture surface are observed for PET injection moulded plaques as well as for the blends PET/PC (80/20), PET/PA (80/20) and PET/PC/PA (80/10/10).

For the blends containing phenoxy, two phases are observed and the crazing phenomena is no longer observed.

Figures 5.37 and 5.38 show the SEM micrographs of the injection moulded plaques of the blends containing larger amounts of compatible polymers PET/PC (70/30), PET/PA (70/30), PET/PA (70/30 + 0.2% NaB + 1%S.

From Figure 5.37(a) and (b) we can see that crazing is more pronounced in the case of PET/PC (70/30) blends than of PET/PA (70/30) blends, but only one phase is observed for both blends. This observation could also be confirmed by the fact that only one Tg was recorded by the DMA tests.

From Figures 5.38(a), 5.39(b) and 5.40(b) we can see that by adding 0.2% NaB and 1% stabiliser to PET/Par blends two phases are clearly observed but the particle size of the dispersed phase (PA) is reduced, especially when phenoxy is added. This strongly suggests that solubilisation of PET and PA results from chemical reactions between the two components and the effectiveness of the stabiliser in inhibiting these reactions.

Figures 5.41, 5.42 and 5.43 show the SEM micrographs of the extruded pellets as well as the injection moulded plaques of PET/MXD6 (80/20), (70/30) and PET/MXD6/PH (80/18/2) blends. Although all these blends were transparent two distinct phases (MXD6 being dispersed aspherical particles) were observed owing to the total lack of miscibility.

The particle sizes of the extruded pellets seems to be much larger than those of the injection moulded plaques, which result from the difference in the shear rate in the two processes.

Figure 5.44 shows the SEM micrographs of the samples taken from the middle and the shear region of the biaxially drawn PET/MXD6 (70/30) blends. Elongated particles are observed as well as some separation of MXD6 particles from the matrix.

Note, however, that the ternary blends containing phenoxy this time do not exhibit the distinct precipitate particles observed for blends containing PC or PA, suggesting such precipitation does not result from the reaction of phenoxy with PET, but with PC or PA.

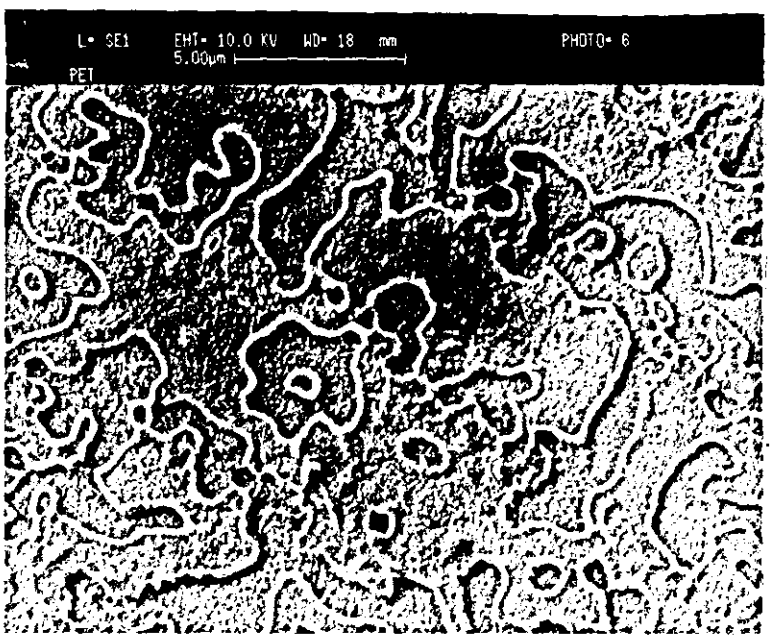

FIGURE 5.33: Scanning electron micrographs obtained from cryogenically fractured injection moulded PET plaques

(a)

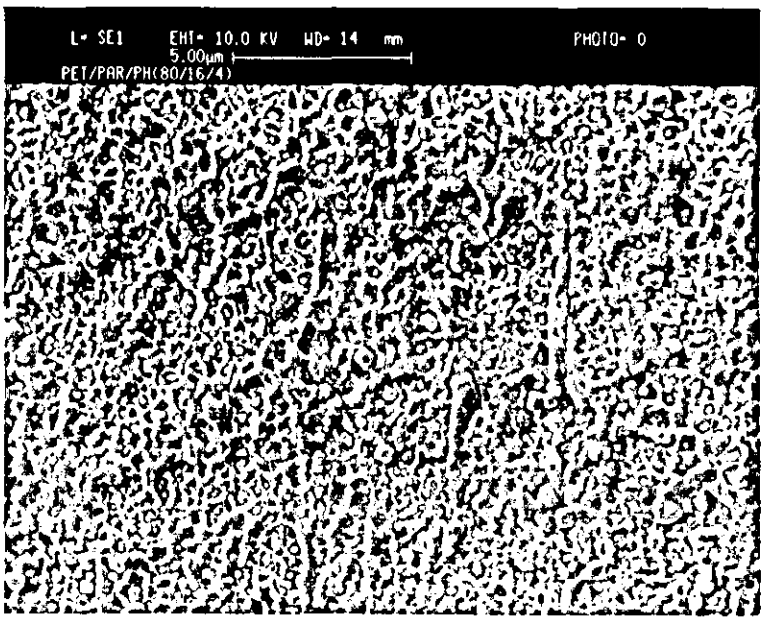

(b)

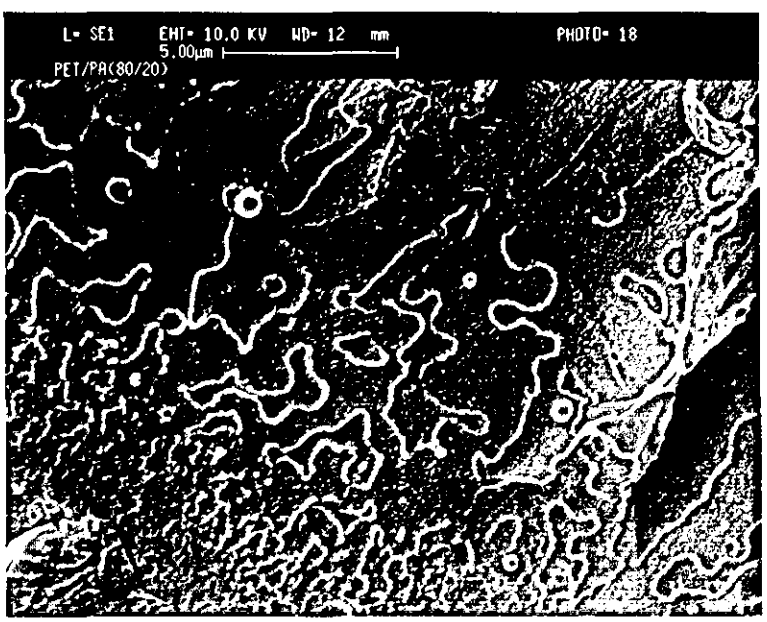

FIGURE 5.34: Scanning electron micrographs obtained from cryogenically fractured injection moulded plaques of PET blends: (a) PET/PA/PH (80/16/4) (b) PET/PA (80/20)

(a)

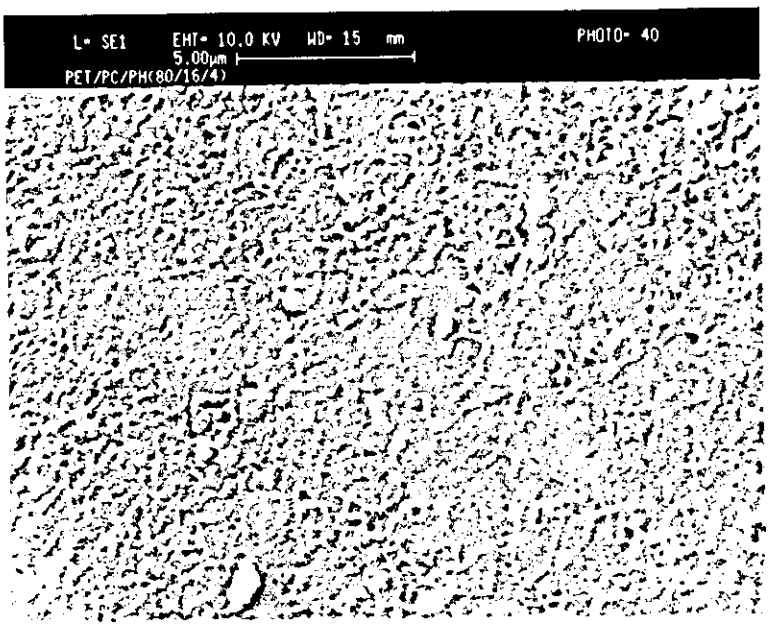

(b)

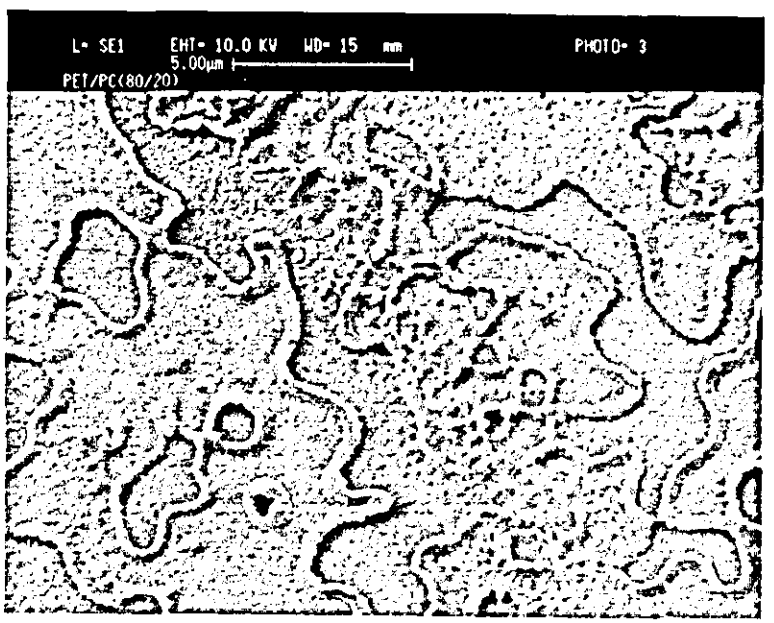

FIGURE 5.35: Scanning electron micrographs obtained from cryogenically fractured injection moulded plaques of PET blends: (a) PET/PC/PH (80/16/4) (b) PET/PC (80/20)

(a)

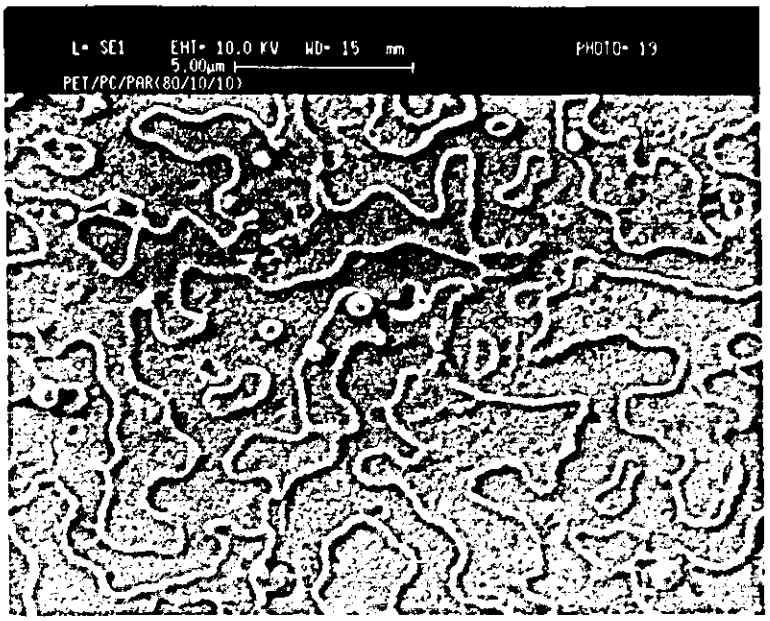

(b)

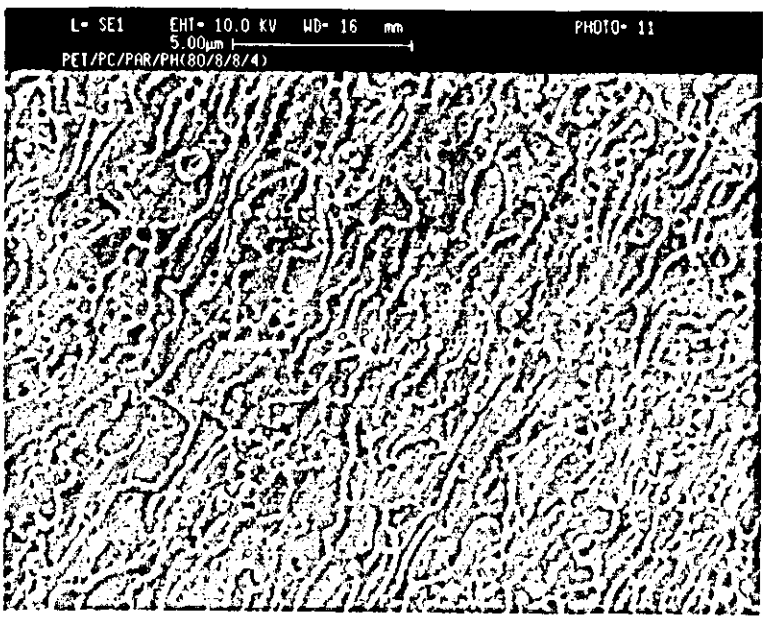

FIGURE 5.36: Scanning electron micrographs obtained from cryogenically fractured injection moulded plaques of PET blends: (a) PET/PC/PA (80/10/10), (b) PET/PC/PA/PH (80/8/8/4)

(a)

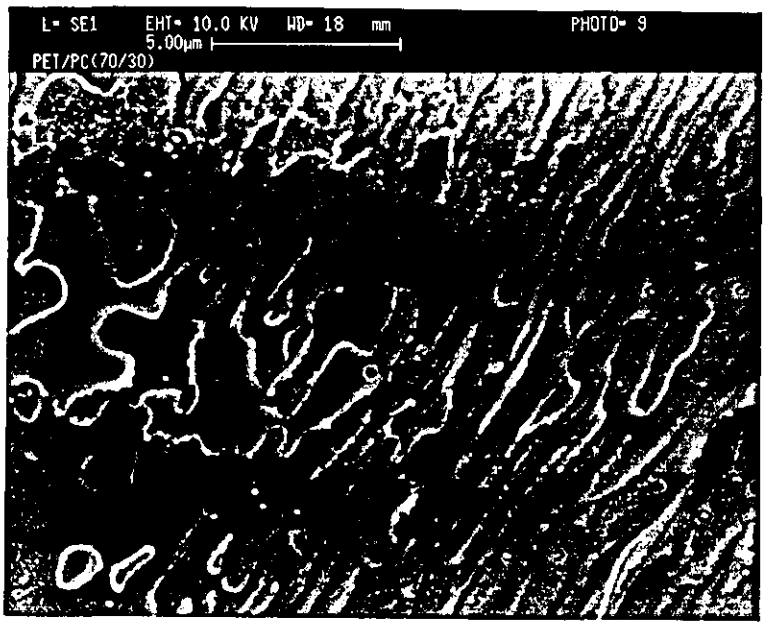

(b)

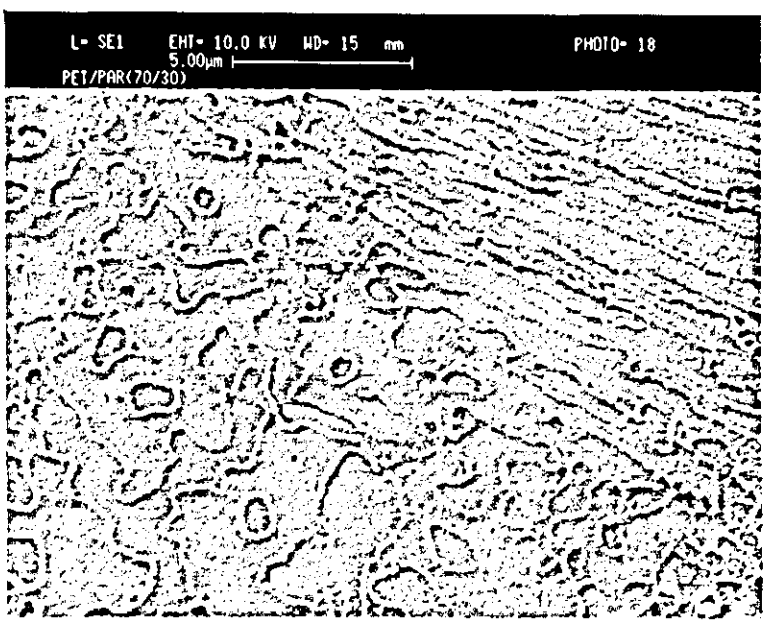

FIGURE 5.37: Scanning electron micrographs obtained from cryogenically fractured injection moulded plaques of PET blends: (a) PET/PC (70/30), (b) PET/PA (70/30)

(a)

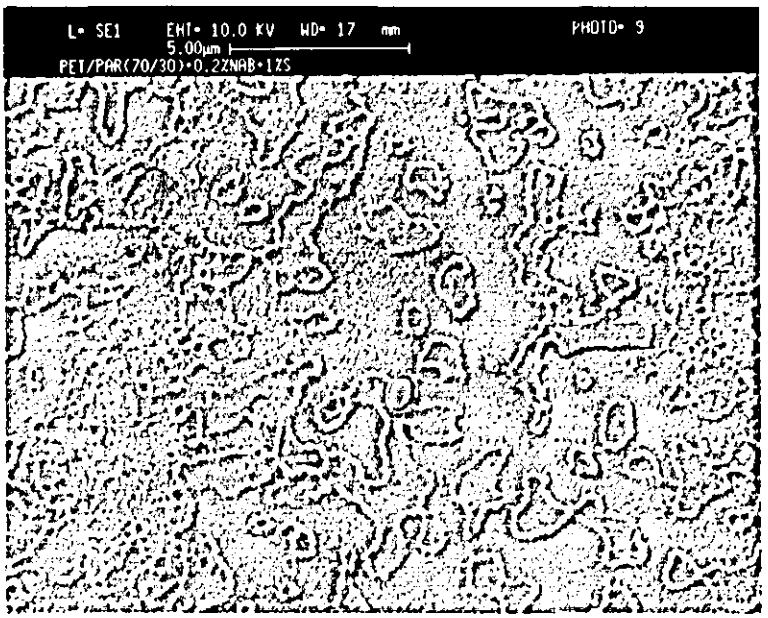

FIGURE 5.38: Scanning electron micrographs obtained from cryogenically fractured injection moulded plaques of PET blends: (a) PET/PA (70/30)+ 0.2% Nab +1% S

(a)

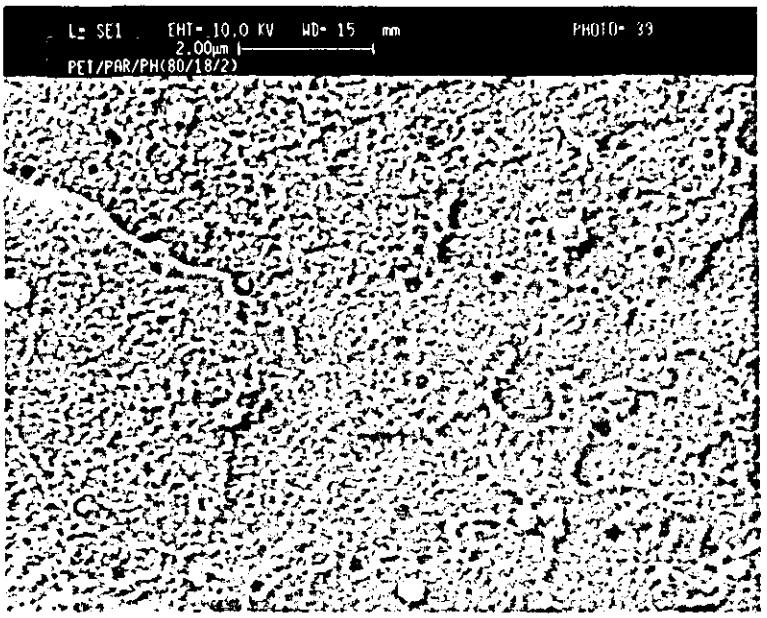

(b)

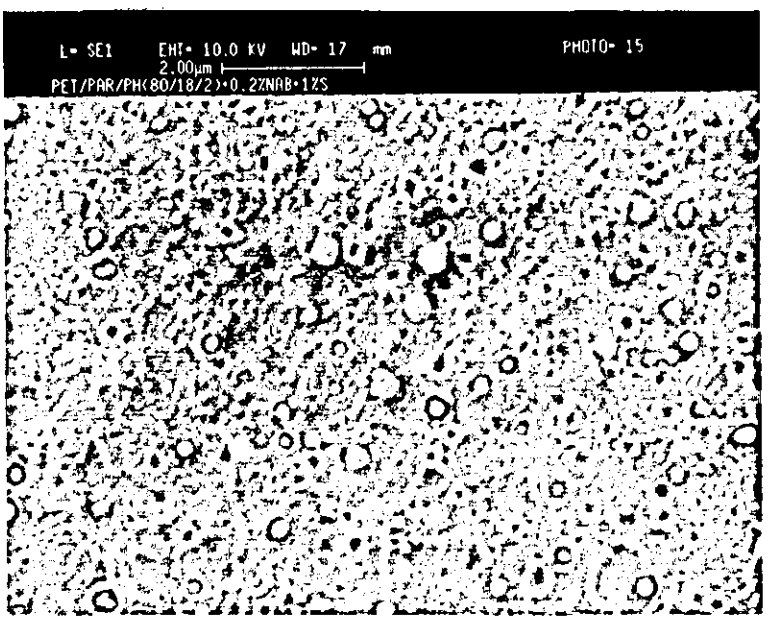

FIGURE 5.39: Scanning electron micrographs obtained from cryogenically fractured injection moulded plaques of PET blends: (a) PET/PA/PH(80/18/2), (b) PET/PA/PH (80/18/2) +0.2% Nab +1% S

(a)

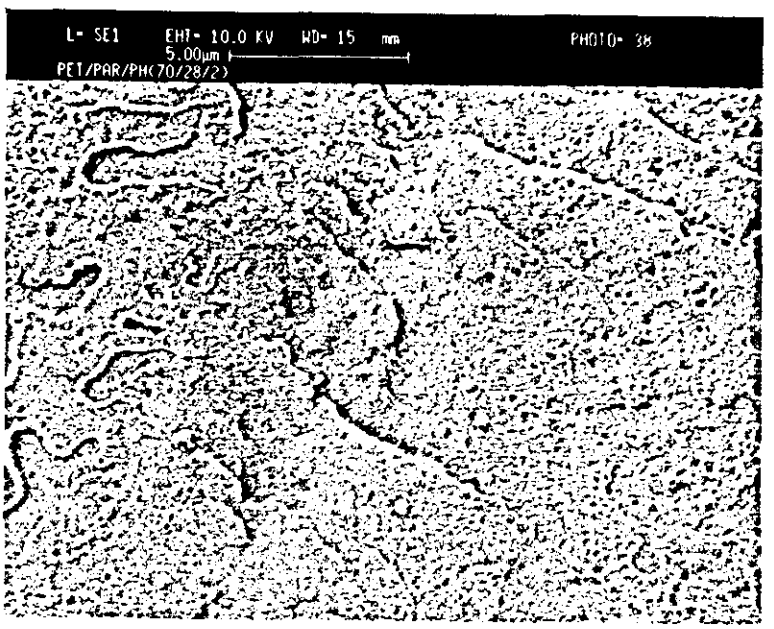

(b)

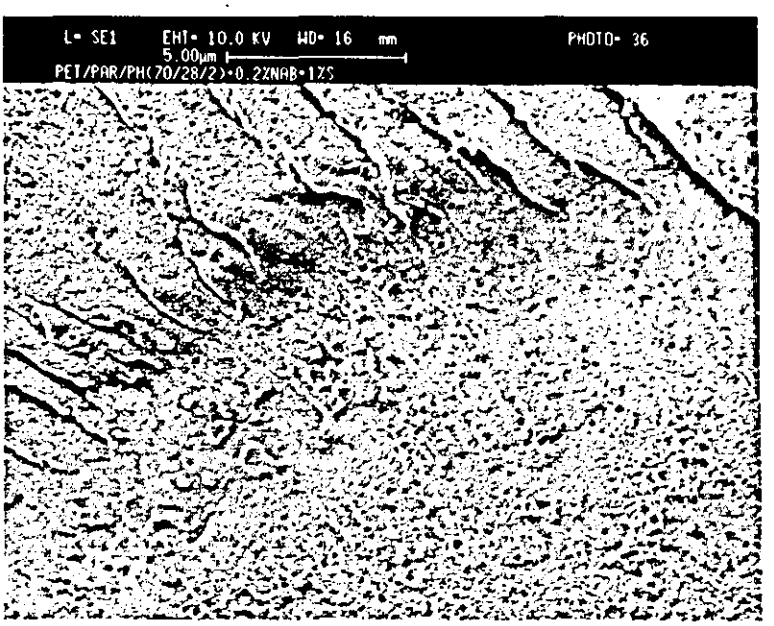

FIGURE 5.40: Scanning electron micrographs obtained from cryogenically fractured injection moulded plaques of PET blends: (a) PET/PA/PH (70/28/2), (b) PET/PA/PH (70/28/2)+0.2% Nab + 1%S.

(a)

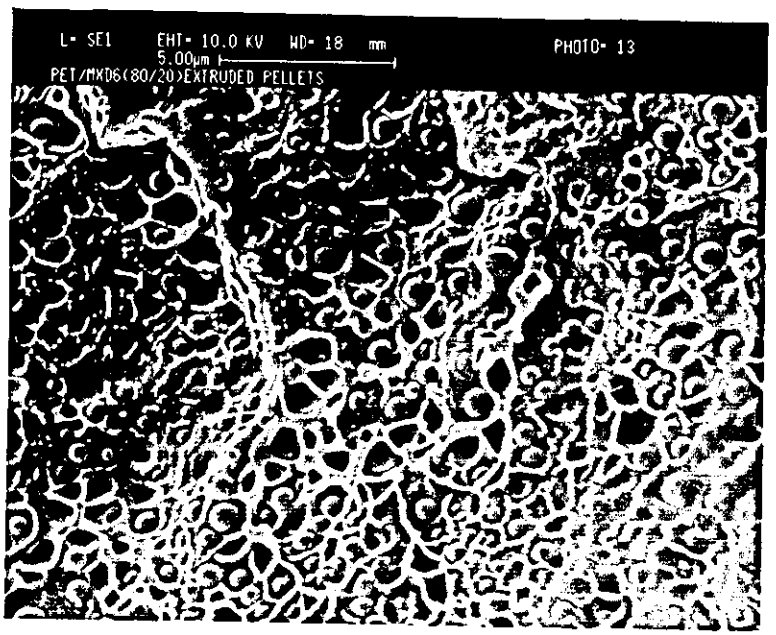

(b)

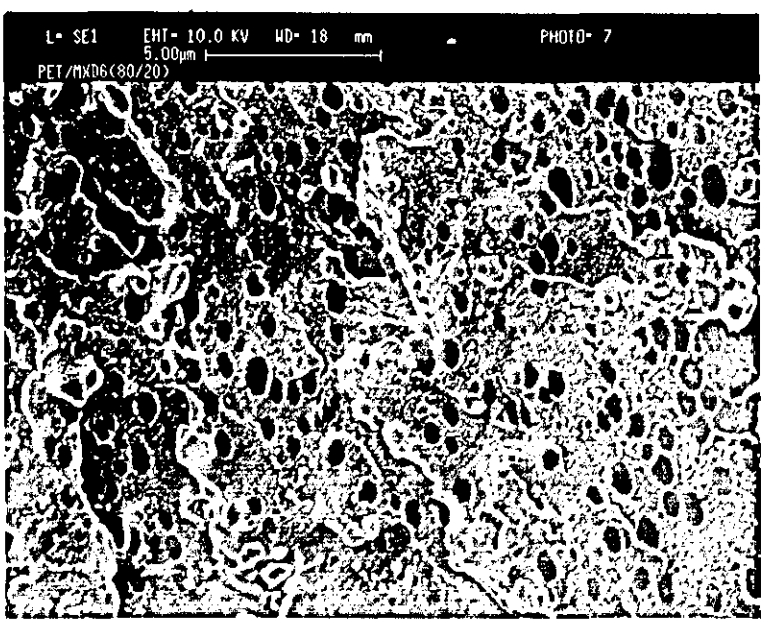

FIGURE 5.41: Scanning electron micrographs obtained from cryogenically fractures of PET/MXD6 (80/20) blend: (a) extruded pellets; (b) injection moulded plaques

(a)

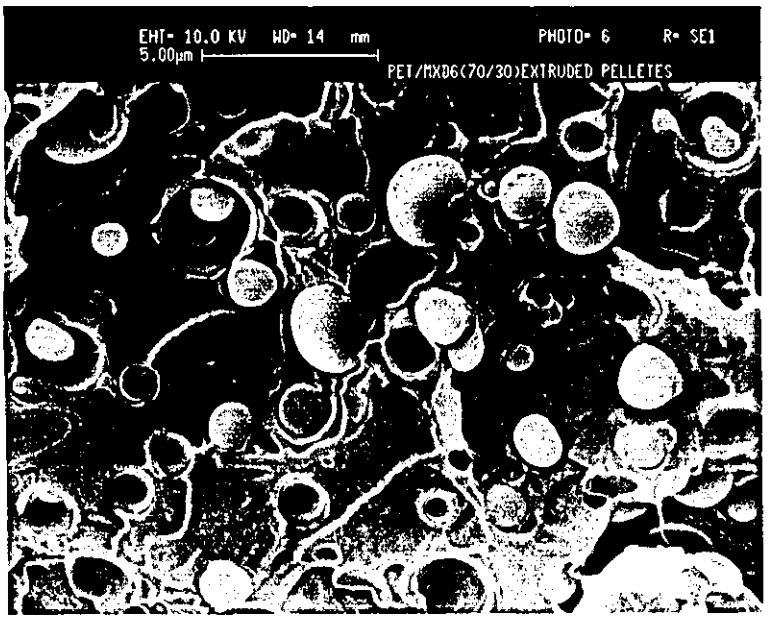

(b)

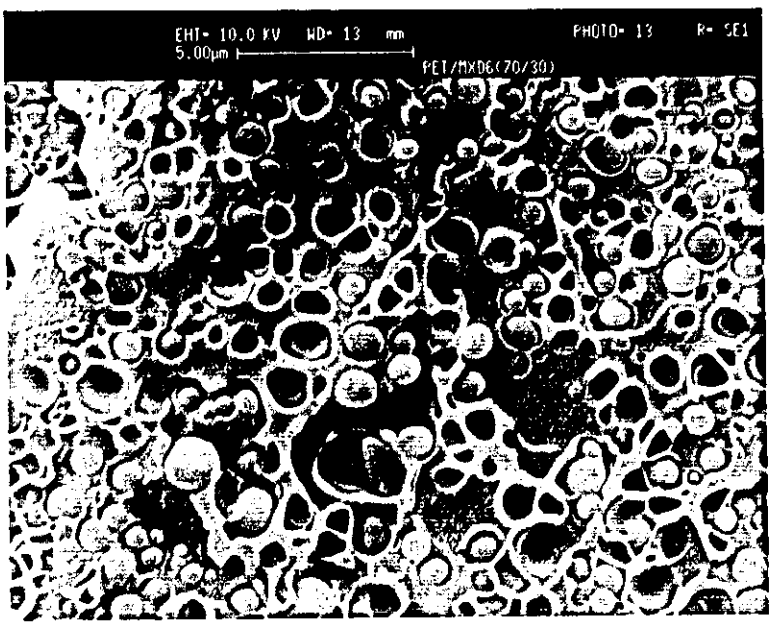

FIGURE 5.42: Scanning electron micrographs obtained from cryogenically fractures of PET/MXD6 (70/30) blend: (a) extruded pellets; (b) injection moulded plaques

(a)

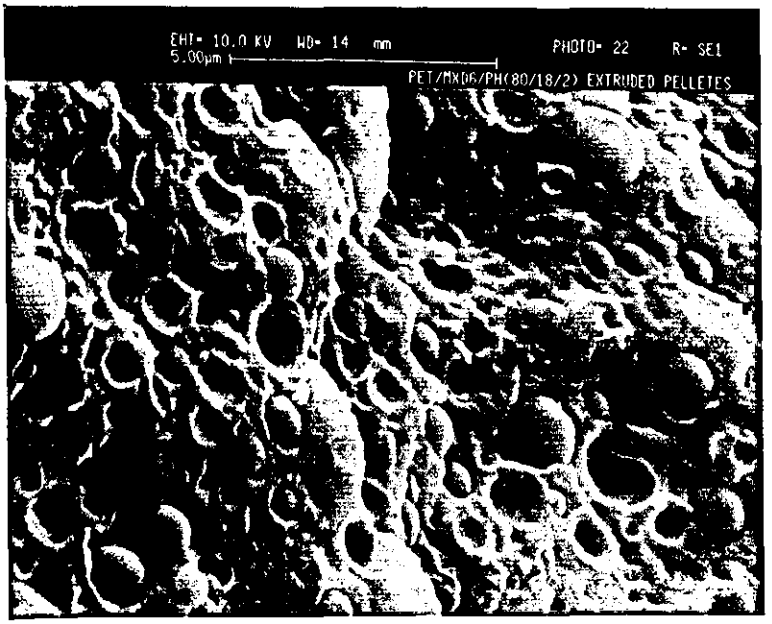

(b)

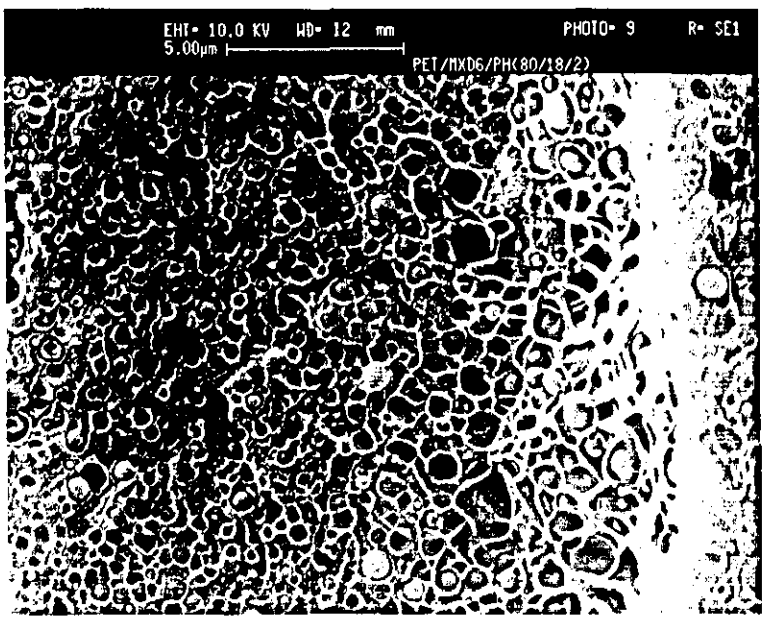

FIGURE 5.43: Scanning electron micrographs obtained from cryogenically fractures of PET/MXD6 (80/18/2) blend: (a) extruded pellets; (b) injection moulded plaques

(a)

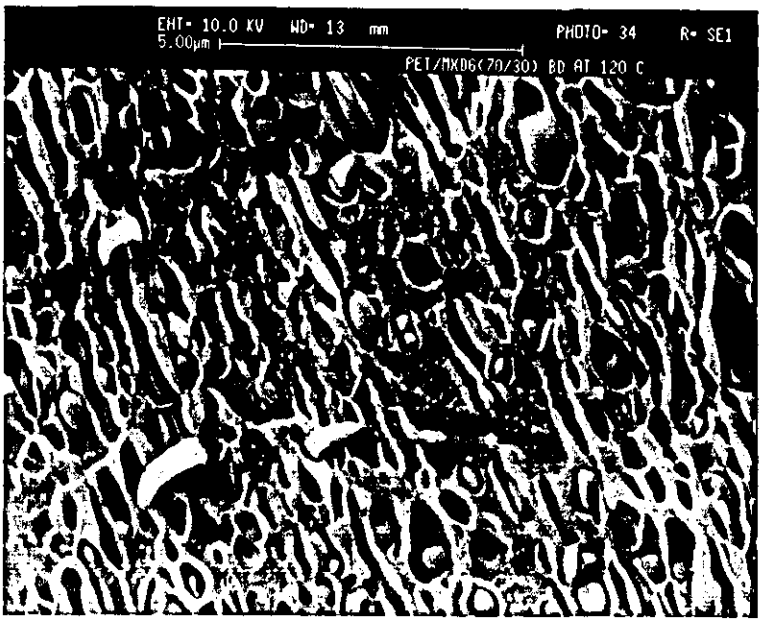

(b)

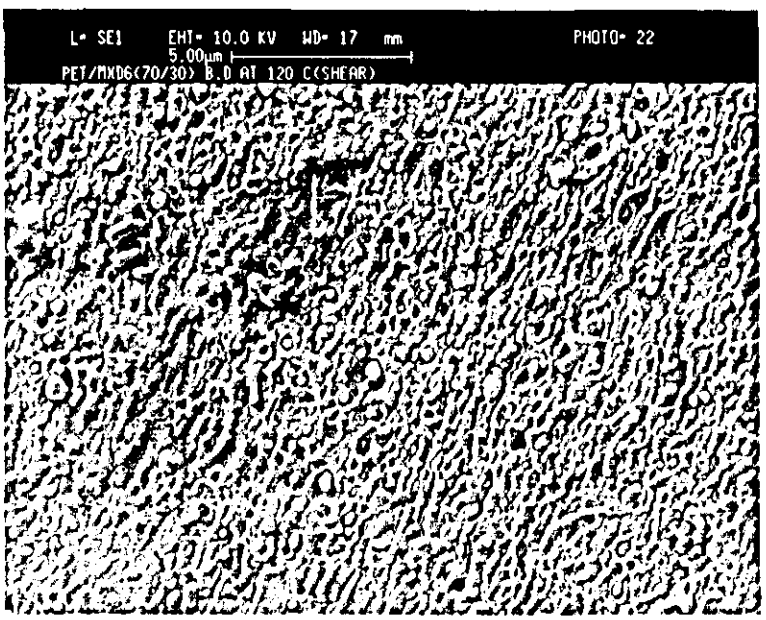

FIGURE 5.44: Scanning electron micrographs obtained from cryogenically fractured biaxially drawn PET/MXD6 (70/30) samples drawn at 120°C (a) samples from the middle, (b) samples from the shear region

5.3.4 Density Results

The density results of biaxially stretched PET/MXD6 (70/30) blends (blend with very low shrinkage) are presented in Figure 5.45 for samples taken from the middle. These show that for the same draw ratio the highest density is obtained for the material showing the lowest shrinkage. Therefore it is possible that the major factor governing shrinkage is the increase in density resulting from the stress-induced crystallisation and not the overall density.

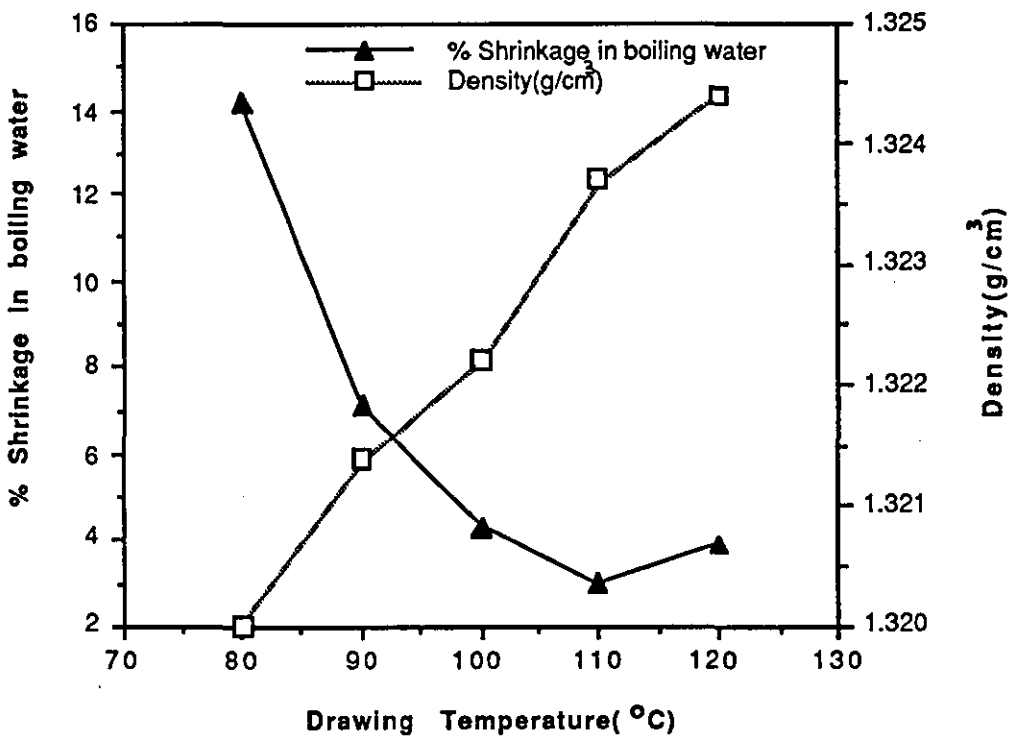

Figure 5.45: Relationship between shrinkage and density for PET/MXD6 (70/30) blend biaxially drawn at draw ratio=3.5:1

CHAPTER 6
DISCUSSION

6.1 UNIAXIAL STRETCHING EXPERIMENTS

As a result of the investigation carried out, a relationship between shrinkage, density and thermal data (DSC) can be obtained, the percent crystallinity, calculated from both DSC and density results, are presented in Figure 6.1, as a function of the drawing temperature.

These results show, however, that the % crystallinity calculated from DSC data displays a minimum at draw temperature of 100°C, which corresponds to the temperature at which maximum shrinkage is observed. These observations are in agreement with those obtained by Sun and Magill [65], who explained that by not taking into account the exothermic nature of the shrinkage process, and the enthalpy associated with it, the calculated values for the degree of crystallinity from DSC data are not correct. Since at a draw temperature of 100°C a high shrinkage is obtained, the "heat of shrinkage" could increase the recorded heat for "cold" crystallisation (ΔH_c) in the DSC scan; this could therefore be one of the reasons for the high value of ΔH_c obtained at that temperature. At a draw temperature of 80°C the percentage crystallinity obtained by DSC is very high due to stress-induced crystallisation giving rise to a high level of orientation, as it was found later from the birefringence measurements. Since shrinkage at this temperature is very low, the shrinkage contribution to the increase in ΔH_c is negligible as shown in Figure 6.2.

At a draw temperature of 125°C and above the percent crystallinity, calculated from DSC is high and reaches a plateau due to the onset of thermal crystallisation, which is confirmed by the observation that the drawn samples become hazy to opaque at draw temperatures around 150°C. As shown in Figure 5.1, the shrinkage at these high draw temperatures is quite low, owing to the onset of thermal crystallisation, which also minimises shrinkage.

As shown in Figure 6.1 the crystallinities calculated from DSC results are different form those obtained from density in the temperature range, between 80°C and 100°C, which is in agreement with those obtained by other workers [65,66,67], and therefore confirm that the crystallinity estimated by DSC for oriented materials has to be corrected by other independent measurement techniques, such as density measurements.

It is found, however, that the percent crystallinity calculated from density results is lower at all drawing temperatures and especially at drawing temperatures of 80°C and 90°C. Since no thermal crystallisation is known to occur at these temperatures but only stress-induced crystallisation, this could lead us to conclude that any increase in density due to the orientation of the amorphous phase has to be smaller than that due to thermal crystallisation. This would then explain the reason why the crystallinity calculated from density is lower for drawing temperatures of 80°C and 90°C.

At a draw temperature of 100°C and above the crystallinity data estimated from density are closer to those obtained by DSC, confirming

once more that the density is more sensitive to thermal crystallisation than to stress-induced crystallisation. However the two methods could be used for a better estimation of the crystallinity for oriented samples and to identify whether molecular disorientration effects associated with shrinkage may contribute to the ΔH values for crystallisation and melting.

From the density results present in Figures 5.12 and 5.13 it is shown that the increase in density with draw ratio is practically independent of draw temperature in the range 80°C-100°C, except at the highest draw ratio (DR = 4:1). In the latter case density increases with increasing stretching temperature, undoubtedly due to the enhanced rate of crystallisation [140], confirming again the increase of crystallinity with drawing temperature for a DR = 4:1.

It is well established [66-141] that the onset of crystallisation is not the only cause for the density increase in oriented PET: the density of the amorphous phase itself is orientation-dependent. Conclusive evidence of this point of view has been recently reported by Ward and others [142], who attribute the observed density increase mainly to the increase in trans-content in the amorphous phase at draw ratio DR $\leq$ 3.5:1.

Moreover the shrinkage results presented in Figure 5.1 are in agreement with those obtained by DeVries et al [43] who suggested that for DR $\leq$ 2:1 the elongational strain is completely recoverable on heating the material above its Tg and ascribed this recovery behaviour to the deformation of an amorphous rubber-like network. For DR > 2:1,

on the other hand, shrinkage decreases with increasing draw ratio due to the evolution of a crystalline phase which opposes the recovery of the amorphous phase, thereby conferring dimensional stability to the drawn material. Moreover, this significant reduction in shrinkage is also attributed, as it was reported by Pereira and Porter [98], to the increase of crystallinity. The crystallites formed during stretching act as immobile crosslinks and restrict shrinkage. This inverse relationship between shrinkage and crystallinity has also been put forward by Smith and Steward [140] in their study of the rate of crystallisation in drawing PET samples.

An analysis of the DSC data reveals some very interesting correlation between the thermal characteristics of the samples and the recorded shrinkage values, as shown in Figures 6.2 and 6.3, these show that shrinkage is directly proportional to the residual heat of crystallisation, irrespective of the drawing temperature of the sample. From Figures 6.2 and 6.3, on the other hand, one can deduce the degree of crystallinity and peak crystallisation temperature for the drawn samples that must be developed in order to eliminate shrinkage.

It would seem however that for monoaxially drawn samples shrinkage is at its minimum when the samples are drawn at temperatures around the Tg of PET.

A relationship between crystallinity and birefringence is presented in Figure 6.4. It is shown that crystallinity is directly proportional to birefringence. Moreover it is shown from Tables 5.3 and 5.4 that at

temperatures below those causing thermal crystallisation, the lowest shrinkage is obtained for the samples exhibiting the highest birefringence, the highest % crystallinity and a strain hardening behaviour during drawing (see Tables 5.3 and 5.4). This illustrates again that stress-induced crystallisation is the cause of the low shrinkage obtained at drawing temperatures 80°C and 90°C. Conclusive evidence of this point of view has also been reported by De Vries et al [43].

It is noted (Figure 5.3) that at the draw temperature of 100°C a very low shrinkage is obtained for samples drawn at 6:1 at a stretching rate of 500 mm/min. This suggests that at this temperature, owing to the high mobility of the chains, one has to use a high draw ratio and a high strain rate to prevent the relaxation of orientation in the amorphous phase.

These data are in agreement with the work of De Vries et al [43] who suggested that the rate of deformation has to be much higher than the reciprocal of the characteristic relaxation time of the polymer network in order to avoid disorientation during stretching. They found that the stretching stress increases with increasing strain rate and with decreasing temperature. Therefore if the temperature is increased, energy dissipation assumes greater importance in comparison to the storage of elastic energy owing to a concomitant reduction in viscosity and relaxation time of the polymer. Lowering the strain rate has a similar effect to increasing temperature because the corresponding increase in time of straining required to attain a given value of strain, allows more disorientation to occur (due to

disappearance of network junctions). This explains why a low birefringence, a low % crystallinity and a high % shrinkage is obtained at stretching rate of 200 mm/min for the samples drawn at 100°C.

For the annealed samples, as shown in Figure 5.7, shrinkage is reduced, for all drawing temperatures, and reaches zero at the annealing temperature of 150°C. These results are in agreement with the work done by Misra and Stein [45] who reported that when drawn PET samples are annealed at temperatures above Tg, the molecules rapidly rearrange to relieve the internal stresses, which is responsible for the reduction in shrinkage. Spruiell et al [143] further suggest that the removal of the internal stresses upon annealing is accompanied by melting of imperfect crystals, which is followed immediately by rapid recrystallisation. This could explain the presence of a second melting peak, at temperatures 10°C to 20°C above the annealing temperature, in addition to the original melting endotherms in the DSC traces.

6.2 BIAXIAL STRETCHING EXPERIMENTS

From the results presented in Sections 5.1 and 5.2 a relationship between uniaxial and biaxial stretching experiments can be obtained. To illustrate this the shrinkage results for both experiments at different drawing temperatures are presented in Figure 6.5. It is found that at a draw ratio (DR) of 2:1 shrinkage decreases with increasing drawing temperature for both uniaxial and biaxial stretched samples. This is due to a low level of orientation, while

contribution to the development of crystallinity from stress-induced crystallisation is negligible.

At the higher draw ratio of 4:1 for uniaxially drawn samples (UDS) and 3.5:1 for biaxially drawn samples (BDS) the minimum in the shrinkage temperature curve is shifted from 80°C for UDS to 110°C for BDS. These results are in agreement with the work of M. Cakmak et al [28], confirming that at 80°C the crystallisation due to thermal effects is negligible [144] and only stress-induced crystallisation can take place at DR > 3:1. As the drawing temperature increases to 100°C and 110°C, the effect becomes more complex because thermal crystallisation makes a significant contribution to the development of crystallinity for both UDS and BDS samples.

Moreover, from the shrinkage and crystallinity results presented in Figures 6.1 and 6.6, it is found that the % crystallinity at 80°C is much higher for UDS than for BDS, but it increases with drawing temperature for BDS. Conclusive evidence of this behaviour has been reported also by M. Cakmak [28] who found that stress-induced crystallisation and thermal crystallisation have a cumulative effect on the overall crystallisation behaviour of biaxially stretched samples.

From the results presented in Section 5.2, a relationship between shrinkage, % crystallinity and the extent of orientation is found for samples biaxially drawn for experiments carried out for both with and without superimposed shear deformations.

In Figure 6.6 is shown the % linear shrinkage versus % crystallinity (calculated from DSC), for samples taken from both the middle and the shear regions of samples drawn by the biaxial stretching jig of square samples (Figure 3.2(a)) without externally imposed shear deformations.

It is shown that shrinkage is inversely proportional to % crystallinity, i.e. samples with the highest amount of crystallinity show the lowest shrinkage. This is in fact the case of the samples taken from the shear region. Moreover, X-ray studies carried out by Guerra [145] on these samples (as a scientific collaboration) have revealed the highest amount of orientation, particularly samples drawn at 90°C and 100°C, see Appendix C. On the other hand a much lower amount of orientation is observed for the samples taken from the middle, particularly samples drawn at 110°C which appear to be without orientation.

These results are in agreement with the DSC results, confirming that samples with high orientation show also a high amount of crystallinity, while those with low orientation show low amounts of crystallinity. Moreover the increase of crystallinity as a result of orientation is caused by stress-induced crystallisation and not by thermal crystallisation, since samples drawn at 110°C appear to be without orientation and with low amounts of crystallinity, resulting from thermal crystallisation. Furthermore the samples drawn at 110°C and above become hazy/opaque but they are transparent when drawn in the temperature range of 80°C to 100°C. This makes the increase of crystallinity due to stress-induced crystallisation more suitable than thermal crystallisation for the production of transparent bottles with low shrinkage at high temperature.

From the shrinkage results presented in Section 5.2 it is shown that a much lower shrinkage is obtained for the samples stretched under combined biaxial drawing with shear deformation than for the samples drawn biaxially with pure biaxial extension. This is mainly due, as it is shown in Figure 6.7, to the increase of crystallinity as a result of stress-induced crystallisation caused by the shear deformation. Moreover, it is found that as the shear extension ratio increases, the shrinkage decreases and the crystallinity increases (see Figures 5.17-5.18 and 6.7). These results reveal that the shear-induced crystallisation is the main cause for the increase of crystallinity and, therefore, to the reduction in shrinkage. Conclusive evidence for this observation has also been reported by M.S. Chun and B.C Tsai [146] in their study of shear induced crystallisation of polyolefins.

6.3 EVALUATION OF BLENDS

The shrinkage and DSC results of PET/PC and PET/PA blends with and without phenoxy presented in Section 5.3, reveal some very interesting correlations between the thermal characteristics of the moulded samples of both PET/PC and PET/PA blends, and the recorded shrinkage values.

It is shown, however, that the Tg of PET is increased by the use of an amorphous high Tg compatible polymer, such as polycarbonate (PC) and polyarylate (PA), but the dimensional stability of the biaxially stretched samples does not improve. Moreover the DSC data show that by using PC and/or PA the crystallisation rate of PET is decreased resulting in a higher value for cold crystallisation temperature (T_c).

The increase of T_c could be the reason for the high shrinkage obtained since the crystallisation of PET has slowed down owing to the greater freedom of the polymer chains to release the internal stresses when heated at high temperature.

These results, however, strongly suggest that it is not the Tg of the blend that determines the level of shrinkage exhibited by the drawn products, but the amount of residual crystallisability of the polymer after drawing [147].

The SEM results, on the other hand, show that for PET/PC and PET/PA (up to 20% PC or PA) blends, a one phase morphology is obtained, and only one Tg is recorded by DSC. This confirm the fact that these blends are compatible but not molecularly miscible as it was confirmed by Kin and Burns [148]. As the amount of PA increases to 30% the compatibility of the blend is improved and especially when a small amount of phenoxy (PH) is added to the blend. This strongly suggests that transesterification reaction takes place between the two components PET and PA whereas some crosslinking reactions could occur between PH and PA, which make the sample more brittle and not stretchable. Supporting evidence for this suggestion can be found in the work of Robeson [121], who found that the polyarylate-PET phase separate before ester exchange reaction takes place, but display a single phase after ester-exchange. A crosslinked single phase has been suggested when PA is mixed with phenoxy.

It is interesting to note that sample stretchability as well as the level of crystallinity are reduced when ester-exchange reaction occurs

when blending PET with PC and PA and that a completely amorphous material is obtained, as shown by DSC, when a single phase system is observed. This confirms that as the amount of PA, PC or PH increases within the blends, the crystallinity is reduced due to ester-exchange or crosslinking reactions and, therefore, a one phase system is observed by SEM. This explains the reason why a stabiliser had to be used to inhibit the ester-exchange reaction for PET/PA blends.

The SEM results confirm the effectiveness of the stabiliser in inhibiting these reactions and two phases are clearly observed. These results are in agreement with those obtained by Cheung et al [138] confirming that the addition of an organophosphite to PET/PA blends effectively retards the ester-exchange reactions.

When this stabiliser is used, however, in PET/PA/PH blends the material is still not stretchable, only one phase is observed by SEM, and therefore, crosslinking reactions between PA and phenoxy are not prevented.

Totally different results are obtained, on the other hand, from shrinkage, DSC, density, and SEM results for PET/MXD6 blends presented earlier in Section 5.3, a relationship between % crystallinity calculated from DSC and shrinkage for PET/MXD6 (70/30) (i.e. blend with the lowest shrinkage) is presented in Figures 6.8 and 6.9.

It is shown, however, that although the Tg of the blend has not been increased, the shrinkage is reduced. The crystallinity of PET, on the other hand, has not been affected and almost the same T_c value as PET

is obtained (see Table 5.13). This confirms the pattern that has continually emerged throughout this work that it is the crystallinity of the samples which determines the level of shrinkage and not the Tg.

From Figure 6.9 it is found that the shrinkage of PET/MXD6 (70/30) taken from the middle of the biaxially drawn samples is inversely proportional to the % crystallinity calculated from DSC. Also the DSC data show that two T_c values are obtained for these blends after stretching, suggesting that the lower T_c is associated with MXD6 and the higher T_c being the one associated with PET. The fact that MXD6 has a lower T_c than PET means that MXD6 will crystallise first under stress and, therefore, may act as a nucleating site for the subsequent crystallisation of PET in PET/MXD6 blends. This could explain the reason why a very low shrinkage is obtained, especially when the amount of MXD6 increases to 30%. This explanation is in concordance with the work reported by Chu and Tsai [146] on PP/HDPE blends, showing that the HDPE phase acts as a nucleating site for the crystallisation of PP. The DSC and density data show that a higher amount of crystallinity is obtained in the samples taken from the shear part compared to the samples taken from the middle. Moreover very low shrinkage is obtained for the shear region samples, therefore the effectiveness of shear deformation to reduce shrinkage is also applicable to blends composed of crystallisable polymers.

Note that even in the absence of thermal crystallisation all the stretched samples were transparent, although the SEM results show two distinct dispersed phases. This is due to the fact that the refractive indices of these two polymers are identical (see Appendix C) and therefore the transparency of the blend is not affected.

It is interesting to note that the first T_c for PET/MXD6 (70/30) blends after drawing corresponds to the T_c value (72°C) extrapolated in Figure 6.3 for a sample with zero shrinkage.

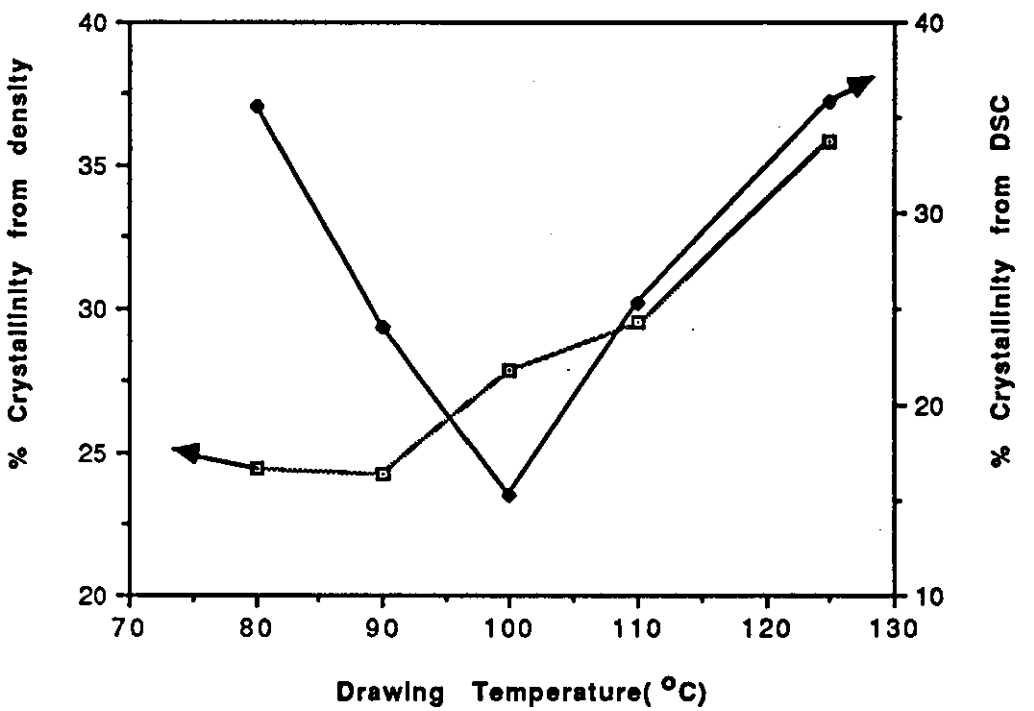

Figure 6.1: Effect of drawing temperature on crystallinity for unaxially drawn non- nucleated PET thick samples (0.8mm) at draw ratio=4:1

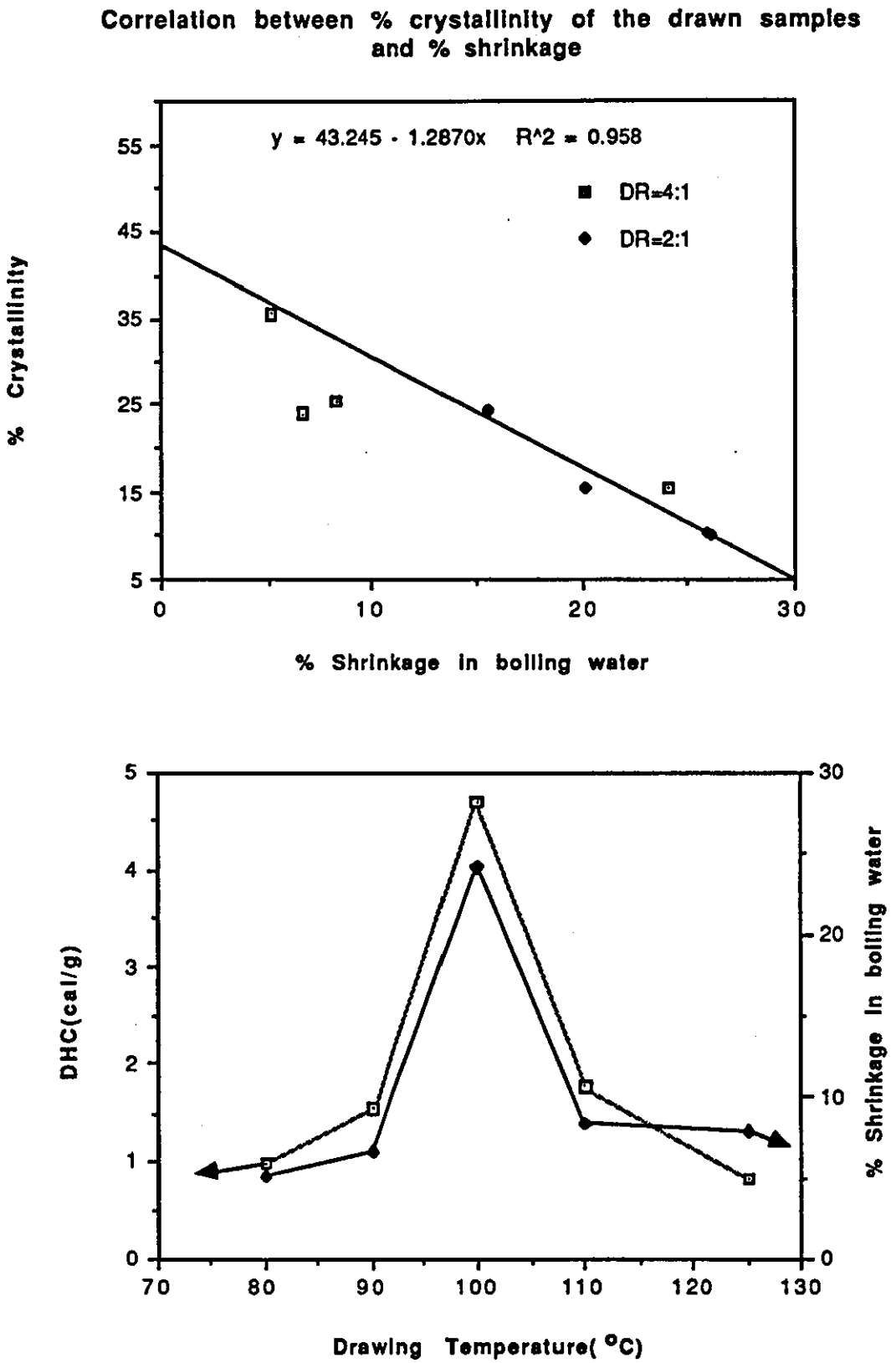

Figure 6.2: Relationship between shrinkage and heat of cold crystallisation temperature for uniaxially drawn non- nucleated PET thick samples (0.8mm) at draw ratio=4:1

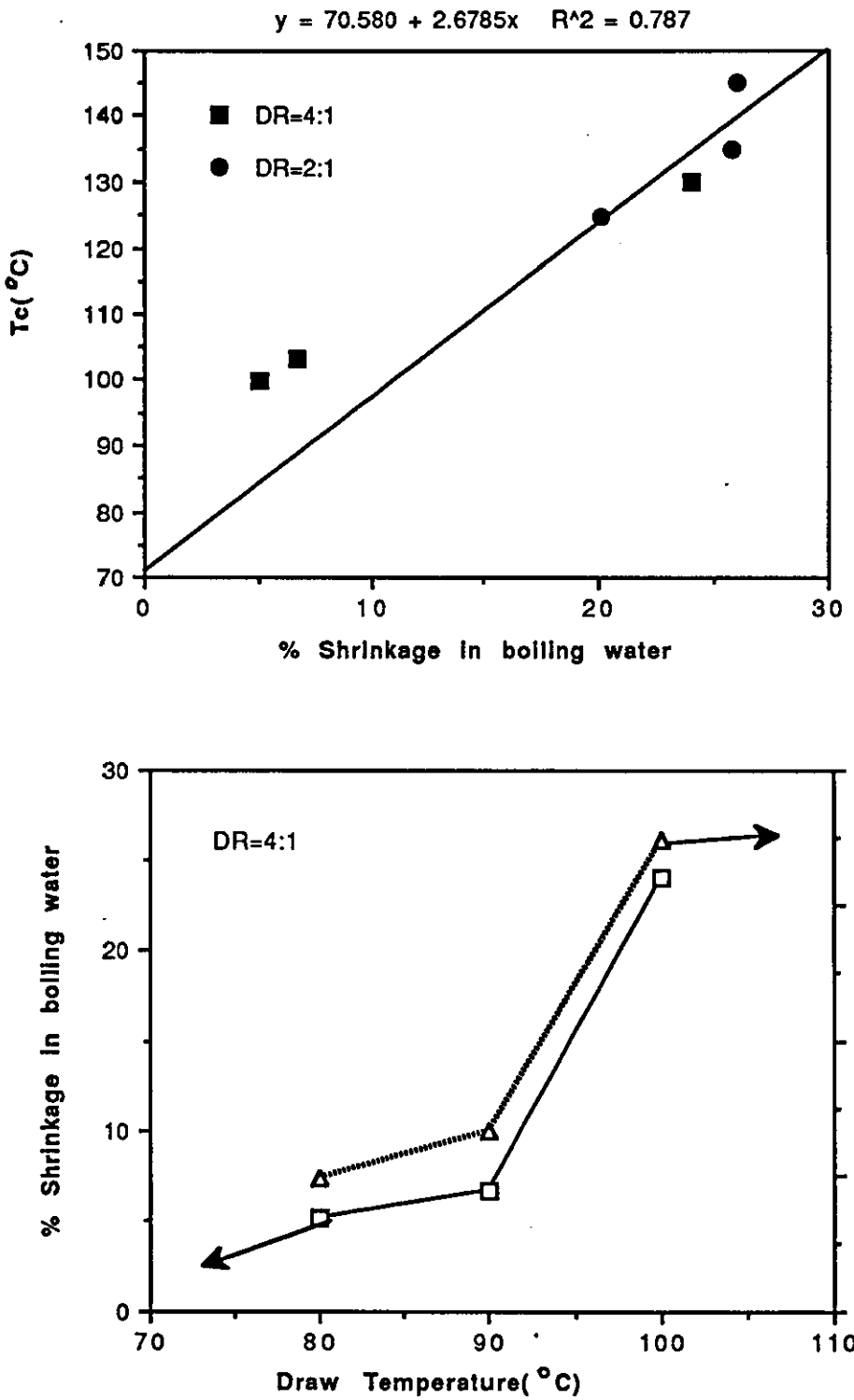

Figure 6.3: Relationship between shrinkage and the cold crystallisation temperature (Tc) for uniaxially drawn non-nucleated thick PET samples

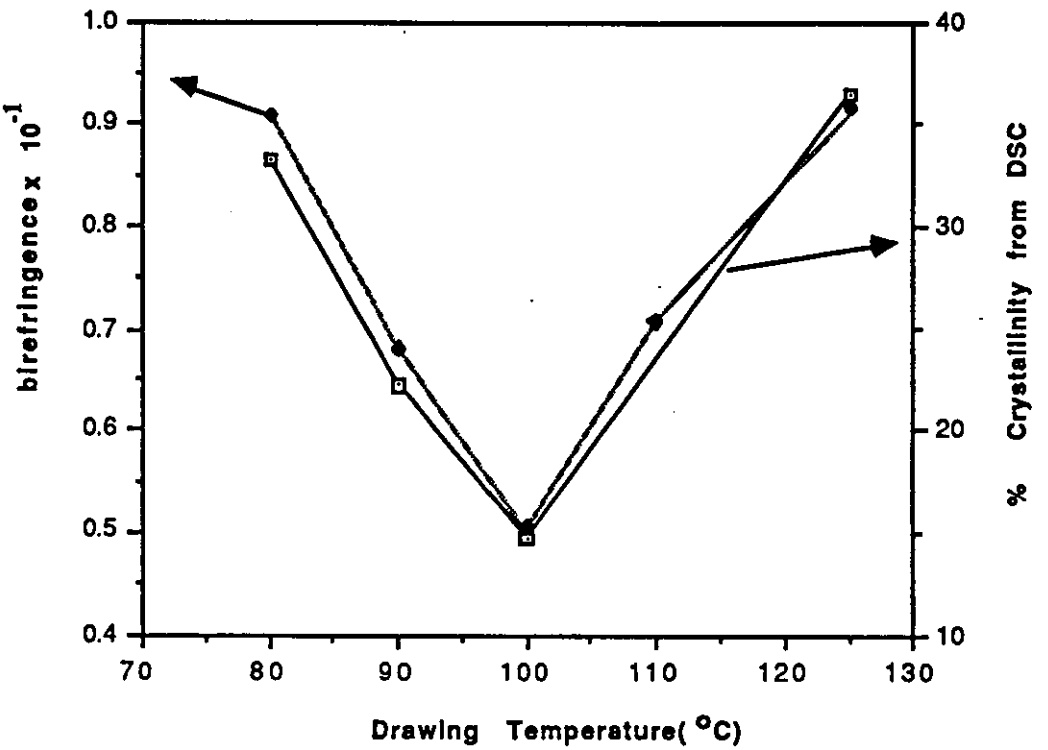

Figure 6.4: Relationship between birefringence and crystallinity foruniaxially drawn PET at draw ratio= 4:1

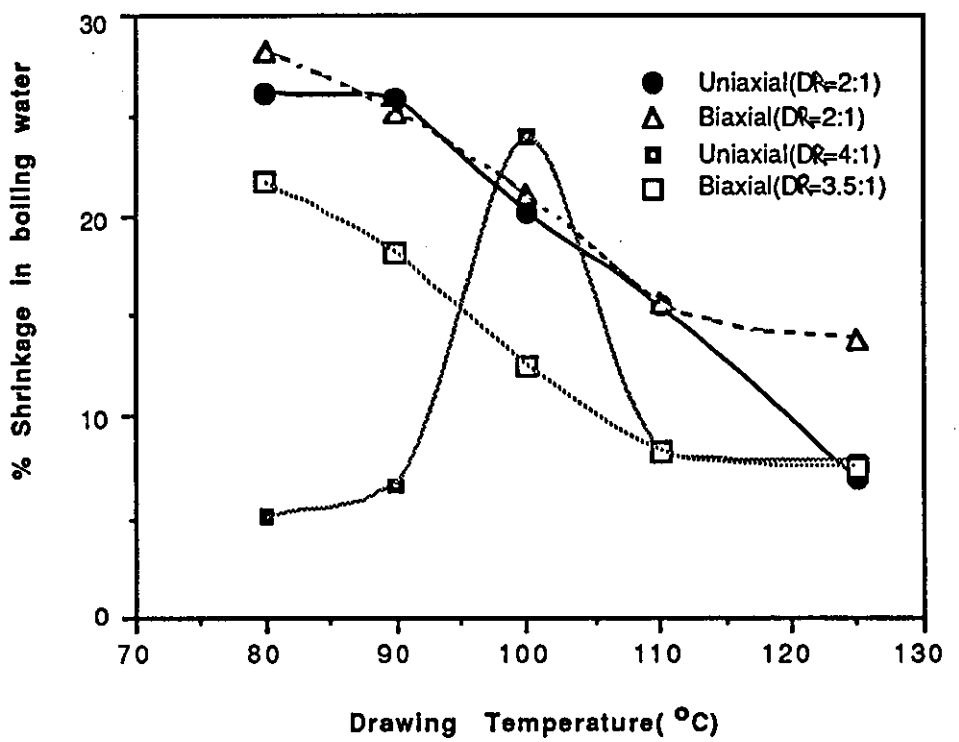

Figure 6.5: Relationship between shrinkage and drawing conditions for both uniaxially and biaxially stretched non- nucleated PET thick samples (0.8mm)

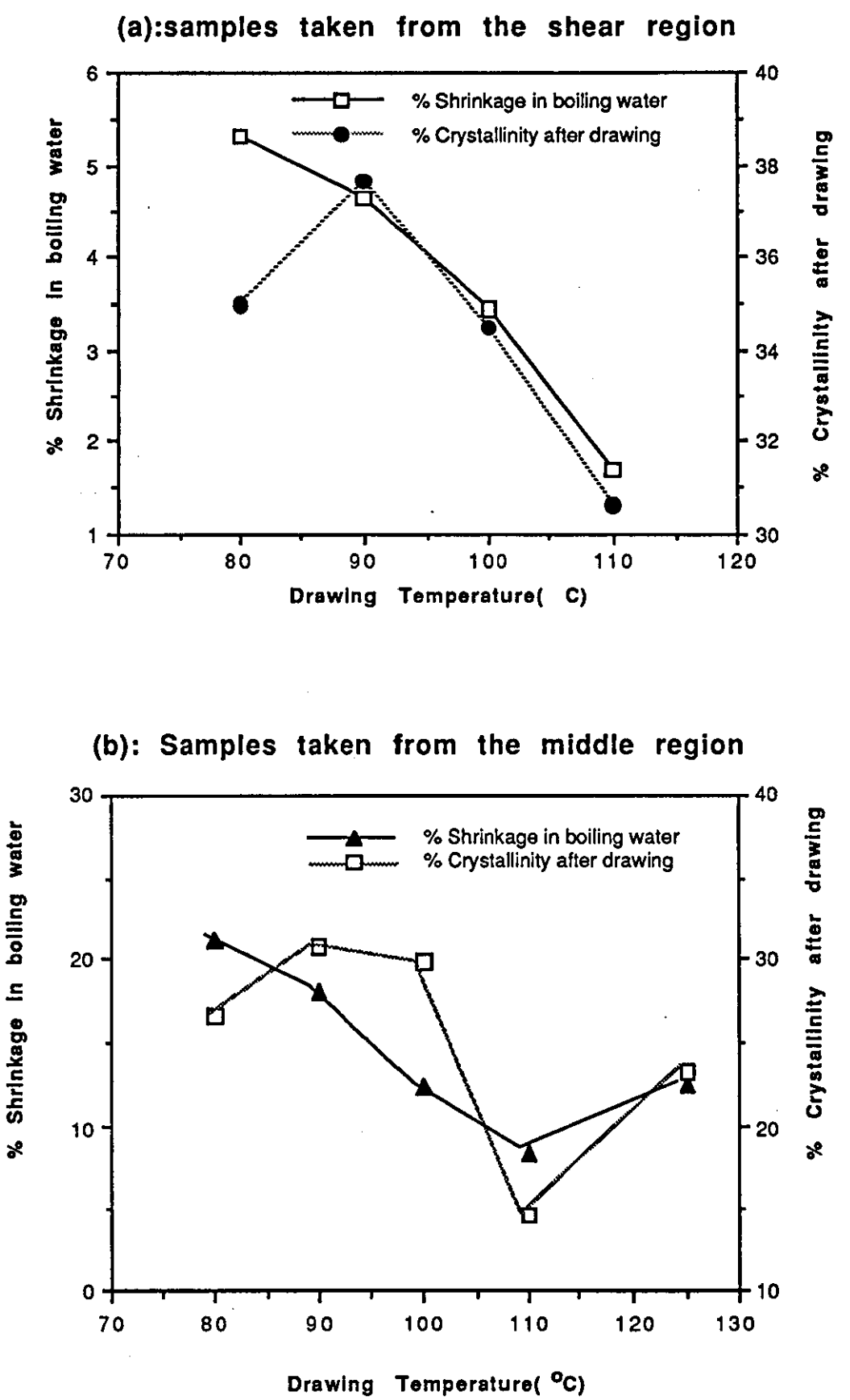

Figure 6.6: Relationship between shrinkage and crystallinity for non-nucleated thick PET sheets(0.8mm) biaxially drawn at draw ratio=3.5:1

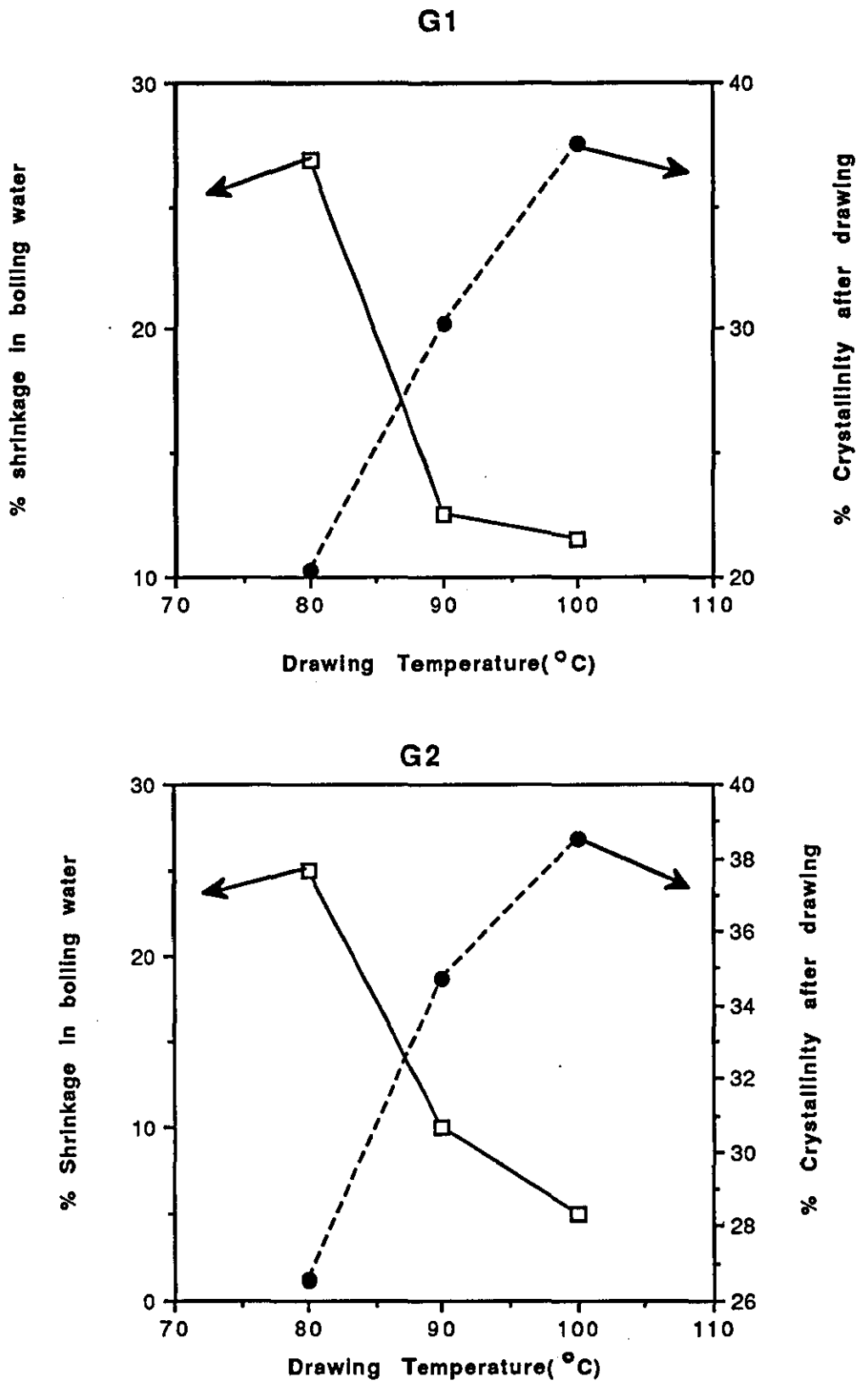

Figure 6.7: Relationship between area shrinkage and crystallinity for biaxially drawn non-nucleated PET samples with superimposed shear deformations

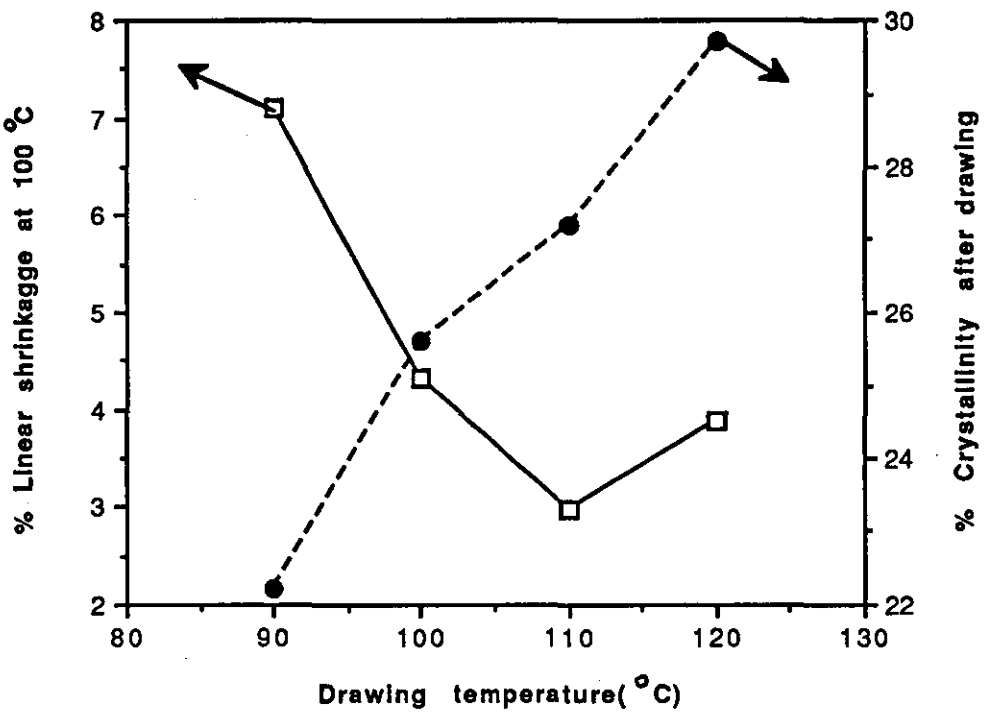

Figure 6.8: Relationship between shrinkage and crystallinity for PET/MXD6(70/30) blend biaxially drawn at draw ratio=3.5:1(samples taken from the middle)

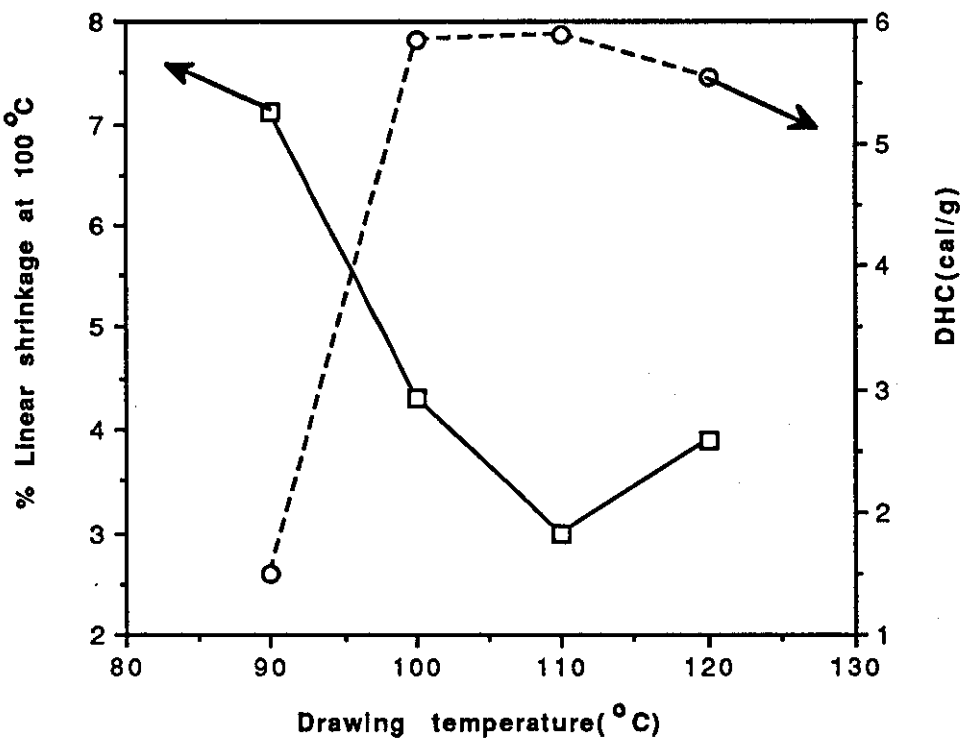

Figure 6.9: Relationship between linear shrinkage and DHC for PET/MXD6(70/30) blend biaxially drawn at draw ratio =3.5:1(samples taken from the middle)

CHAPTER 7
CONCLUSIONS AND SUGGESTIONS FOR FUTURE WORK

From the present study it can be concluded that:

1. The main factors controlling the level of shrinkage of oriented products, when subsequently exposed to high temperature, is the degree of crystallinity developed during drawing i.e. the stress-induced crystallisation. The higher the crystallinity developed during stretching the lower is the shrinkage.

2. By using faster rates of stretching the minimum level of post-drawing shrinkage i.e. when the product is exposed to high temperatures, occurs at higher draw temperatures. This is also associated with the highest level of stress-induced crystallisation taking place at higher temperatures.

3. The post-processing shrinkage seems to decrease with increasing thickness of the original sheet, for both nucleated and non-nucleated samples. This is due to the higher level of crystallinity developed in the thin samples during preheating in the air oven of the tensile machine before stretching, which decreases the amount of crystallinity developed during stretching.

It is suggested, however, that further work could be carried out to study the effect of thickness on shrinkage by using a different heating source, e.g. infra-red heaters, which generate

heat within the bulk of the material, thereby minimising differences in level of crystallinity developed with changing sample thickness.

4. Imposing in-plane shear deformations during axial stretching increases the amount of stress induced crystallisation and therefore, reduces the high temperature shrinkage of the drawn samples. The required shear deformations for the expansion of tubular products, such as bottles, would have to be applied through torsions caused by the rotation of the "spigot" during the vertical stretching of the preform.

   The amount of shear required to achieve the best results for a given axial draw ratio is not known. Hence further work could be carried out to evaluate how the relative ratio of shear to biaxial extension affects the kinetics of stress induced crystallisation and the extent orientation of the crystals. It would be of interest to study also such a phenomenon in relation to diffusion properties.

5. PET/PC and PET/PA blends exhibit a higher Tg than the base PET polymer for all compositions evaluated in this study but the level of shrinkage at high temperature remains high. This high level of shrinkage is caused by the decrease in the amount of crystallinity that is being developed during stretching owing to the reduced molecular mobility of PET chains in the blend.

6. By blending PET with polymethaxylene adipade (MXD6), the Tg of the blend is the same as for pure PET but the post-orientation shrinkage is lower due to larger amounts of stress-induced crystallisation developed as the result of possible nucleating effects of MXD6 on PET. This effect needs further study, e.g. WAXS, in order to understand better the crystalline nature of the blend and to evaluate the difference between the crystal orientation of the two polymer phases.

7. By using 30% MXD6 in the blend the post-orientation shrinkage decreases to very low levels, suggesting that this blend could be used for the production of biaxially oriented products exhibiting dimension stability at high temperatures.

REFERENCES

1. Petukhov, B.V. The Technology of Polyester Fibres, Pergamon Press, Oxford, (1963).

2. Press, J.J. (ed). Man-made Textile Encyclopaedia, Textile Book Publishers Inc., New York, (1959).

3. Hawthorne, J.M. and Heffelfinger, C.J. "Polyester Fibres" in Encyclopaedia of Polymer Science and Technology, Vol. 11, p.1-41, John Wiley and Sons (1969).

4. Kodapak PET - Thermoplastic Polyester, Eastman Chemical Products Inc., Kingsport, USA (1982).

5. Neth, Pat. 7,203,971 (Sept. 28, 1972); US Pats 3,803,275 (April 9, 1974) and 3,745,150 (July 10, 1973), W.L. Corsover, (to E.I. Du Pont Nemours and Co Inc).

6. US Pat. 3,733,309 (May 15, 1973), N.C. Wyeth and R.N. Roseveorve (to E.U. Du Pont de Nemours and Co Inc).

7. Aust. Pat. 315,511 (May 27, 1974) (to Ciba-Geigy Corp).

8. US Pat. 3,814,786 (June 4, 1974); Brit. Pat. 1,437,492 (May 26, 1976); UAS Pat. 3,931,114 (Jan. 6, 1976), J.S. Gall and G.W. Halek (to Celanese Corp).

9. Fritz, H.G., Kunststoffe, 68, 450, (1978).

10. Plast. Technol. 25 (March 1980).

11. Shen, M. and Kawai, H. AIChEJ, 24(1), 1 (1978).

12. Roovers, J. Meth. Experim. Phys., 16C, 275 (1980).

13. Barlow, J.W. and Paul, D.R. Poly. Eng. and Sci., Vol. 21, 985, (1981).

14. Krouse, S.A., J. Macromol. Sci., Rev. Macromol. Chem., 7, 251 (1972).

15. Siegmann, A. J. Appl. Polym Sci., 24, 2333, (1979).

16. Siegmann, A. J. Appl. Polym. Sci., 27, 1053, (1982).

17. Nassar, T.R., Paul, D.R. and Barlow, J.W. J. Appl. Polym. Sci., 23, 85 (1979).

18. Cruz, C.A., Barlow, J.W. and Paul, D.R. Macromolecules 12, 726, (1979).

19. Mohn, R.N., Paul, D.R., Barlow, J.W. and Cruz, C.A., J. Appl. Polym. Sci., 23, 575, (1979).

20. Encyclopaedia of Polymer Science and Engineering, Vol. 12, p.425, John Wiley and Sons.

21. Robeson, L.M. J. Appl. Polym. and Sci., Vol. 30, 4081 (1985).

22. Ward, I.M. "Structure and properties of oriented polymers". Applied Science Publishers, London, 1975.

24. Yang, H.H., Chouinard, M.P. and Lingg, W.J. EI. J. Polym. Sci. Polym. Phys. Vol. 20, 981, (1982).

25. Axtell, F.H. PhD Thesis, p.299, (1987).

26. Alexander, L.E. X-ray diffraction methods in polymer Science, Wiley, New York, (1969).

27. Cakmak, M., Spruiell, J.E. and White, J.L. Polym. Eng. and Sci., Vol. 24, 1390, Dec. (1984).

28. Cakmak, M., Spruiell, J.E., White, J.L. and Lin, J.S. Polym. Eng. Sci., Vol. 27, 893, (1987).

29. Samuels, R.J. Structural Polymer Properties, John Wiley, New York (1974).

30. Holdsworth, P.J. and Turner-Jones, A. Polymer, 12, 195 (1971).

31. Kanetsuna, H. and Maeda, K. Kagyo Kagaku Zasshi 1966, 69, 1784.

32. Roberts, R.C. Polymer, 10, 117, Lond. 1969.

33. Bell, J.P. and Murayama, T. J. Polym. Sci. (A-2) 7, 1059, (1969).

34. Keller, A., Lester, G. and Morgan, L.B. Phil. Trans. Roy. Soc. A247, 23, (1954).

35. Zachmann, H.G. and Stuart, H.A. Makromol. Chem., 41, 148, (1960).

36. Le Bourvellic, G., Monnerie, L. and Jarry, J.P. "Kinetics of induced crystallisation during stretching and annealing of poly(ethylene terephthalate) films. Polymer, Vol. 28, p.1712-1716, September 1987

37. Hughes, M.A. and Sheldon, R.P. J. Appl. Polym. Sci., 8, 1541, (1964).

38. Bair, H.E., Salovey, R. and Huseby, T.W. Polymer, 8.9, Lond. 1967,

39. Cobbs, W.H. and Burton, R.L. J. Polym. Sci., 10, 275, (1953).

40. Cakmak, M., White, J.L. and Spruiell, J.E. J. Polym. Eng. Vol. 6, 291, (1986).

41. Petermann, J. and Rieck, U. "Morphological and mechanical properties of PET films crystallised under high strain rate". J. Polym. Sci., Polym. Phys., Vol. 25, p.279-293, (1987).

42. Klement, J.J. and Geil, P.H. "Deformation and annealing behaviour. Thick polyethylene terephthalate films". J. Macromol. Sci-Phys. B5(3), p.535-558, (1971).

43. De Vries, A.J., Bonnebat, C. and Beautemps, J. "Uni- and biaxial orientation of polymer films and sheets". Journal of Polymer Science, Polymer Symposium, Vol. 58, 109-159 (1977).

44. Matsuo, M., Tamada, M., Terada, T., Sawatari, C. and Nawa, M. Macromolecules, 15, 988, (1982).

45. Misra, A. and Stein, R.S. J. Polym. Sci., Polym. Phys. Edn. 17, 235, (1979).

46. Bragato, G. and Gianatti, G. Eur. Polym. J., 19, 803, (1983).

47. Koenig, J.L. and Mele, M.D. Makromol. Chem., 118, 128 (1968).

48. Sodamatsu, S. "Reports on Progress in polymer physics in Japan". Vol. VIII, p.97 (1965).

49. Spruiell, J.E. "Structure development in blow moulding polyethylene terephthalate", 912, Antec 85.

50. Manaresi, P., Parrini, P., Semeghini, G.L. and Defornasari, E. Polymer, 17, 595 (1976).

51. Hennessey, W.J. and Spatarico, A.L. Polym. Eng. Sci., Vol. 19, p.462-467, (1979).

52. Yeh, G.S.Y. and Geil;, P.H. J. Macromol. Sci., B1, 235 (1967).

53. Yeh, G.S.Y. and Geil, P.H. Ibid., B1, 251 (1967).

54. Casey, M. Polymer, 18, 1219, (1977).

55. Prevorsek, D.C. J. Polym. Sci., 32, 343, (1971).

56. Prevorsek, D.C., Haque, P.J., Sharma, R.K. and Reimschussel, R.C. J. Macromol. Sci. Phys., 138, 127, (1973).

57. Lemanska, G. and Narebska, A. J. Polym. Sci., Polym. Phys. Edn. 18, 917, (1980).

58. Gupta, V.B. and Kumar, S. Polymer, 19, 953, (1978).

59. Xanthos, M., Young, M.W. and Biesenberger, J.A. Polym. Eng. and Sci., Vol. 30, 355, March 1990

60. Muller, A.J., Feijoo, J.L., Alvarez, M.E. and Febles, A.C. Polym. Eng. and Sci., Vol. 27, 796, June 1987,

61. Starkweather, H.W., Zoller, P. and Jones, G.A. J. Polym. Sci., Polym. Phys. Ed. 21, 295 (1983).

62. Sun, D.C. and Magill, J.H. Polym. Eng. and Sci., Vol. 29, 1503, mid-Nov. 1989,

63. Kavesh, S. and Schultz, J.M. Polym. Eng. and Sci., Vol. 9, 331, September 1969.

64. Le Bourvellec, G., Monnerie, L. and Jarry, J.P. Polymer, Vol. 27, 856, (1986).

65. Wunderlich, B. 'Macromolecular Physics', Vol. 1, Academic Press, New York, 1973.

66. Farrow, G. and Ward, I.M. Polymer, 1, 330, (1960).

67. Nobbs, J.H., Bower, D.I. and Ward, I.M. Polymer, 17, 25, (1976).

68. Hermann, K., Gerngross, O. and Abitz, W. (1932). Z. Phys. Chem., B10, 371.

69. Schuur, G. Some Aspects of the Crystallisation of High Polymers, Thesis, Delft, (1955).

70. Frank, F.C., Keller, A. and O'Connor, A. Phil. Mag., 3, 64, (1958).

71. Thompson, A.B. J. Polym. Sci., 34, 741 (1959).

72. Yeh, G.S.Y. and Geil, P.H. J. Macromol. Sci., Part B, 1, 251 (1967).

73. Ludewig, Herman. "Polyester Fibres Chemistry and Technology". Wiley Interscience, New York (1971).

74. Hillier, K.W. "Homopolymers" in 'Man-Man Fibres, Science and Technology', Vol. 3 pp 1-20, H.F. Mark, S.M. Atlas and E. Cernig, Eds., Interscience Publishers (1968).

75. Hawthorne, J.M. and Heffelfinger, C.J. "Polyester Films" in 'Encylopaedia of Polymer Science and Technology', Vol. 11, John Wiley and Sons (1969).

76. Spencer, A.W., Eastman Kodak Co. "Poly(ethylene terephthalate) Films". Fr. 1, 477, 269, April 14, 1967, CA67, 74266W (1967).

77. Granata, J. "Injection Blow Moulding of PET", 825, ANTEC 86.

78. Lohmar, J.O. Kunststoffe German Plastics 76, 6, (1986)

79. Lohmar, J.O, Kunststoffe, Vol.76, p.481, (1986).

80. Thompson, A.B. in Fibre Structure, J.W.S. Hearle and R.H. Peters, eds., Butteworths, Washington, DC, (1963).

81. Thompson, A.B. and Marshall, I. Proc. R. Soc. London, Ser. A, 211, 541 (1954).

82. Sheldon, R.P. Polymer, 4, 213 (1963).

83. Jabarin, S.A. Polym. Eng. and Sci., Vol. 24, 376, (1984).

84. Nicolas, P., Lane, A.R., Carter, T.J. and Hay, J.N. Polymer, Vol. 29, 894, (1988).

85. Keller, A. J. Polym. Sci., 21, 363 (1958).

86. Kashiwagi, M., Cunningham, A., Manual, A.J. and Ward, I.M. Polym. 14, 111 (1973).

87. Heffelfinger, C.J. and Schmidt, P.G. J. App. Polym. Sci., 9, 2661 (1965).

88. Newman, S. J. Polym. Sci., 27, 583 (1963).

89. Asan, T. and Setom, T. Polym. J., 5, 72 (1973).

90. Klement, J.J. and Geil, P.H. J. Macromol Sci. Phys., B5(3), 535, (1971).

91. de P. Daubeny, R., Bunn. C.W. and Brown, C.J. Proc. Roy. Soc. (London), Ser. A, 226, 531 (1954).

92. Bonart, R. Kolloid-Z, 199, 136 (1964).

93. Statton, W.O. and Goddard, C. J. Appl. Phys., 28, 1111 (1957).

94. Elsner, G., Zachman, H.G. and Milch, J.R. Makromol. Chem., 182, 657 (1981).

95. Fischer, E.W. and Fakirov, S. J. Mater. Sci., 11, 1041 (1976).

96. Heffelfinger, C.J. and Lippert, E.L.J. Appl. Polym. Sci., 15, 2699 (1971).

97. Bonart, R., Kolloid Z. Z. Polymere, 199, 136 (1964).

98. Pereira, J.R.G. and Porter, R.S. Polymer, Vol. 25, 877, (1984).

99. Perkins, W.G., ANTEC, 39th Proceedings Conference 012, Boston p.705-7, May 1981.

100. Bhatt, G.M. and Bell, J.P. J. Polym. Sci, Polym. Phys., 14, 575, (1976).

101. Liska, E. Kolloid, Z. Z. Polym., 251, 1027, (1973).

102. Statton, W.O., Koenig, J.L. and Hannon, M.J. Appl. Phys., 4290, (1970).

103. Prevorsek, D.C., Tirpak, G.A., Harget, P.J. and Reimschwessel, A.C. J. Macromol. Sci. Phys., B9,733, (1974).

104. Wilson, M.P.W. Polymer, 15, 277, (1974).

105. Nobbs, J.H., Bower, D.I. and Ward, I.M. Polymer, 17, p.25, (1976).

106. Heffelfinger, C.J. and Schmidt, P.G. J. Appl. Polym. Sci., 9, 2661, (1965).

107. Sattler, H. Kolloid, Z., 187, 12 (1963).

108. Pinnock, P.R. and Ward, I.M. Trans. Faraday Soc., 62, 1308 (1966).

109. Dumbleton, J.H. Text. Res. J., 70, 1035, (1970).

110. Samuels, R.J. J. Polym. Sci., A-2, 9, 781 (1972).

111. Wilson, M.P.W., Polymer, 15, 277 (1977).

112. Dumbleton, J.H. J. Polym. Sci., A-2, 7, 667 (1969).

113. Sun, D.C. and Magill, J.H. Polym. Eng. and Sci., Vol. 29, No. 21, mid-Nov. (1989).

114. Murff, S.R., Barlow, J.W. and Paul, D.R. J. Appl. Polym. Sci., 29, 3231 (1984).

115. Huang, J.H. and Wang, L.H. Makromol. Chem., Rapid. Comm., 7, 255 (1986).

116. Hanrahan, B.D., Angeli, S.R. and Runt, J. Polym. Bull., 15, 455 (1986).

117. Olabisi, O., Robeson, L.M. and Shaw, M.T. Polymer-Polymer Miscibility, Academic Press, New York, Chap.3, (1979).

118. MacKnight, W.J., Karasz, F.E. and Fried, J.R. in Polymer Blends, D.R. Paul and S. Newman, Eds., Academic Press, Vols. 1 and 2, Chap 5, New York, (1978).

119. Kim, W.N. and Burns, C.M. J. Appl. Polym. Sci., 32, 2989 (1986).

120. Kim, W.N. and Burns, C.M. J. Appl. Poly, Sci., 34, 945 (1987).

181
+ 180
Bound
in wrong
order.

assigned to Unitika Ltd, March 23, (1976).

134. Kimura, M., Salec, G. and Porter, R.S. J. Appl. Polym. Sci., Vol. 29, p.1629, (1984).

135. Equizabel, J.I., Ugar, G., Cartozar, M. and Irwin, J.J. Polymer Vol. 27, p.2013, (1986).

136. Olabisi, O., Robeson, L.M. and Shaw, M.T. in Polymer-Polymer Miscibility, Chapter 2, Academic Press, New York, (1979).

137. Robeson, L.M. J. Appl. Polym. and Sci., 17, 3607 (1973).

138. Robeson, L.M. in Polymer Compatibility and Incompatibility Principles and Practices (K. Solc, ed), MMI Press, Symposium Series, Vol. 2, Harwood Academic, New York, p.177, (1982).

139. Cheung, M.F., Golovoy, A., Carter, R.G. and Van Oene, H. Ind. Eng. Chem. Res., 28, 476, (1989).

140. Smith, F.S. and Steward, R.D. Polymer, 15, 283, (1974).

141. Lindner, W., Polymer, 14, 9, (1973).

142. Cunningham A., Ward, I.M., Willis, H.A. and Zichy, V. Polymer, 15, 749, (1974).

143. Spruiell, J.E., McCord, D.E. and Beuerlein, R.A. Trans. Soc. Rheol. 16 (3), 535, (1972).

144. Stein, R.S., Hashiyama, M. and Parport, M.K. p.371, Gordon and Breach, London (1979).

121. Kim, W.N. and Burns, C.M. Macromolecules, 20, 1876 (1987).

122. Imken, R.L., Paul, D.R. and Barlow, J.W. Polym. Eng. Soc. 16, 593 (1976).

123. Murff, S.R., Barlow, J.W. and Paul, D.R. Rev. Past. Mod. 48, No. 337, p.48, (1984).

124. Legras, R., Bailly, C., Doumerie, M., Dekenink, J.M., Mercier, J.P., Zichy, V. (Mrs), and Nield, E. Polymer, Vol. 25, 835, (1984).

125. Bier, G. Polymer, 15, 527 (1974).

126. Korshak, V.V. and Vinogradova, S.V. Polyesters, Pergamon Press, Oxford, (1965).

127. Domine, J.D., 37th ANTEC of SPE, p.655, New Orleans, LA, May 7-10, (1979).

128. Freitag, D. and Reinking, K. Kunststoffe, 71(1), 46 (1981).

129. Sakata, H., SPE, 32nd ANTEC, p.459, April 13-16, San Francisco, California, (1974).

130. Mondragon, I., Cortazar, and Guzman, G.M. Makromol. Chem., 184, 1741 (1983).

131. Robeson, L.M. US Pat. No. 4,259,458, assigned to Union Carbide Corp., March 31, (1981).

132. Robeson, L.M. US Pat. No. 4,231,922, assigned to Union Carbide Corp., Nov. 4, (1980).

133. Sakata, H., Okamoto, T. and Hasegawa, H. US Pat. No. 3,946,091,

145. Guerra, G. University of Naples, Chemistry Dept (private communication).

146. Chun, M.S. and Tsai, B.C. Polym. Mater. Sci. Eng., Vol. 61, p.166, (1989).

147. Mascia, L., Fekkai, Z. Polymer Blends. Third European Symposium E16/1, July (1990).

148. Woo Nyon Kin and Burns, C.M. J. of Polym. Sci., Part B, Polym. Phys.Vol. 28, p.1409 (1990).

149. Benham, P.P., and Warnock, F.V. "Mechanics of solids and structures." Pitman international. London. (1982).

APPENDICES

APPENDIX A

TABLE A1: DENSITY RESULTS OF UNIAXIALLY DRAWN PET SAMPLES FROM THICK SHEETS (0.8 mm) AFTER ANNEALING

Drawing Temp (^{o}C)	Draw Ratio	Drawing Speed mm/min	Annealing Temp (^{o}C)	% Shrinkage in boiling water	Density (g/cm^3)
80	2:1	200	150	0	1.3709
80	2:1	200	180	0	1.3769
80	4:1	200	180	0	1.3783
90	2:1	200	180	0	1.3752
90	4:1	200	180	0	1.3778
100	4:1	200	180	0	1.3787

TABLE A2: DENSITY RESULTS OF UNIAXIALLY DRAWN PET SHEETS OF 0.40 mm THICKNESS

Material	Drawing Temp (^{o}C)	Draw Ratio (DR)	Drawing Speed mm/min	% Shrinkage in boiling water	Density (g/cm^3)
Non-nucleated PET sheets	80	3:1	200	15.55	1.3555
Non-nucleated PET sheets	80	4:1	200	13.8	1.3563
Nucleated Ca Montanate (0.5%)	80	41	200	11.8	1.3593
Non-nucleated	90	4:1	200	27.77	1.3590
Nucleated Ca Montanate (0.5%)	90	4:1	200	6.67	1.3608

FIGURE A1: CALIBRATION CURVE FOR DENSITY TESTS OF UNIAXIALLY DRAWN PET

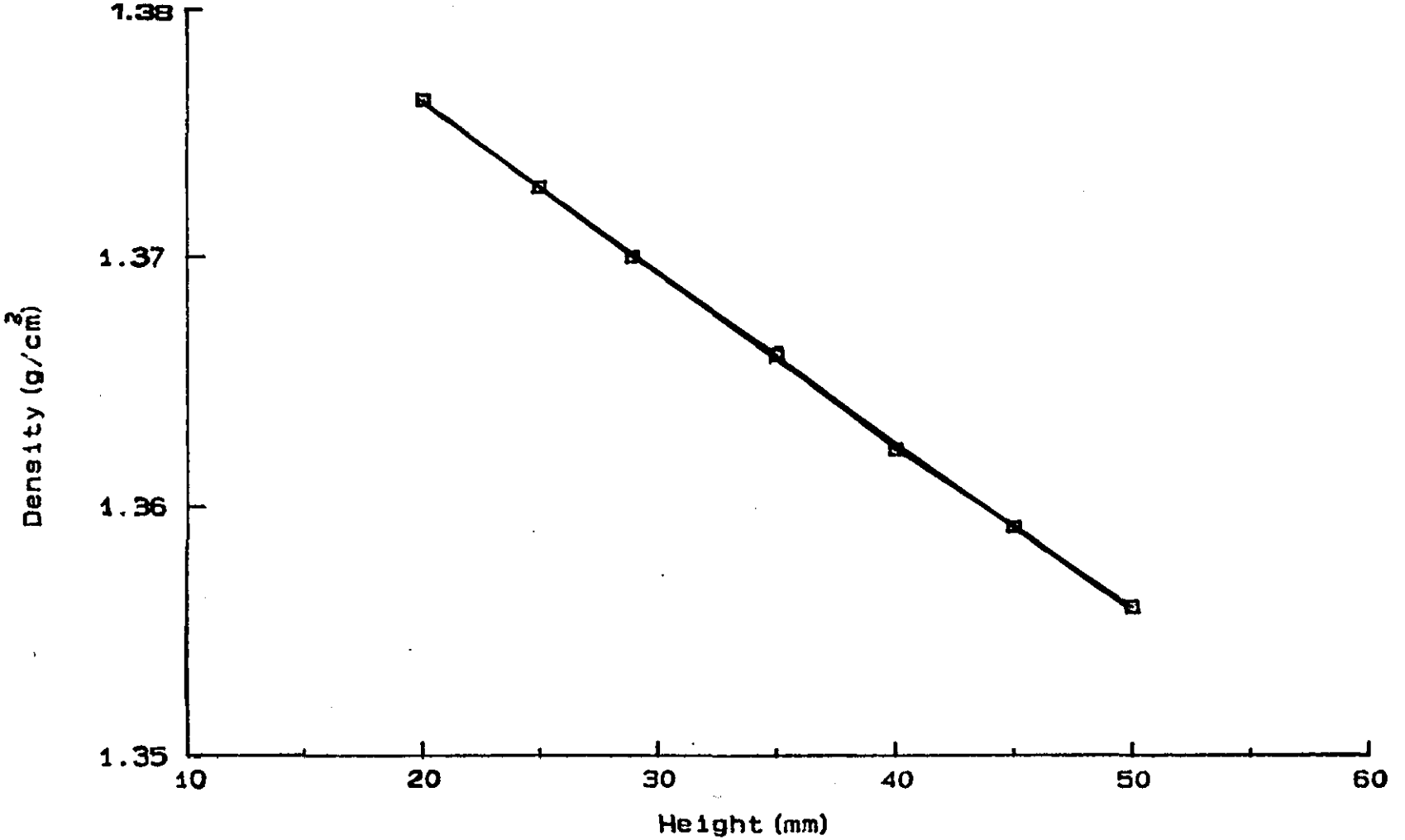

FIGURE A2: CALIBRATION CURVE FOR DENSITY TESTS OF PET/MXD6 (70/30) BLEND

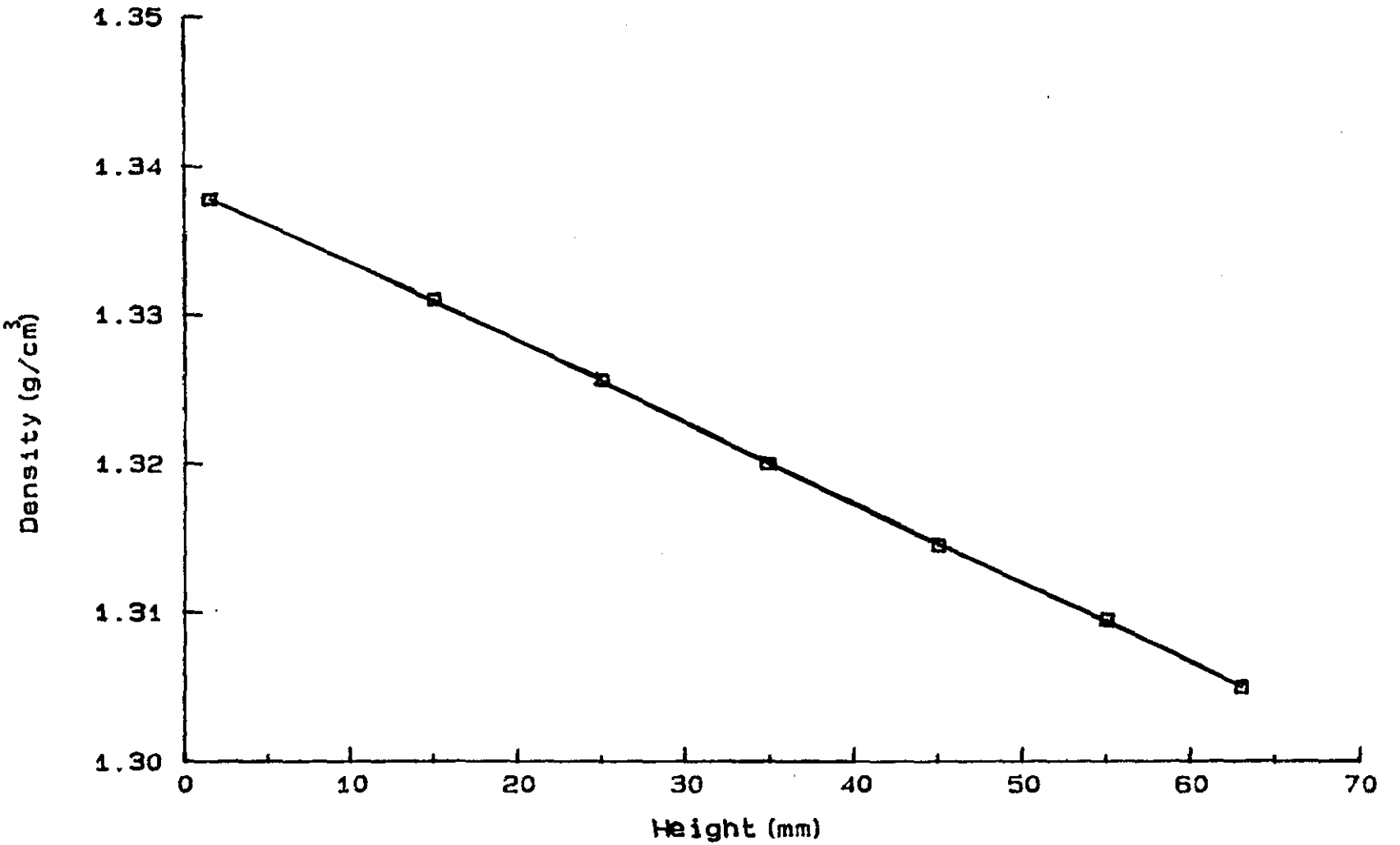

APPENDIX B

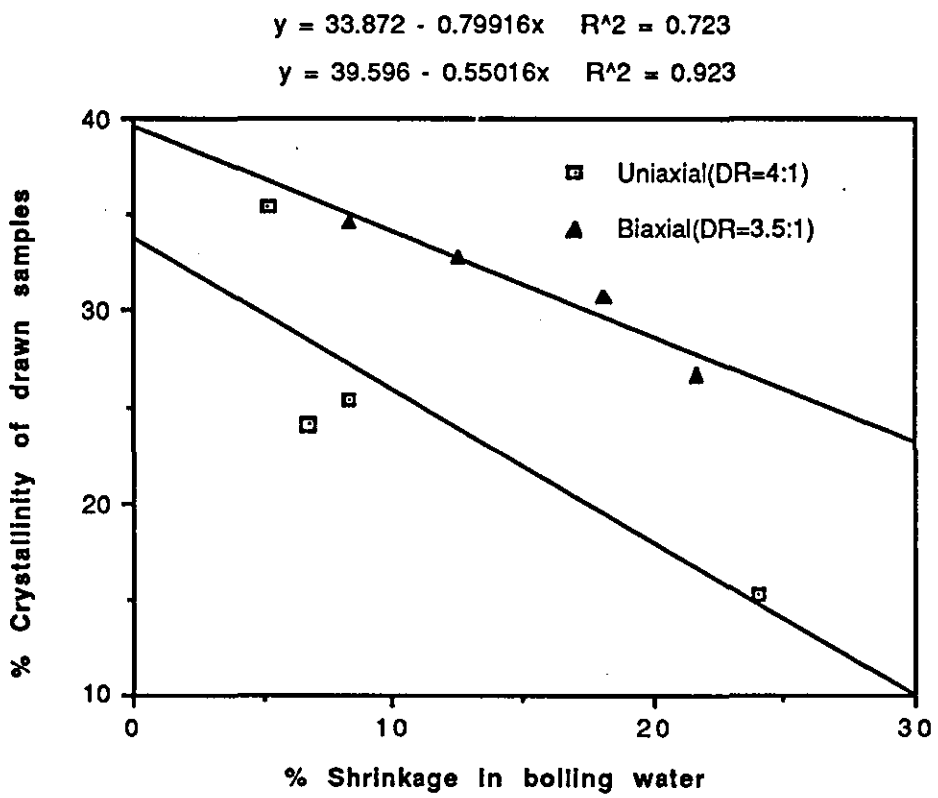

Figure B1: Relationship between % crystallinity of drawn non-nucleated thick PET samples(0.8mm) and shrinkage in boiling water

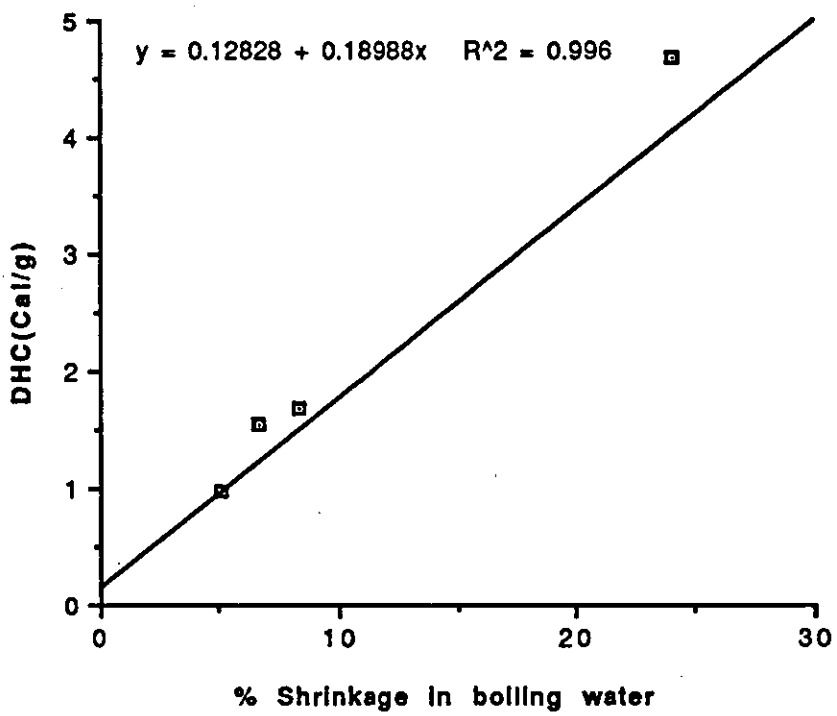

Figure B2 : Relationship between the heat of cold crystallisation temperature(ΔHC)and shrinkage in boiling water for uniaxially drawn thick PET samples (0.8mm) at 80 C for DR=4:1

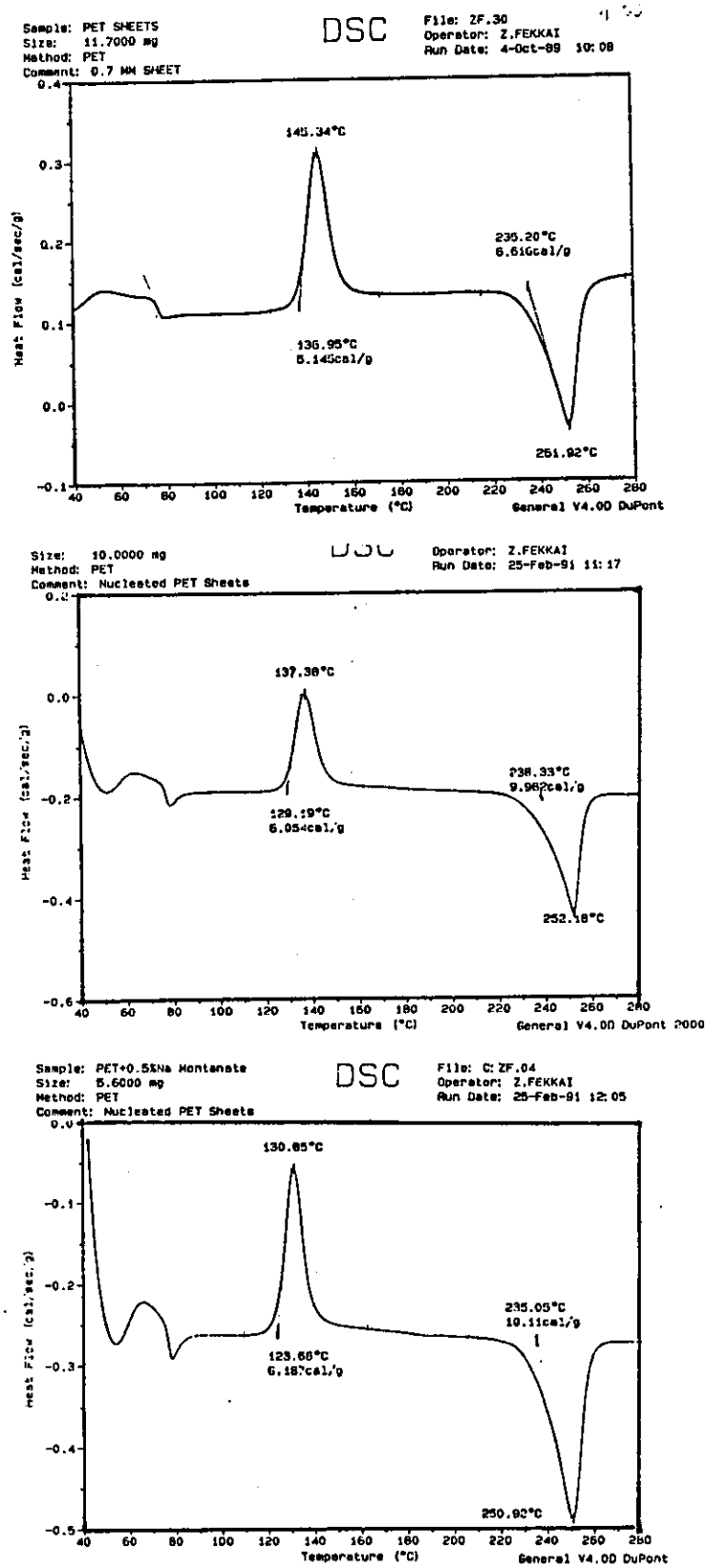

FIGURE B3: DSC traces at 20 C/min heating rate of nucleated and non-nucleated thick PET sheets (0.8 mm)

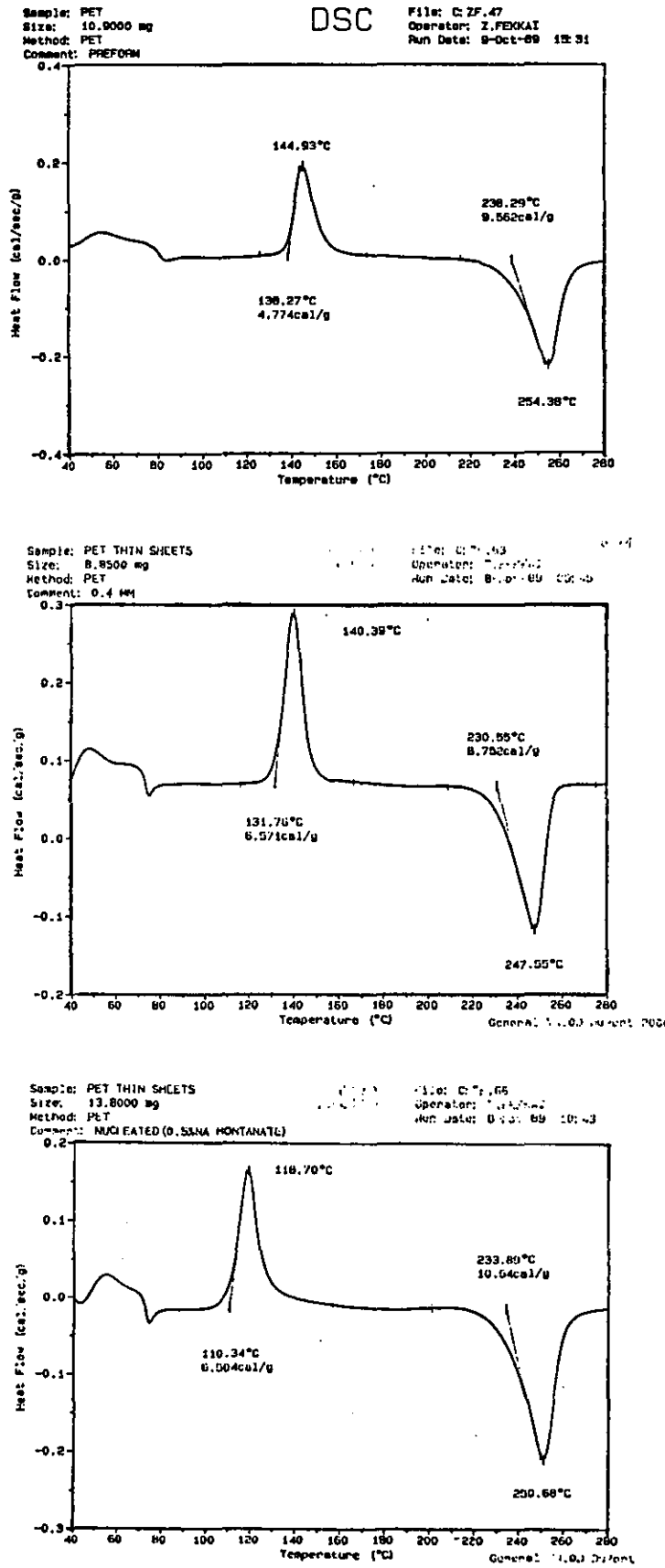

FIGURE B4: DSC traces at 20 C/min heating rate of PET preform, nucleated and non-nucleated thin PET sheets (0.4 mm)

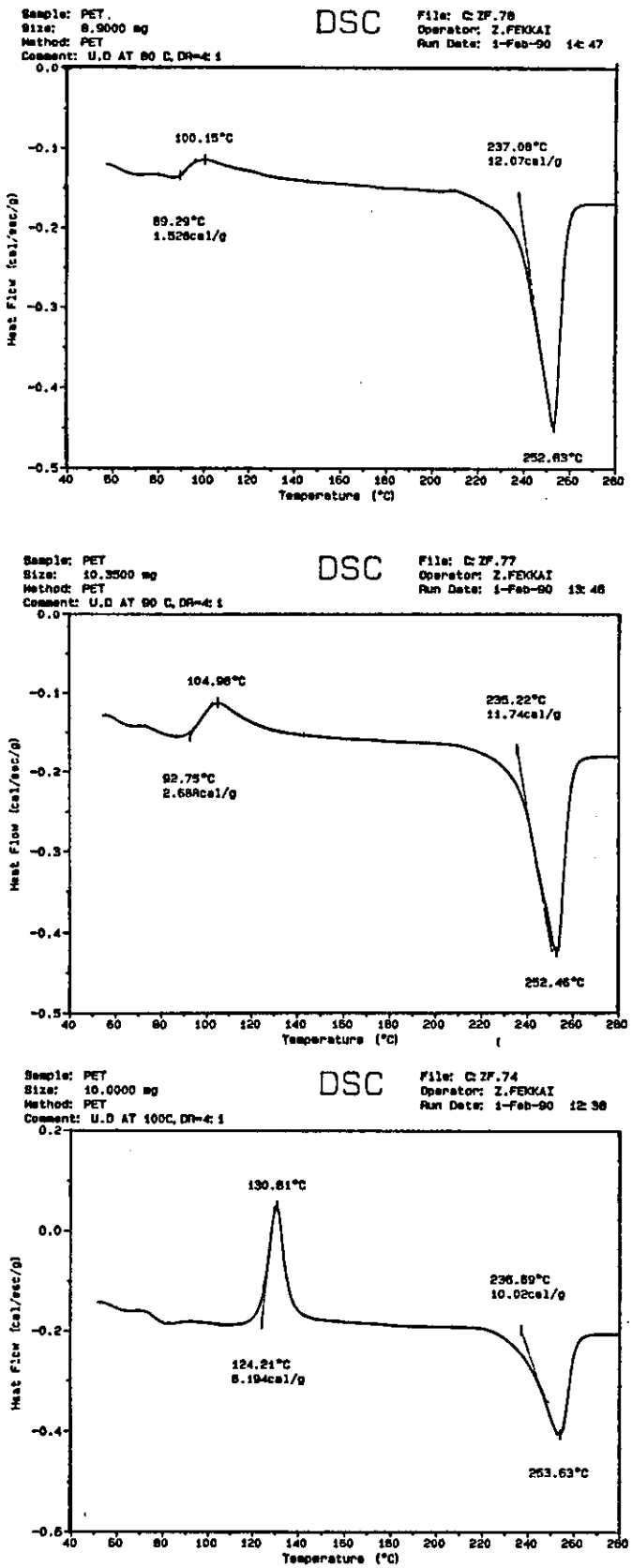

FIGURE B5: DSC traces at 20 C/min heating rate of uniaxially drawn non-nucleated thick PET samples (samples from injection moulded plaques)

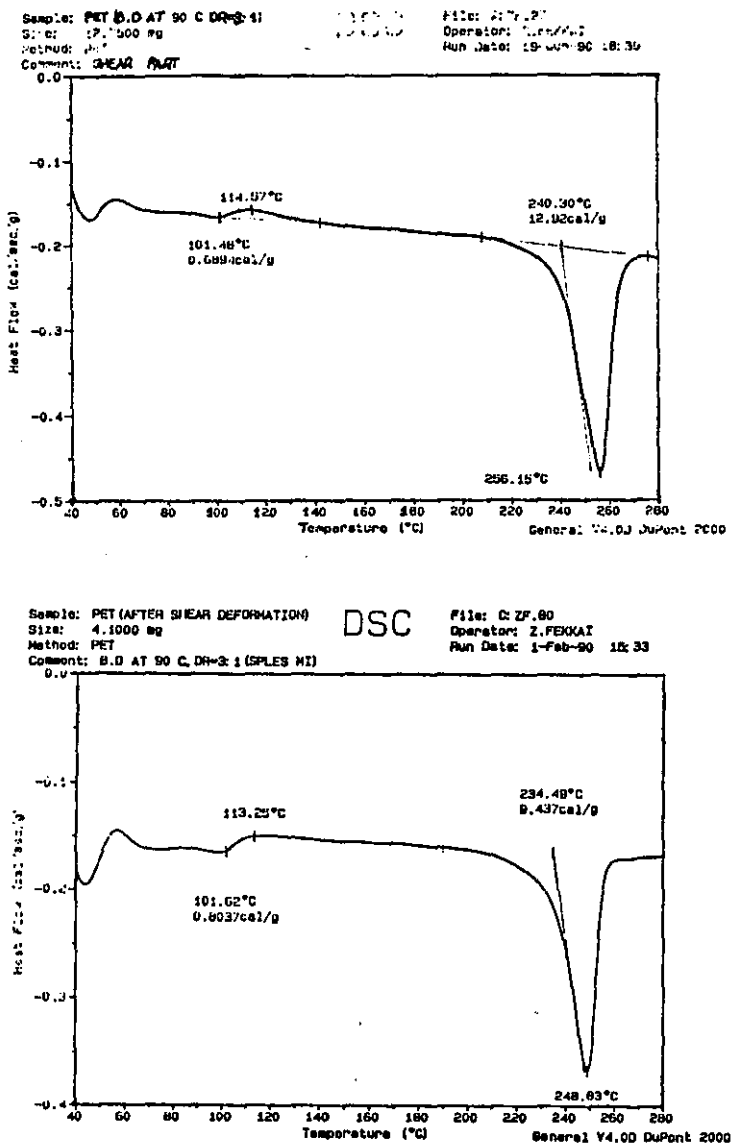

FIGURE B6: DSC traces at 20°C/min heating rate of biaxially drawn PET with and without shear deformation

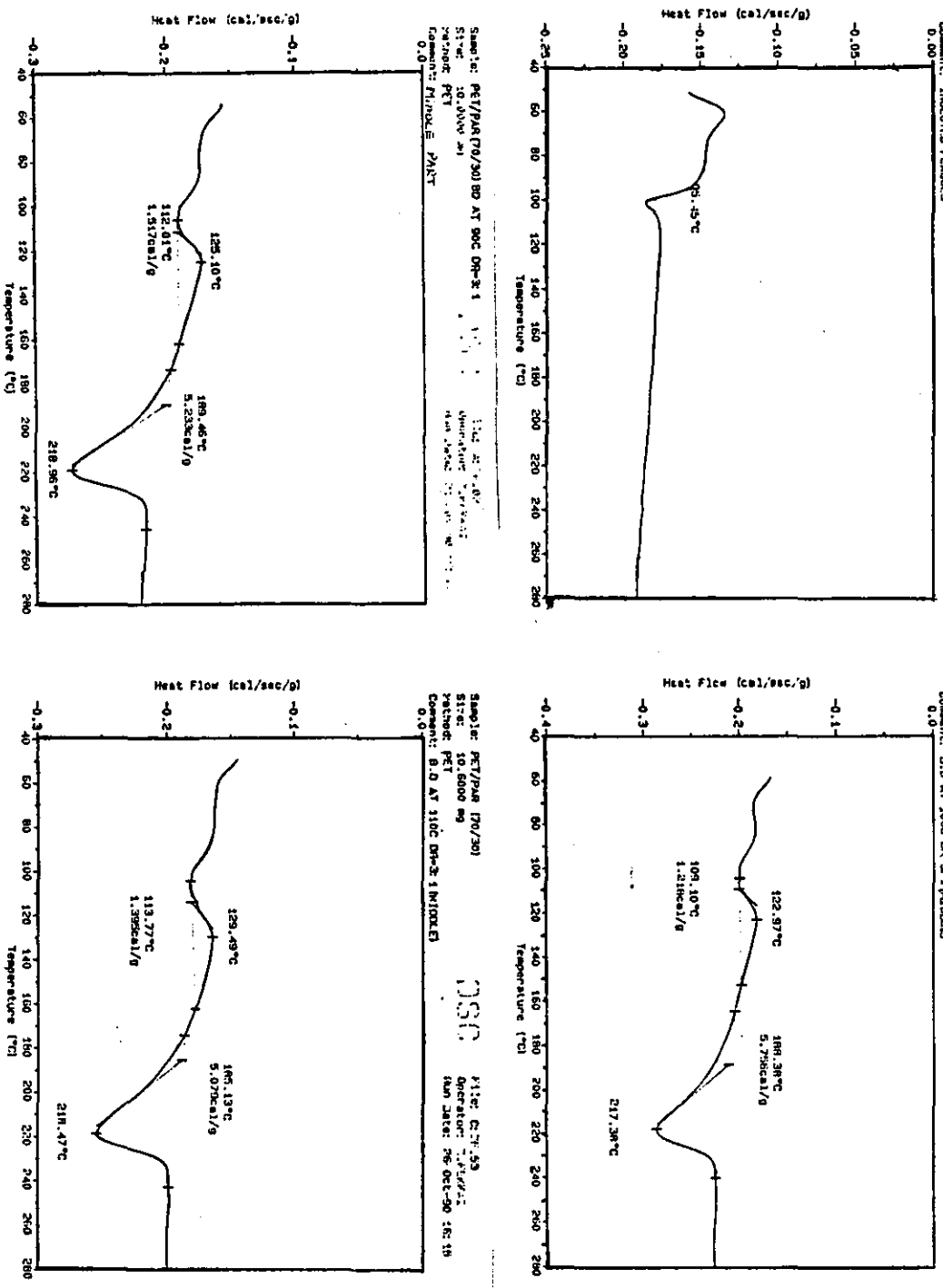

FIGURE B7: DSC traces at 20°C/min heating rate of the samples taken from the middle of biaxially drawn PET/PA (70/30) blend

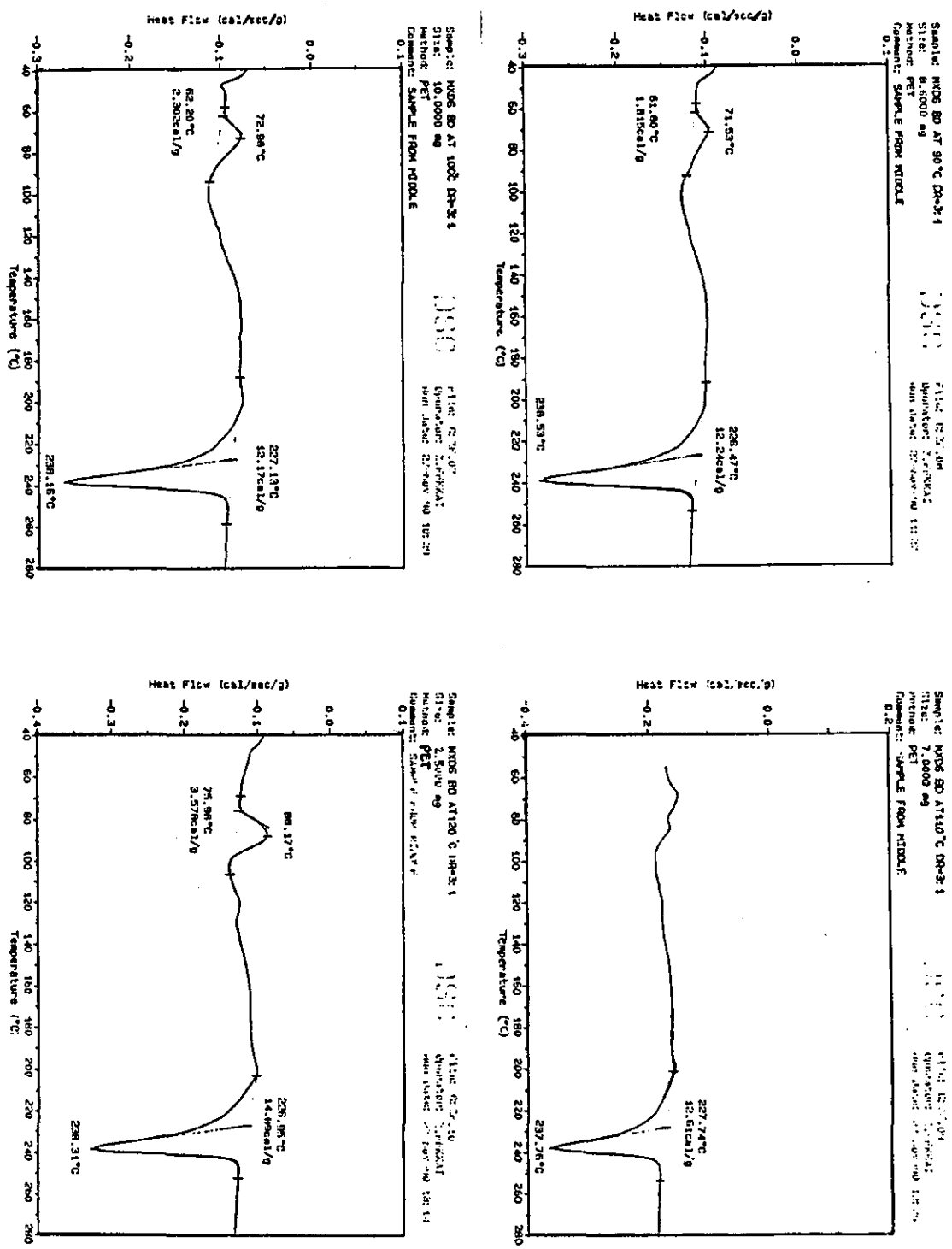

FIGURE B8: DSC traces at 20°C/min heating rate of samples taken from the middle of biaxially drawn MXD6

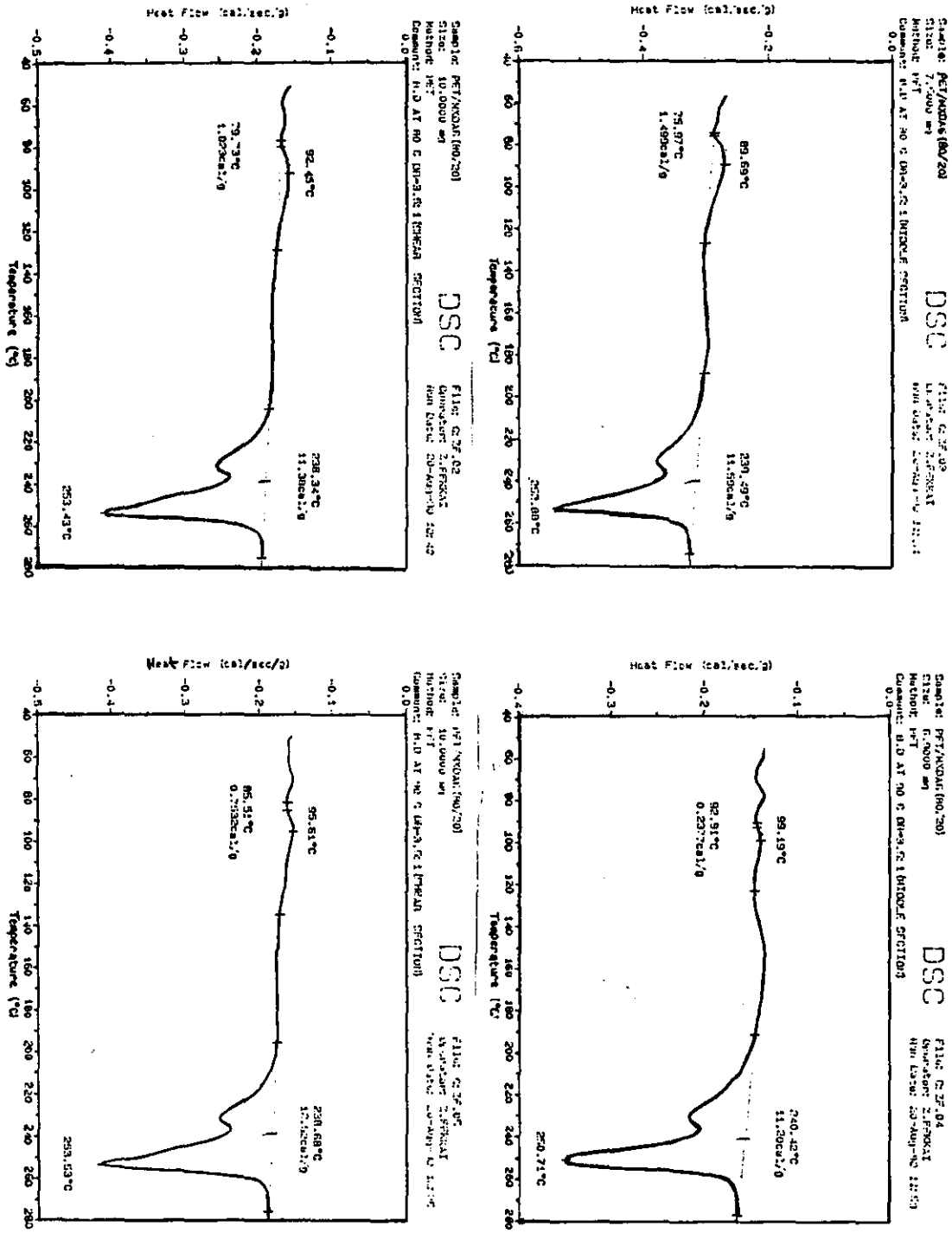

FIGURE B9: DSC traces at 20°C/min heating rate of biaxially drawn PET/MXD6 (80/20) blend at 80°C, and 90°C for DR = 3.5:1 (samples taken from the middle and the shear region)

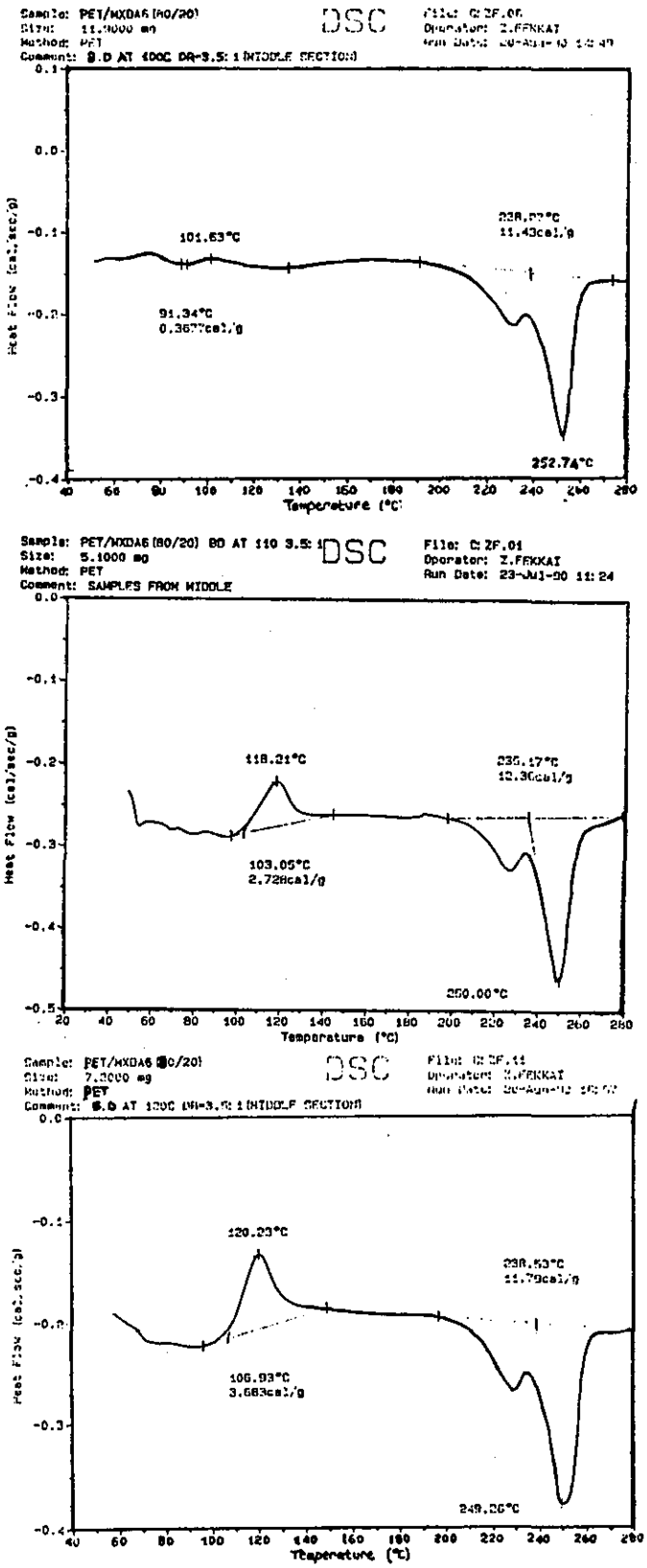

FIGURE B10: DSC traces at 20°C/min heating rate of samples taken from the middle of biaxially drawn PET/MXD6 (80/20 blend)

APPENDIX C

REFRACTIVE INDICES RESULTS

The refractive index of PET and MXD6 has been evaluated by using the Abbe refractometer (see Chapter 1, Section 1.3.1 for the principal measurements of the refractive index).

The results showed that the refractive indices of these two polymers are identical and equal to 1.582.

(a)

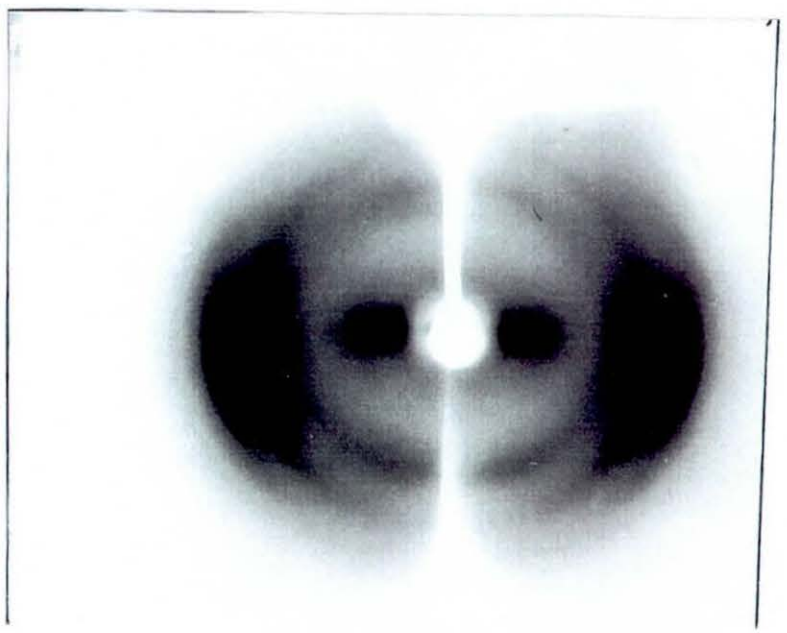

(b)

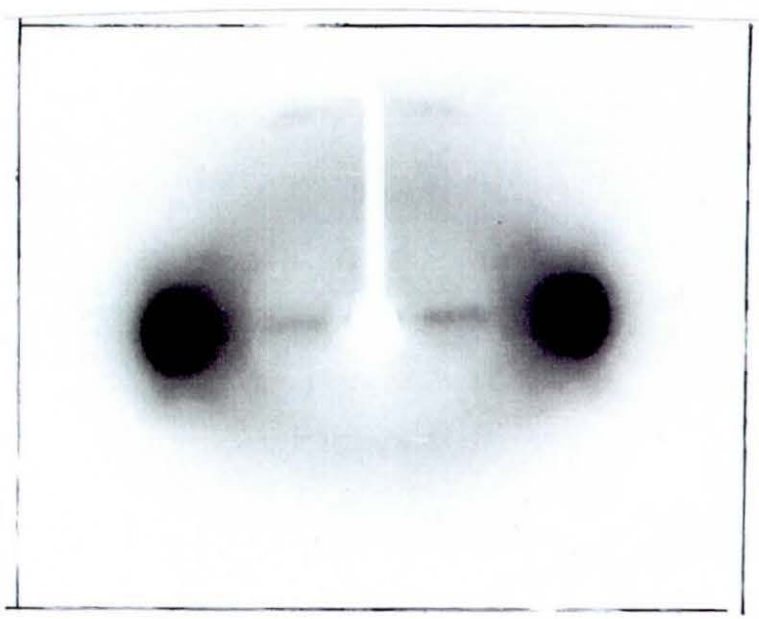

FIGURE C1: Wide angle X-ray pattern of biaxially drawn non-nucleated PET samples at TD = 90°C and DR = 3.5:1
a) samples taken from the middle region
b) samples taken from the shear region

(a)

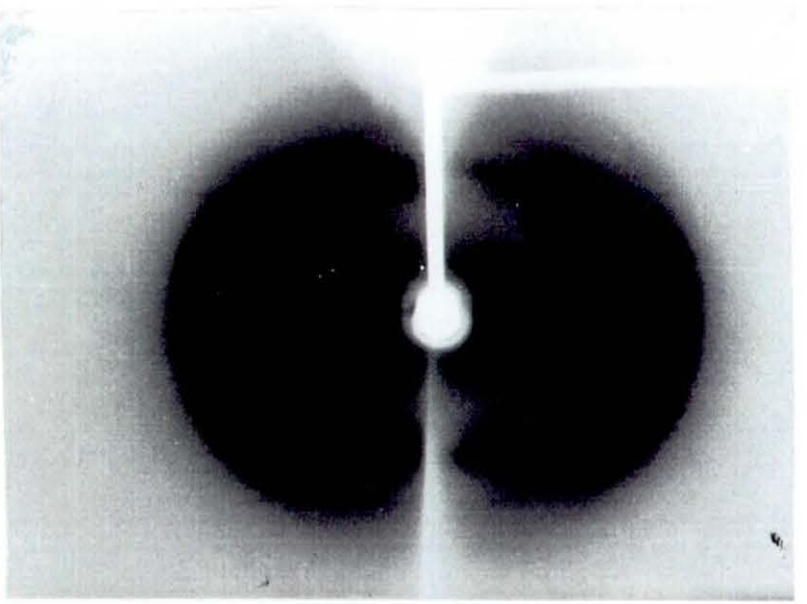

(b)

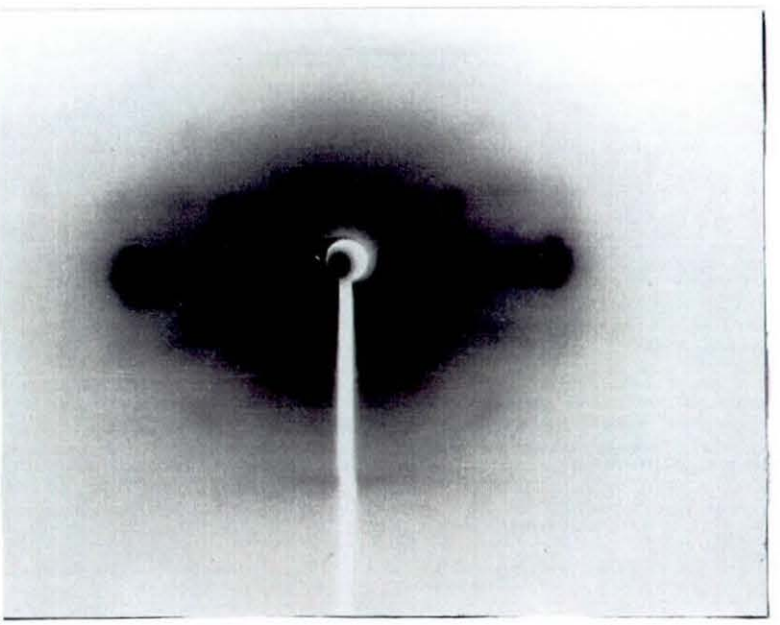

FIGURE C2: Wide angle X-ray pattern of biaxially drawn non-nucleated PET samples at TD = 100°C and DR = 3.5:1
a) samples taken from the middle region
b) samples taken from the shear region

(a)

(b)

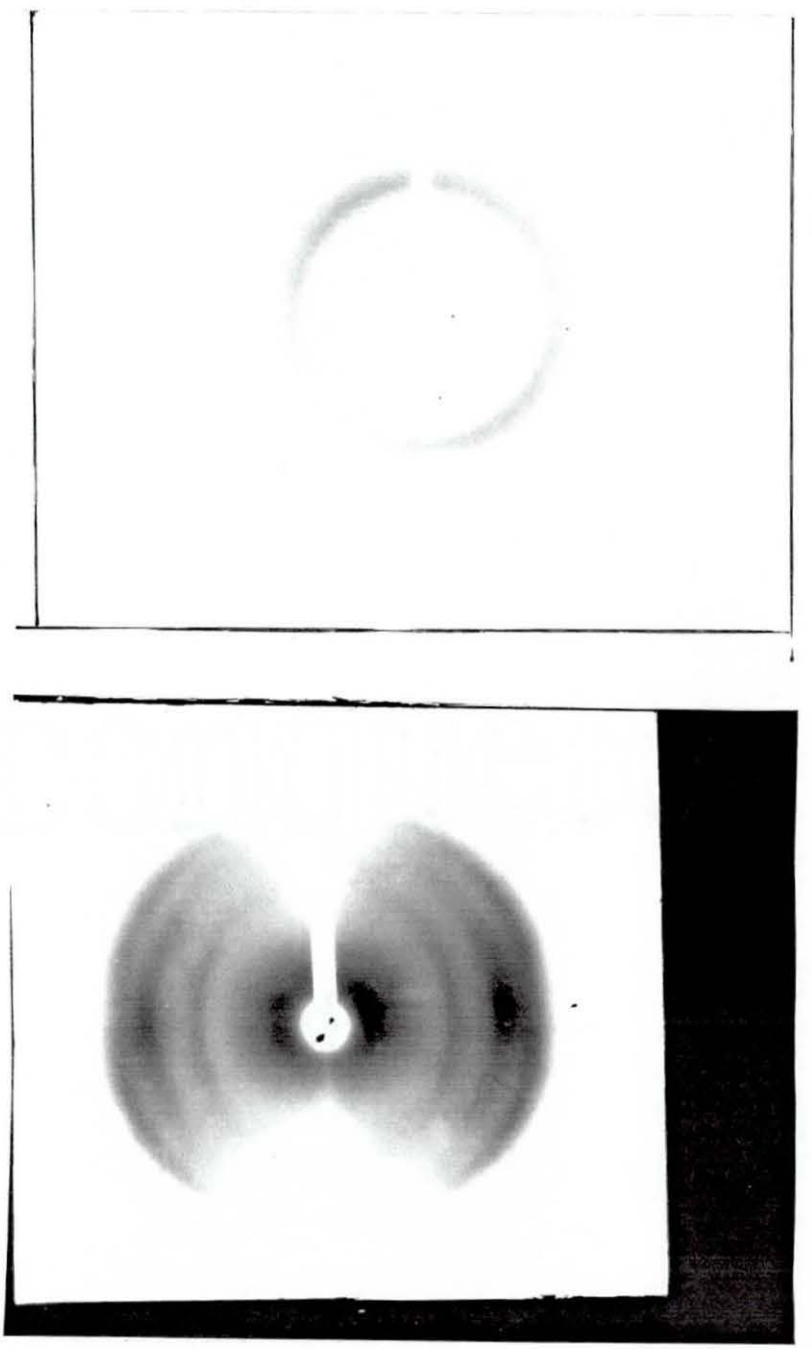

FIGURE C3: Wide angle X-ray pattern of biaxially drawn non-nucleated PET samples at TD = 110°C and DR = 3.5:1
a) samples taken from the middle region
b) samples taken from the shear region